PLANNING AND 4D VISUALISATION OF THE MARINE CONTROLLED SOURCE ELECTROMAGNETIC METHOD

Report No.: GPH 7/08

by Andrew Pethick

BSc (Geophysics) Curtin and BCs (Computer Science) UWA

This report is presented as part of the requirement for the units Geophysics Honours Dissertation 494 Part A & B, units totalling 50 credit points in the BSc (Geophysics) Honours from Curtin University of Technology. The work is the result of supervised research; however, the report has been prepared **by the student who is solely responsible for its contents.**

DEPARTMENT OF EXPLORATION GEOPHYSICS
Curtin University of Technology

November 2008

Abstract

Marine controlled source electromagnetics has developed rapidly as a hydrocarbon exploration technique. Companies have conducted 3D over 2D surveys to improve target resolution. Planning requires extra consideration as the cost and complexity of these surveys rise. I analysed a range of planning procedures and developed a four step methodology since detailed methodologies for marine CSEM weren't publicly available. The four steps were; (1) create geoelectric model (2) initialise forward modelling parameters (3) optimise survey parameters (4) evaluate survey design. I designed a software package (CSEMoMatic) which facilitated importing and exporting survey designs. This overcame the lack of existing software for exporting file formats for 4D visualisation software packages. It was developed using object oriented programming (OOP) in Java. EM fields and survey configurations are easily stored, modified and represented by OOP. The package contains new processing techniques constructed to evaluate survey designs. 4D visualisation techniques for the MCSEM method have been underappreciated. Several of these techniques have been applied to assist survey planning. Findings included (1) 3D polygons can represent the geometry and resistivity of geoelectric bodies. (2) Polarisation ellipses simplify the 4D motion of the EM vector field. (3) Polarisation ellipses and streamlines assist in optimising receiver positions by showing the direction of maximum coupling to the scattered response.

Additional findings indicated survey design should incorporate vertical electric dipole receivers since E_z is effective at detecting hydrocarbon reservoirs. Further research in MT, MCSEM and seismic surveys is needed to achieve cost effectiveness and efficiency in using marine CSEM.

Acknowledgements

I'd like to thank my family, my parents Peter and Connie and my brothers David and Michael, for all the support they have given me. I would never be where I am today without them. I would also like to thank my supervisors Brett Harris and Andrew Squelch for not only lending their expertise and experience but encouraging me every step of the way.

Finally I would like dedicate this thesis to my fiancée and future wife Karen Lam. I love you more than anything on this earth. I can't wait to spend the rest of my life with you

Table of Contents

List of Figures

List of Tables

1 Introduction

1.1 Research Objectives

The main objectives are to:

1) Develop a software package to facilitate MCSEM survey design and visualisation
2) Examine a range of visualisation techniques to represent EM fields
3) Develop a planning procedure for marine CSEM

Objective 1:

Develop a software package

The plan is to develop a software package to interface with forward modelling software. The software is to be designed to:

i. Import forward modelled spectral 3D CSEM data
ii. Process forward modelled data
iii. Export processed data in several file formats
iv. Be intuitive

Objective 2:

Study a range of visualisation techniques

The secondary goal is to apply visualisation techniques to represent low frequency EM field propagation. The visualisation representations to facilitate survey design include:

i. 3D Polygons

ii. 3D scalar planes

iii. Isosurfaces

iv. Streamlines

v. Polarisation ellipses

Objective 3:

Analyse planning procedures for marine CSEM

The planning methodology will incorporate:

i. Normalisation plots

ii. Geometric response indicator grids

iii. 3D visualisation techniques

1.2 Marine CSEM

Electromagnetic (EM) methods for hydrocarbon exploration can be divided into active and passive categories. The use of passive sources such as MT has shifted to active EM methods such as the controlled source electromagnetic (CSEM) method. MCSEM has been used to detect and appraise thin resistive hydrocarbon reservoirs in a conductive surrounding. Controlled source electromagnetic method is also known as, CSEMi, sea bed logging or SBL. CSEM detects electrical resistivity contrasts (Kong, 2002). Originally developed for deepwater studies of oceanic lithosphere in the only 20th century (Cox, 1981) the first commercial MCSEM surveys completed in 1979 (Spiess et al., 1980). These early surveys concentrated on shallow water exploration targets (Chave et al., 1981) however the method has expanded onto both locating deep and shallow water targets. In the last couple of decades the MCSEM method has expanded through the efforts of various university and industry researchers such as Scripps Institute of Oceanography, The University of Toronto, Cambridge and later Southampton University. The original research combined both natural and active EM sources to image resistivity variations beneath the sea floor. Prior to MCSEM, MT identified resistivity variations on large scale structures at basin level. MCSEM now ascertains the shape and resistivity of thin resistive bodies (Peace, 2005).

MCSEM detects resistivity rather than acoustic properties hydrocarbon saturation can be characterised more accurately than by using seismic attributes. The response in MCSEM correlates with the saturation percentage, which is unlike seismic which can only detect accurately between 0 and 10% with amplitude and velocity analysis techniques (MacGregor, 2006); this can be seen in Figure 1-1. Marine CSEM can detect petroleum, natural gas, gas hydrates and other resistive zones provided a

sufficient resistivity contrast exists. It is also able to predict the hydrocarbon saturation for a potential reservoir ahead of drilling (Phillips, 2007). Marine CSEM surveys are becoming more popular in deep water due to the increasing expense of seismic surveys and the cost of drilling prospects (Spiess et al.,1980). The method must be applied under suitable geoelectrical conditions. Commercial projects are always preceded by a feasibility study evaluating the electromagnetic responses of the expected target and background geoelectric structure. A survey plan can be designed from the results of the feasibility study.

1.3 Project background

The controlled source electromagnetic method is used when seismic method is restricted by low velocity zones such as magma chambers or high velocity layers in sub-basalt or sub-salt areas. MCSEM is not perfect, its use is restricted when applied beneath thick tabular salt/basalt targets or where the target is thin, deep and has low resistivity comparable to the surrounding geology (see Table 1-1). MCSEM is useful in deep water turbidites and deltas, over stacked reservoir sequences or where there are large resistivity contrasts such as in shallow gas hydrates (MacGregor, 2006). Geological environments such as reservoirs at the edges of salt diapirs and in carbonates can be explored by the MCSEM method. Despite these advancements there are two areas still in need of research, these include visualising MCSEM data and survey planning.

Marine controlled source electromagnetic surveys have become an integral part of deep ocean petroleum exploration and appraisal (Gribenko and Zhdanov, 2005) and future use for monitoring purposes may be possible. Some are now performed in 3D rather than 2D. For 3D MCSEM, planning has become increasingly important for the success of a survey (Kong et al., 2005).

Practicality	Geology
Works Well	Deep water turbidites Deep water deltas Stacked seservoir sequences Under shallow gas or gas hydrates
Feasible	Flanks of salt diapirs Carbonate sequences Shallow water areas
Needs Research	Beneath thick tabular salt/basalt Thin deep, low resistivity targets

Table 1-1: The practicality of the MCSEM method in different geological environments. MCSEM works in a variety of geological environments however in some geological settings MCSEM may not work. (MacGregor, 2006).

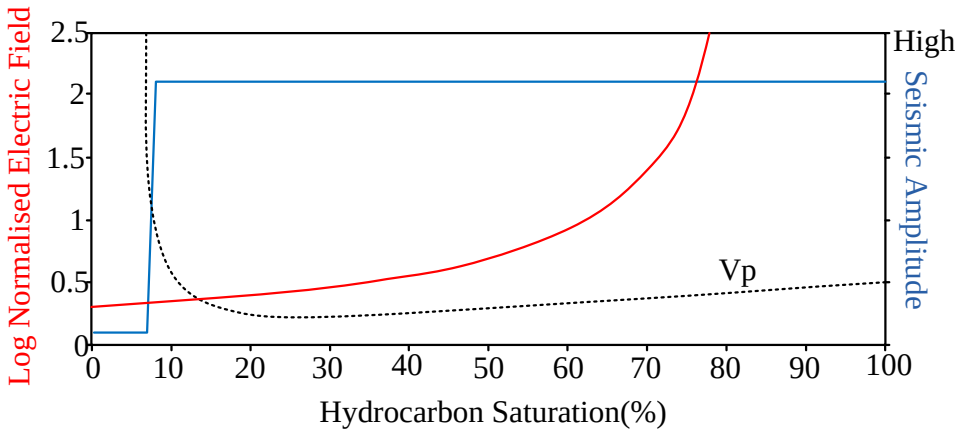

Figure 1-1: The effect of Hydrocarbon saturation on seismic and MCSEM electric field observations. MCSEM electric field response characterise the hydrocarbon saturation more precisely because the increase in signal corresponds to the hydrocarbon saturation, while the seismic method fails to distinguish between 10 and 100 percent (Modified from MacGregor, 2006)

1.4 The controlled source electromagnetic method

There is a typically a resistivity contrast between the conductive host rock and the resistive hydrocarbon. Saturated mudstone rocks, sandstones and shales with low resistivity dominate deep water environments. A hydrocarbon reservoir can be 10 to 100 times greater in resistivity (Eidesmo et al., 2002). This physical property can be exploited by the marine CSEM method by recording the disturbances from an active electromagnetic source.

Typical marine CSEM surveys work by using a horizontal electric dipole to transmit a low frequency 0.1 to 5Hz square wave under high power up to 1000 Amps (MacGregor, 2006). A horizontal electric bipole is a 100-1000m long electric field transmitter towed 50m above of the ocean bottom (MacGregor, 2006). Receivers can be placed to record the perturbations in the electric and magnetic fields for all Cartesian directions. In modern surveys E_x, E_y, H_x and H_y components are typically recorded.

The transmitted wave diffuses through the through the water column and into seabed (as seen in Figure 1-2). Electric fields attenuate less in resistive mediums. The increase in electrical field due to the reservoir can measured at the seafloor at offsets roughly double the depth of the reservoir below the seabed. The magnetic field circulates around the electric field and is responsive to secondary fields.

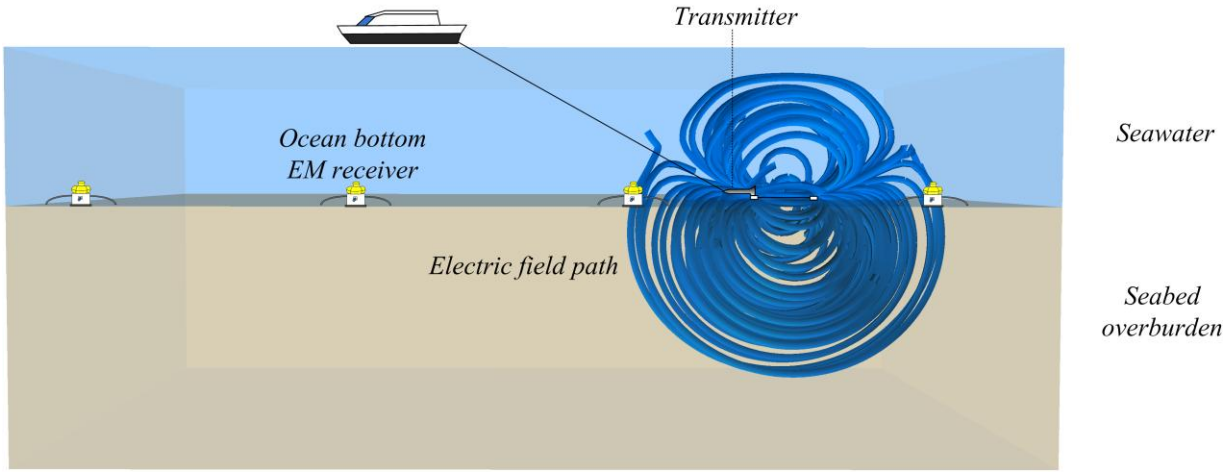

Figure 1-2: A schematic of a MCSEM survey showing the path of the transmitted electric field. The electric field will channel above the resistive boundaries such as at air and hydrocarbon interfaces.

2 Background

This chapter will overview the use of the marine controlled source electromagnetic method for hydrocarbon exploration.

i. The current state of the marine controlled source electromagnetic technique for hydrocarbon exploration.

ii. Physics of low frequency electromagnetic

iii. Instrumentation

iv. Survey parameters

v. Factors affecting survey design

vi. Possible survey designs

2.1 The current state of the marine CSEM method

2.1.1 Survey planning methodologies

Few papers have stated clear survey planning methodologies, the papers written by Peace (2005) and Flosadóttir et al. (1996) are overviews of the main areas of survey planning and MacGregor (2002) and MacGregor et al. (2006) only skim the topic surface. Currently there is no publicly available material that provides an in depth planning methodology, specifically in the area of 3D multispectral survey design and only Ridyard D. Et al. have provided insight into evaluating MCSEM survey designs.

2.1.2 CSEM component representation

It appears that the conventional representations of MCSEM data include 1D profiles, grids and in more extraordinary cases 3D contours, such as Peace (2005), Mittet et al. (2004), Phillips (2007). The use of 3D visualisation techniques is limited. Polarisation ellipses have been mentioned by MacGregor (2006) but only on a 2D

plane. Streamlines, isosurfaces, polarisation ellipses and polydata are scarcely applied to MCSEM data.

2.2 Physics of low frequency electromagnetics

2.2.1 Skin depth

The depth of penetration as a relationship of frequency and conductivity is described by the skin depth. From looking at previous MCSEM surveys MacGregor et al. (2001), MacGregor et al. (1998) and Ellingsgrud et al. (2002).

Skin depth is the effective depth of penetration of electromagnetic energy in a conducting medium when the amplitude of a plane wave has been attenuated to $^1/_e$ (or 37 percent) (Sherriff, 1991). This relationship is described by the skin depth in equation 1.

$$\delta = \sqrt{\frac{2}{\mu_0 \sigma \omega}}\text{m} \approx 503\sqrt{\frac{1}{f\sigma}}\text{m} \quad (1)$$

μ_0 = Magnetic permeability in a vacuum $\left(Hm^{-1}\right)$ *Density*
ω = Angular frequency $\left(Radians\right)$
σ = Conductivity $\left(Sm^{-1}\right)$
f = Frequency $\left(Hz\right)$

The formula can only be used in an isotropic conductive environment. The skin depth equation can only provide an indication of decay lengths for more complex geoelectric models.

Sea water is generally considered highly conductive and acts as a low pass filter to incident MT source fields (Constable et al., 1998). Frequency also affects the depth of penetration because energy is lost for every cycle of the wave, causing higher frequencies to be attenuated more as seen in Figure 2-1. The electromagnetic skin depth is shortest at high frequency.

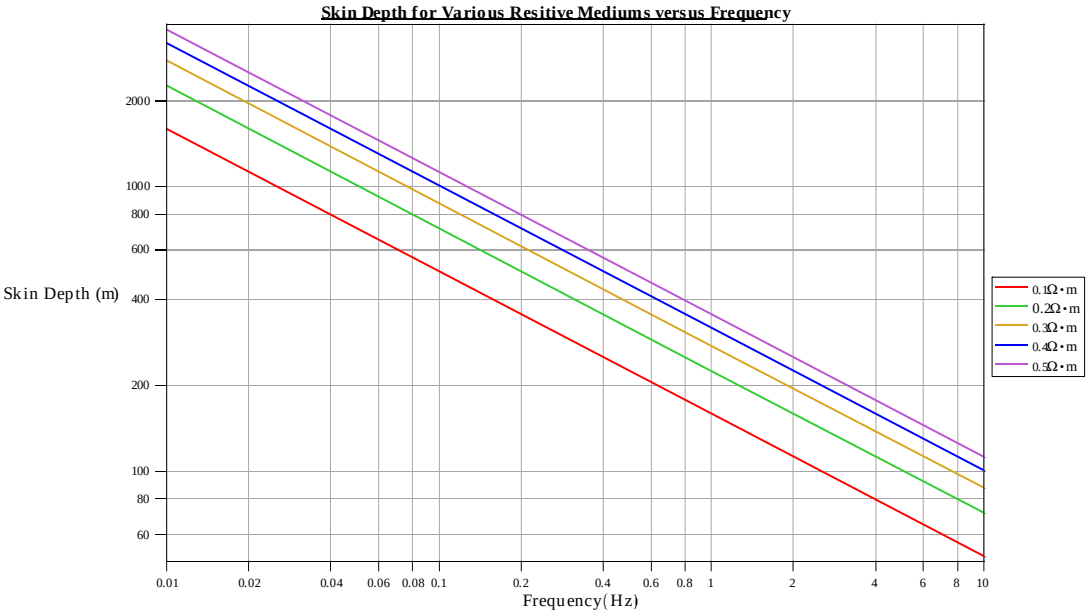

Figure 2-1: The relationship of skin depth for frequency and conductivity. The skin depth decreases as the conductivity or frequency increases.

2.3 Survey parameters

2.3.1 Transmitted waveform

The waveform dictates the frequency content. The frequency content influences the depth of investigation, resolution and sensitivity to the hydrocarbon body. Another attribute to consider includes the waveform stability. The waveform must be stable to ensure consistent signal phase measurements. To ensure this in the field, MCSEM waveform monitoring is used (MacGregor, 2006).

The MCSEM method traditionally uses a continuous harmonic square wave signal with fundamental frequency (and odd harmonics) typically within the range of 0.01-10Hz (Pound, 2007). The Square and Cox are two commonly used waveforms as seen in Figure 2-2. They are used due to phase stability and the wide frequency content (MacGregor, 2006). Unfortunately there is a trade-off between resolution and depth of penetration. In most cases high frequencies resolve near surface resistivity variations, which can be used to constrain the geoelectric model for both the inversion and final interpretation. The waveform should contain multiple frequencies so that both near and far surface resistivity variations can be resolved whilst also maximising the depth that can be detected.

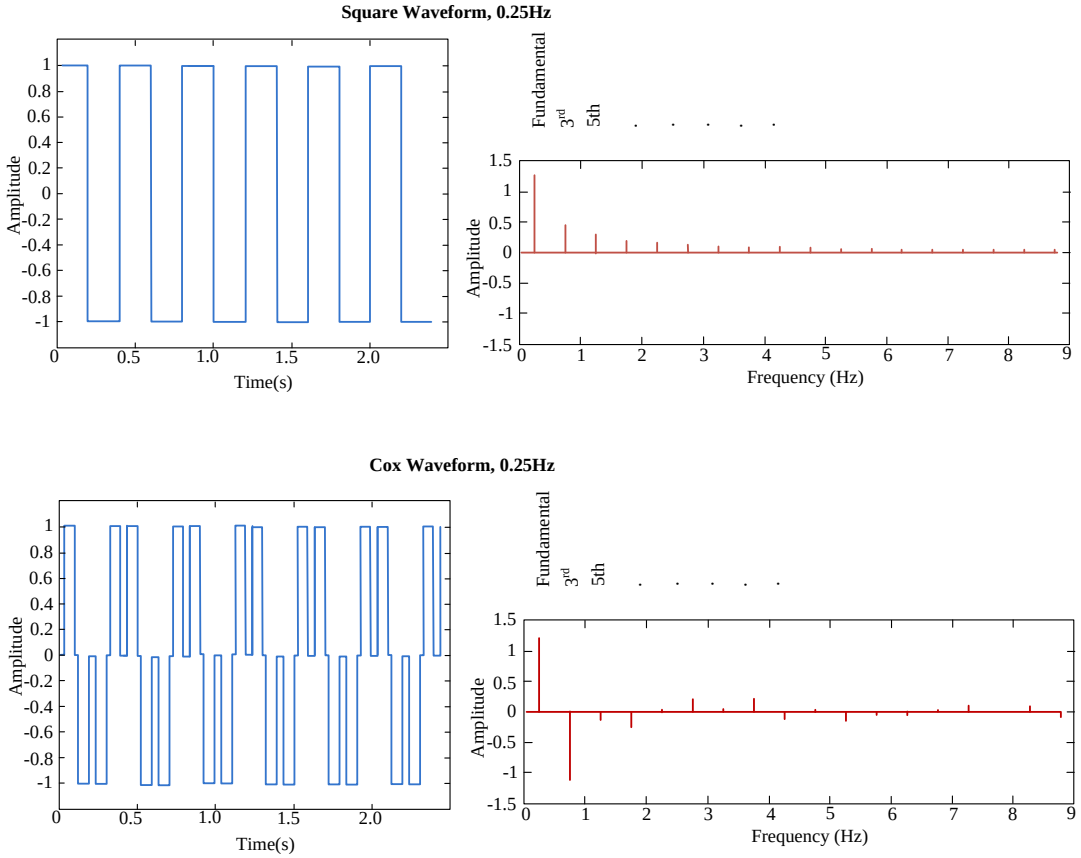

Figure 2-2: Typical transmitted MCSEM waveforms and the associated frequency spectra. The frequency spectrums are usually dominated by the fundamental frequency and its harmonics. Waveforms with both low and high frequencies allow both near surface and target geoelectric properties to be resolved (Modified from MacGregor, 2006).

2.4 Factors affecting survey design

2.4.1 CSEM noise sources

A number of noise sources that must be considered. Sources include sea water currents, magnetotelluric activity, bipole vibration, internal electrode and amplifier noise and cultural effects, as seen in Table 2-1 and Figure 2-3.

Internal amplifier and electrode noise limits the instrument's high frequency noise floor. Vibrations of the dipole receiver arms can also induce an unwanted signal. A vibration of less than 1mm for a 10m dipole can produce an induced voltage comparable to the target signal. These movements can be limited by using bottom weights, weighting each electric receiver dipole arm with glass rods and by using farings on dipole arms (MacGregor, 2006). These issues are not as influential in deeper waters so the receiver dipole arm length can be increased.

At lower frequencies (<1Hz) spheric noise and ocean induced fields can contaminate the received data. The magnitude of spherics noise reaching the receivers varies with water depth. Increases in water depth improve noise recording conditions of surveys because seawater acts as a shield from external magnetotelluric signals (Kong et al., 2002). The motion of a conductor in an electric field will have a voltage induced in accordance with Faraday's law. Seafloor water currents can dominate the intermediate frequencies in a survey. Therefore care must be taken when planning surveys in areas with fast moving water currents.

Noise Source	Description
Seafloor currents (<1Hz)	The motion of a conductor in an electric field will induce a voltage.
Spherics (<1Hz)	Lightning and ionic field disturbances resulting in a low frequency noise. Spheric noises reduce with water depth.
Cultural	Highly conductive or resistive materials close to the receiver will skew the signal
Bipole vibration (>1Hz)	Vibrations of the electric dipole receiver arms can induced a voltage comparable to the target signal
Internal electrode and amplifier noise (>1Hz)	The instruments internal noise.

Table 2-1: Noise sources to consider.

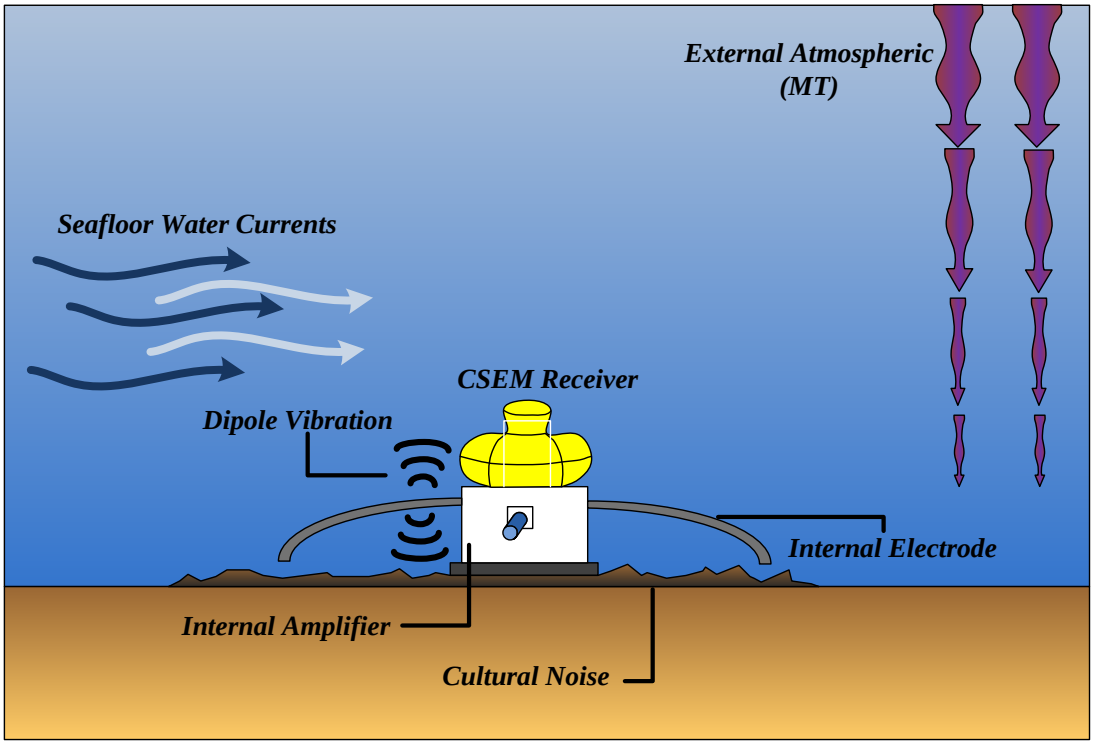

Figure 2-3: Noise sources. The noises can be split into two areas, external and internal. Internal sources are within the instruments which are internal amplifier and electrode noise, whilst external noises are caused by seafloor water currents, magnetotelluric (MT) signals, dipole vibration and cultural noises. It is best to conduct a survey in deep water to reduce the effect of seafloor water currents and external atmospheric noise.

2.4.2 Target style considerations

The target style greatly influences survey planning. Considerations include water depth, target depth, geological type of target, reservoir style, resistivity contrast, resistive non-hydrocarbon geological targets, reservoir complexity and the purpose of survey (Peace, 2005).

Water depth and bathymetry influences the onset of the airwave. Water bottom channels, canyons and sloping or having the target sit above the water bottom when surveying off a shelf edge, all need to be considered. Secondly the target depth from the water bottom and aerial size of the target compared to the depth affects the detectability of the target. Targets smaller in aerial extents than their depth are harder to detect. Thirdly the geological type and shape of target influences the response receiver on the ocean floor. Resistivity contrast also influences a survey plan. If the resistivity contrast between the hydrocarbon and the host is insufficient, no survey could detect the hydrocarbon. Non-hydrocarbon resistive structures could also lead to false positives. Therefore it is necessary to model a range of geological settings. Lastly the purpose of the survey influences the final survey design. For example recognisance surveys utilise widely spaced receivers and transmitter lines to target hydrocarbons. 3D surveys use many closely spaced receivers and densely positioned transmitter line locations at multiple azimuths to characterise or appraise a known field (See Figure 2-4).

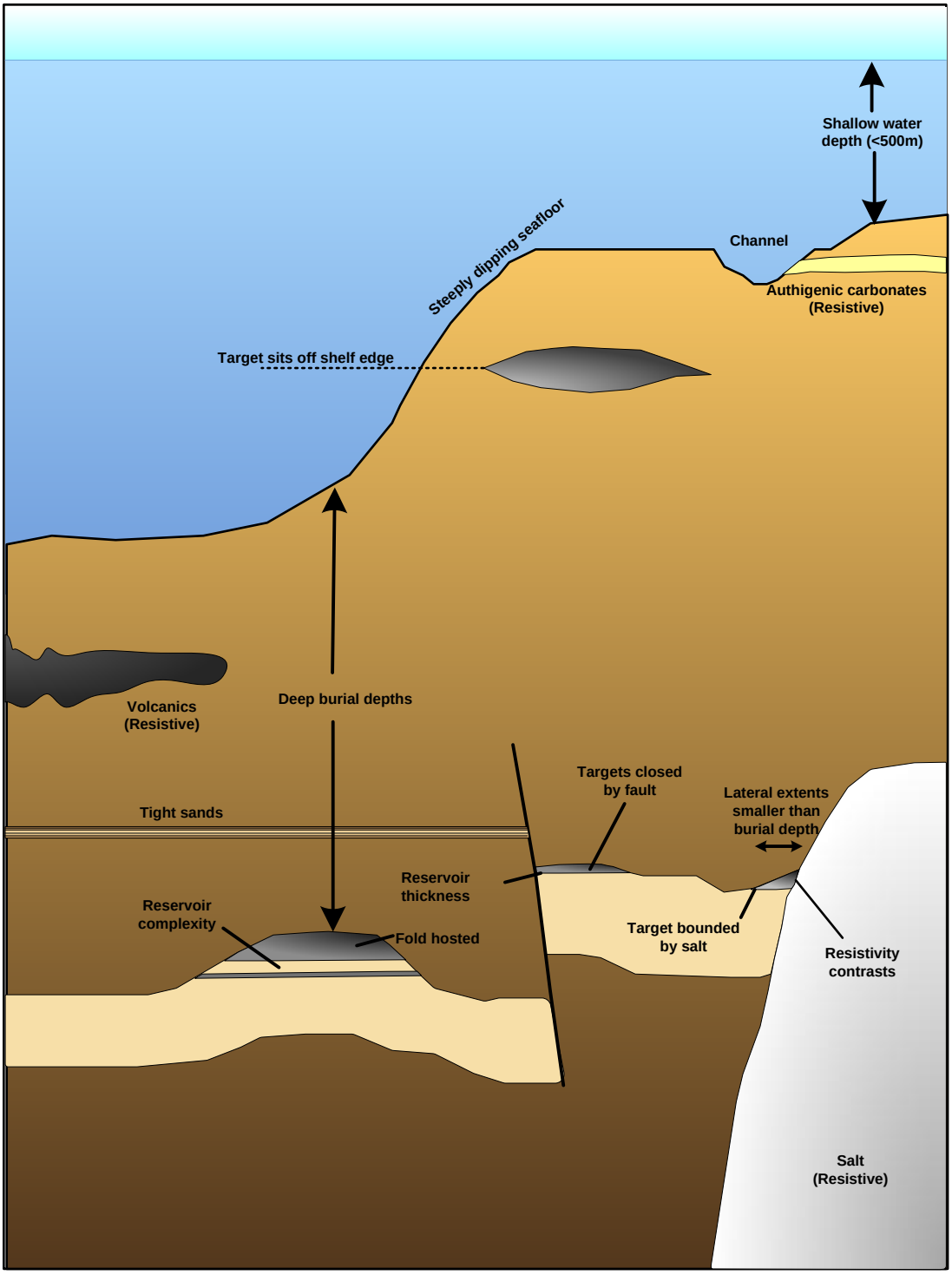

Figure 2-4: Geological considerations for MCSEM survey planning

2.4.3 The airwave problem

The airwave is a complex interference effect between the air and the water and seabed layering. The airwave poses problems for MCSEM surveys because it tends to dominate received signals at far offsets; masking seabed response (Eidesmo et al., 2002). It can be identified by a gradient break in inline electric field profiles, there is also a total phase lag which dependant on the offset and water depth (Eidesmo et al., 2002). The airwave is affected by the transmitter-receiver offset, transmitter dipole orientation, transmission frequency, resistivity structure and the water depth.

Eidesmo et al., (2002) and MacGregor (2006) have offered solutions to the airwave problem but none offer a 'silver bullet' solution. It is an ongoing problem for industry, EMGS and OHM that are working to resolve it by using various data processing techniques and also by limiting its effect by using novel acquisition practices (Eidesmo and Ellingsrud, 2002). Possible solutions to the airwave problem include selecting acquisition parameters that limit the generation of an airwave, signal processing and even using information in the airwave (MacGregor, 2006; Eidesmo and Ellingsrud, 2002l Eidesmo et al., 2002). Forward modelling can provide information regarding the effect of the airwave prior to surveying (Mittet et al., 2004; Johansen et al., 2005). Forward modelling calculates the onset of the airwave response. Modelling of these transmitter-receiver geometries will indicate the influence of the airwave.

Constable and Weiss (2006) have suggested that by using a vertical electric dipole transmitter the airwave can be limited. The coupling of the air-water interface is influenced by the orientation of the transmitter. Horizontal current loops create PM modes which strongly couple with this interface, while vertical current loops create TM modes and have no strong airwave effect (MacGregor, 2006).

The choice of transmission frequency is important because it affects the onset and amplitude of the airwave. Not only do higher transmission frequencies amplify the airwave effect, but the onset of the wave arrives sooner as seen in Table 2-2. Therefore the benefits of low frequency must be balanced against reduced resolution (MacGregor, 2006).

The maximum depth of investigation before contamination of the airwave can be calculated by using localisation (Eidesmo et al., 2002). The depth at which this occurs can be calculated by multiplying the scale factor from Equation 3 (α) with the water depth (Tompkins et al., 2004). For example if α=1.76 and the water depth is 1000m, then the maximum depth of investigation would be 1760m.

$$\frac{\mathrm{Re}\left\{k_{H_2O}\right\}}{\mathrm{Re}\left\{k_{Earth}\right\}} \cong \sqrt{\frac{\omega\mu\sigma_{H_2O}}{2}} \Big/ \sqrt{\frac{\omega\mu\sigma_{Earth}}{2}} = \sqrt{\frac{\sigma_{H_2O}}{\sigma_{Earth}}} = \alpha \qquad (3)$$

Water Depth (m)	Frequency			
	0.25Hz	0.5Hz	1.0Hz	2.0Hz
500	4.8	4.0	3.4	3.0
600	5.2	4.3	3.9	3.5
700	5.7	4.7	4.3	3.8
800	6.1	5.0	4.6	4.1
900	6.5	5.4	4.9	4.5
1000	6.9	5.8	5.4	4.9
1200	7.6	6.7	6.1	5.6
1400	8.5	7.5	6.8	6.2
1600	9.3	8.3	7.5	7.1
1800	10.1	9.0	8.3	7.8
2000	11.0	9.8	8.9	8.4

Table 2-2: The distance from the source (in km) at which the airwave starts to dominate the overall response. The point at which the response is dominated by the airwave is represented as function of water depth and the signal frequency. (Reproduced from Eidesmo et al., 2002)

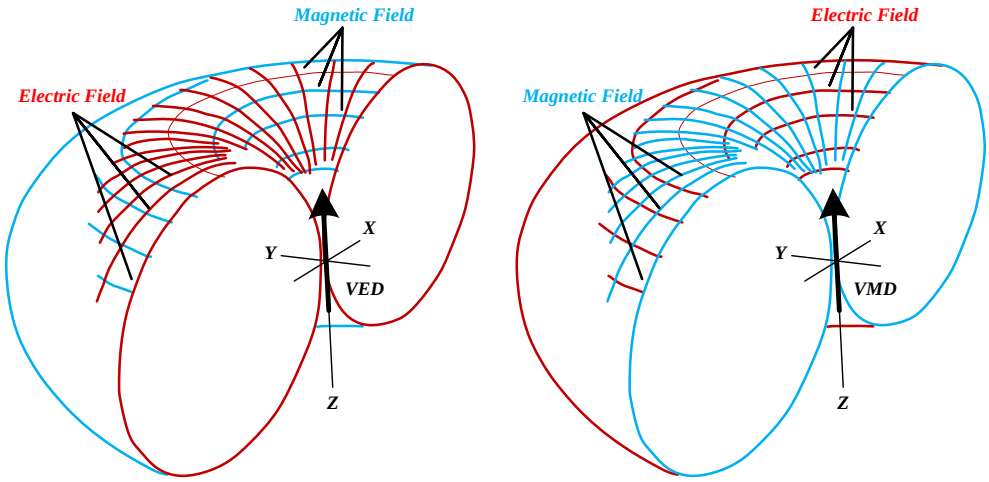

Figure 2-5: The magnetic and electric field patterns from vertical electric (VED) and magnetic (VMD) dipoles. Horizontal current loops strongly couple with the air water interface resulting in a large air wave response. The air wave phenomenon can be minimised by using a vertical electrc dipole.

2.4.4 Seawater conductivity

Seawater constitutes a large portion of the geoelectric model. Determining the correct seawater conductivity is important for both forward modelling and inversion. The conductivity of the fluid varies in the water column and also in the seabed structure itself. Auxiliary instruments record seawater conductivity over the duration of most MCSEM surveys (an example can be seen in Figure 2-6). Sea water varies in resistivity due to temperature, salinity and pressure as described in equation 4.

$$\sigma = 3 + \frac{T}{10} Sm^{-1} \qquad \begin{boxed} \sigma = \text{conductivity of sea water} \\ T = \text{Temperature in degrees C} \end{boxed} \tag{4}$$

Sea water conductivity is around $0.3\Omega \cdot \text{m}$ at typical ocean floor temperatures, it reaches a minimum conductivity of $0.04\Omega \cdot \text{m}$ at $350°\text{C}$. This large variation in conductivity has a significant effect on the bulk resistivity of the formation. Archie's 1942 law can be used to find the saturated formation's true resistivity in $\Omega \cdot \text{m}$ (see equation 5).

$$\text{Archies Law}: \quad F = \frac{R_0}{R_w} = \frac{\phi^m}{a} \qquad S_w^n = \frac{R_0}{R_t}$$

F = Formation factor
R_0 = Formation resistivity when 100% saturated
R_w = Resistivity of fluid
ϕ = Porosity
m = Cementation factor (between 1.3 and 3)
a = Formation constant
S_w = Water saturation

(5)

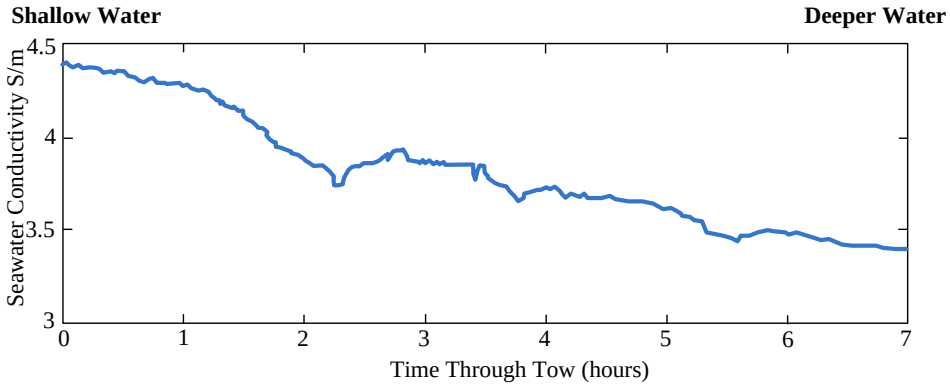

Figure 2-6: Typical seawater conductivity measurement over the duration of a typical MCSEM survey. The conductivity varies over time and position and the recorded data should be incorporated into the geoelectric model for forward modelling or inversion (Reproduced from MacGregor, 2006).

2.4.5 Hydrocarbon saturation and formation resistivity

When dry, reservoir formations extremely resistive. Interstitial saline pore fluid allows the electrical current to flow. Archie's law relates the electrical conductivity of sedimentary rocks with its porosity and brine saturation. Hydrocarbons increase the formation resistivity when it displaces brine from a formation. Hydrocarbon saturation increases the overall formation resistivity. MCSEM measurements can detect the increase in hydrocarbon saturation.

2.4.6 Bathymetry

The marine CSEM method is affected by variations in seafloor bathymetry. The HED transmitter should be towed at a constant height above the receivers, following the shape of the bathymetry. Bathymetry should be taken into account because a seafloor rise can produce the same response as a reservoir and only quantitative interpretation such as inversion may be able to establish the true geoelectric properties (Mehta et al., 2006).

2.5 Multispectral instrumentation

Marine CSEM instrumentation has developed rapidly with ocean bottom receivers reaching higher levels of sensitivity while horizontal electric bipole sources are becoming increasingly powerful. The choice of instrumentation is a significant step in planning because it affects the noise-floor of the survey.

2.5.1 Multi component receivers

Technology during the late 1990s underwent major advancements notably by organisations such as Scripps Institution of Oceanography (Constable et al., 1998). The MCSEM method uses receivers modelled on marine magnetotelluric instrumentation from this period. The receiver records magnetic and electric field time series data. The receivers have a number of recording devices, including a digital magnetic compass/tilt-meter which records the orientation, a timing system which is synchronised pre and post deployment and magnetic and electric sensors recording multiple axial directions. Horizontal electric field receivers are composed of silver-silver chloride electrodes which are between 1 and 10m in length (MacGregor et al., 2006). A highly sensitive vertical arm can be used to measure the vertical field. The magnetic fields are measured by highly sensitive, light weight induction coil magnetometers (Keys, 2003). The typical components which are detected by commercial designs are x and y magnetic and electric field directions. The vertical electric field could also be used for commercial uses. Currently this orientation is not recorded because the vertical electric field dipoles are still too noisy to be used practically.

There are numerous receiver parameters to be considered when choosing the most suitable receivers for the survey (as seen in Table 2-3). Key attributes to consider prior to surveying include the noise floor of the instrument, timing calibration, timing

stability, battery type and energy use, recording capacity, response calibration, navigation and seafloor orientation (MacGregor, 2006). The dynamic range of the instrument is important because there is a large variation in the signal strength. Therefore 24-bit analogue to digital converters with pre-amplifiers enable high resolution data to be recorded at all source-receiver offsets without signal saturation.

The noise level of a receiver affects receiver selection during planning. The main source of electric field receiver noise above 1Hz is caused by amplifier and electrode induced noise rather than ambient noise (Hoversten et al., 2006). There is an inverse relationship between the noise level of electric field receivers and the frequency. For example OHM's EFMALS III, has a noise floor of 1nV/m / $\sqrt{Hz}$ (MacGregor, 2002). In effect, the receiver can detect and resolve smaller amplitudes for higher frequencies. WesternGeco (2008) use receivers that have the capability to resolve values as low as $3\times10^{-15}\,\mathrm{V/Am^2}$ at 1Hz. Deep seafloor environments are typically electrically quiet. Most MCSEM receivers have a noise floor electromagnetically around $10^{-15}\,\mathrm{V/Am^2}$ for electric fields and $4\times10^{-12}\mathrm{T}$ at 1Hz for magnetic fields.

To improve the signal to noise ratio of the receiver, the antenna length can be extended. This voltage is proportional to the receiver dipole length (Flosadóttir, Á et al., 1996). Synchronous stacking can be used to also recover a repetitive signal from the random ambient or instrument noise.

Technology is improving and the limits and features will drastically over next few decades. Hence the features seen in Table 2-3 should only be taken as a guide. In summary the main features to consider when planning a survey are the noise threshold of both the E-Field and B-Field sensors and which electric and magnetic axial directions the device will record.

Receiver Features	Typical Attribute
E-Field Noise Floor	$<10^{-15}$V/Am^2 (at 1Hz)
B-Field Noise Floor	$<10^{-6}$nT^2/Hz (at 0.1Hz)
Timing Stability	<1 in 10^6 intervals result in drift (<1ms/day)
Battery Capacity	6-18 days continuous logging
Storage Capacity	>1Gb
Receiver Length	1-10m
Electric Field Receivers	E_x(Inline) and E_y(Broadside)
Magnetic Field Receivers	H_x(Inline)
Sampling Frequency	128Hz
Dynamic Range	24 bit
Sensitivity	Around 2 pV/count
Depth Rating	3000-6000m
Other Recording Devices	Temperature sensor, magnetic compass, inclinometer, Horizontal magnetic field channels

Table 2-3: Typical receiver features to consider when planning a MCSEM survey. These values have been taken from two commercial contractors, OHM's EFMALS III and WesternGeco receivers. The main attributes to consider when choosing the correct receiver when planning a survey are the electric and magnetic field receivers, their associated instrument noise and axial direction. (Reproduced from WesternGeco, 2008 and OHM Surveys, 2008)

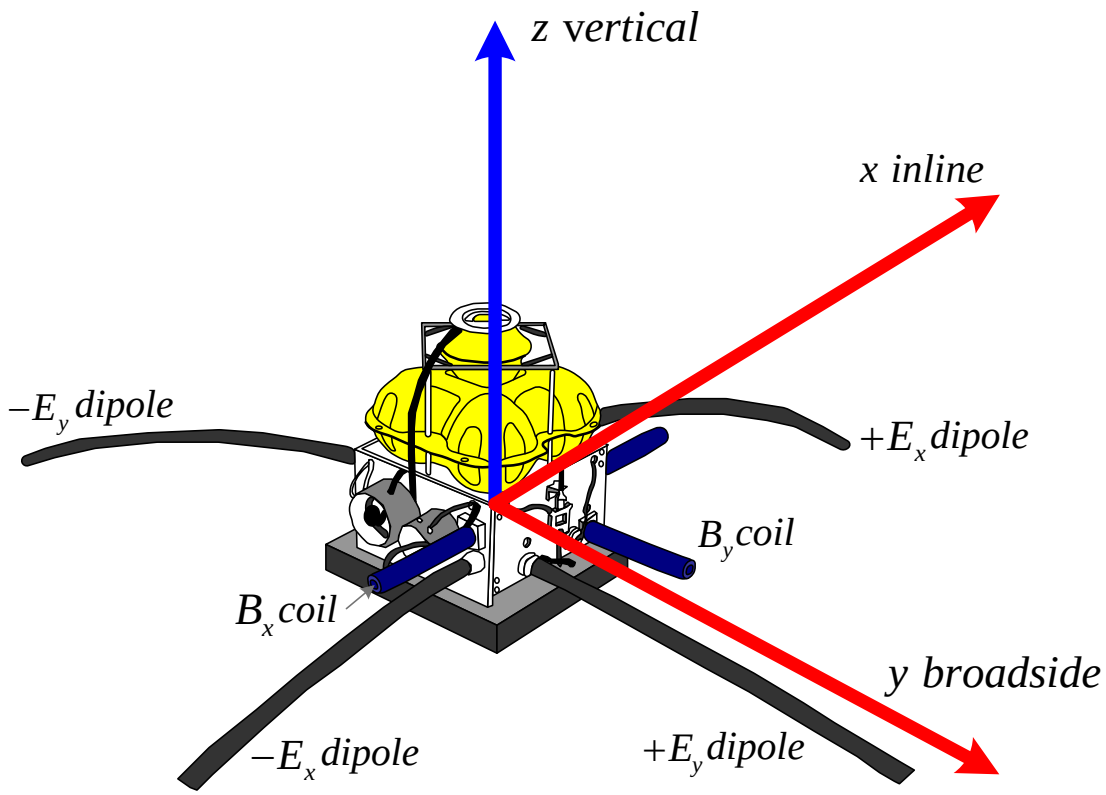

Figure 2-7: Diagram of a typical marine CSEM multicomponent receiver. The receiver is the Scripps Institute of Oceanography Mark III design only records inline magnetic and electric fields and broadside electric field (Constable et al., 1998; reproduced from Keys, 2003)

2.5.2 Transmitter

The marine controlled source electromagnetic method uses a horizontal electric dipole as a transmitter. The transmitter consists of two electrodes separated between 100-300m. The Transmitter is towed 25-50m above the seabed at a speed of 1.5 to 2.0 knots (WesternGeco, 2008). The transmitter uses a powerful source generates around 1000A. There are numerous commercially available transmitters that can be selected prior to surveying.

Important attributes to consider when selecting a good transmitter include the peak output dipole moment and the stability of the output waveform. Waveform polarity transitions have a temperature-dependent latency (1-2μs) that decreases as the transmitter temperature rises and stabilises (WesternGeco, 2008). The output waveform's phase must be stable to around 1 part in 10^8 (1ms/day) otherwise the received waveform will be artificially out of phase with the transmitted waveform. Phase is controlled by GPS and consistently monitored during the survey.

The dipole moment is the length of the electrodes multiplied by the transmitted current. If the dipole moment is doubled the amplitude recorded at the receiver are also doubled.

The source is deep-towed to optimise signal coupling with the sea floor and to reduce the conductive losses. Heights of around 25-50m are chosen but can be varied in accordance to bathymetry, ocean conditions and the coupling required. The altitude of the transmitter is constantly monitored by using an altimeter on the source. The tow speed of the transmitter should be considered prior to surveying as it affects the quality of the received data. A receiver records 50 transmitter cycles every 100m for

a given frequency of 0.5Hz and a towing speed of 1m/s. Stacking reduces the noise by a $1/\sqrt{N}$ times and improves with slower towing speeds (Hoversten et al., 2006).

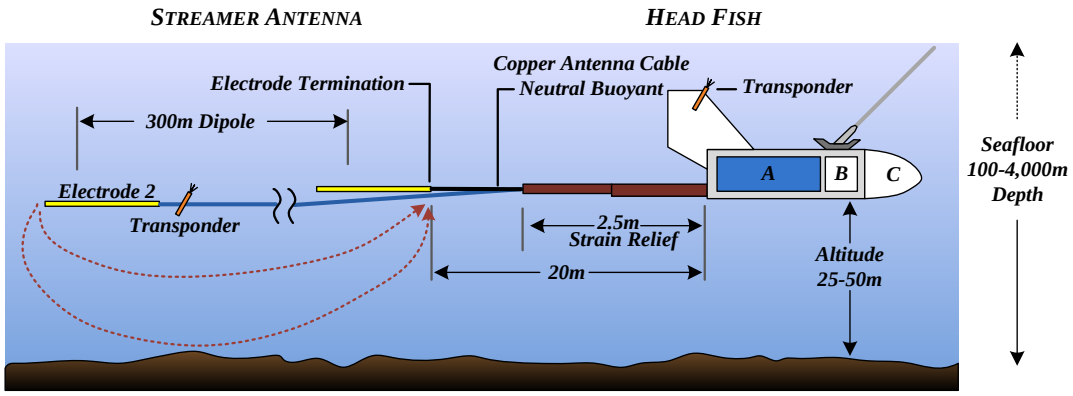

A) ORCA transmitter power section
B) Telemetry and signal conditioning
C) Instrument suite: Altimeter, pressure, compass DVL/MRU, SV and CTD

Figure 2-8: Typical schematic of a marine CSEM transmitter and HED (Reproduced from WesternGeco, 2008).

2.6 The use of forward modelling for survey planning

Forward modelling of a prospects geoelectric response prior to surveying fulfils several purposes.

- To optimise transmission parameters to reduce noise and maximise resolution
- Design transmitter-receiver geometries to enhance the response of the target reservoir

2.6.1 Optimisation of transmitter receiver geometry

Transmitter receiver geometry affects the response detected from the prospective hydrocarbon. For example, inline electric field receivers detect a larger electric field component whilst the magnetic field mainly influences the broadside geometry. There is a link between transmitter-receiver offsets and depth of investigation. Large transmitter-receiver offsets are sensitive to deep targets, while short offsets are responsive near surface resistivity variations.

Inductive effects dominate the broadside geometry while galvanic effects are much stronger in the inline receiver geometry. Errors due to azimuthal scattering (associated with surface heterogeneities) reduces with the increase in the number of receivers in accordance with $\frac{1}{\sqrt{n}}$, where n is the number of data with independent transmitter and receiver locations.

2.6.2 Survey Design Options

The survey design includes both receiver and transmitter positions. This geometry determines how well the target can be detected and characterised. There are a number of options available to MCSEM practitioners ranging from simple 1D lines to a multi-azimuthal survey which ‘illuminates’ the target from all directions as seen

in Figure 2-9. The type of survey design depends on the objective of the survey. (McGregor, 2006). For example reconnaissance surveys identify resistivity variations on a regional scale, detection surveys need to identify commercial resistive targets and appraisals require a more detail constraint of an identified prospect. The purpose of the survey determines the receiver and transmitter line spacing.

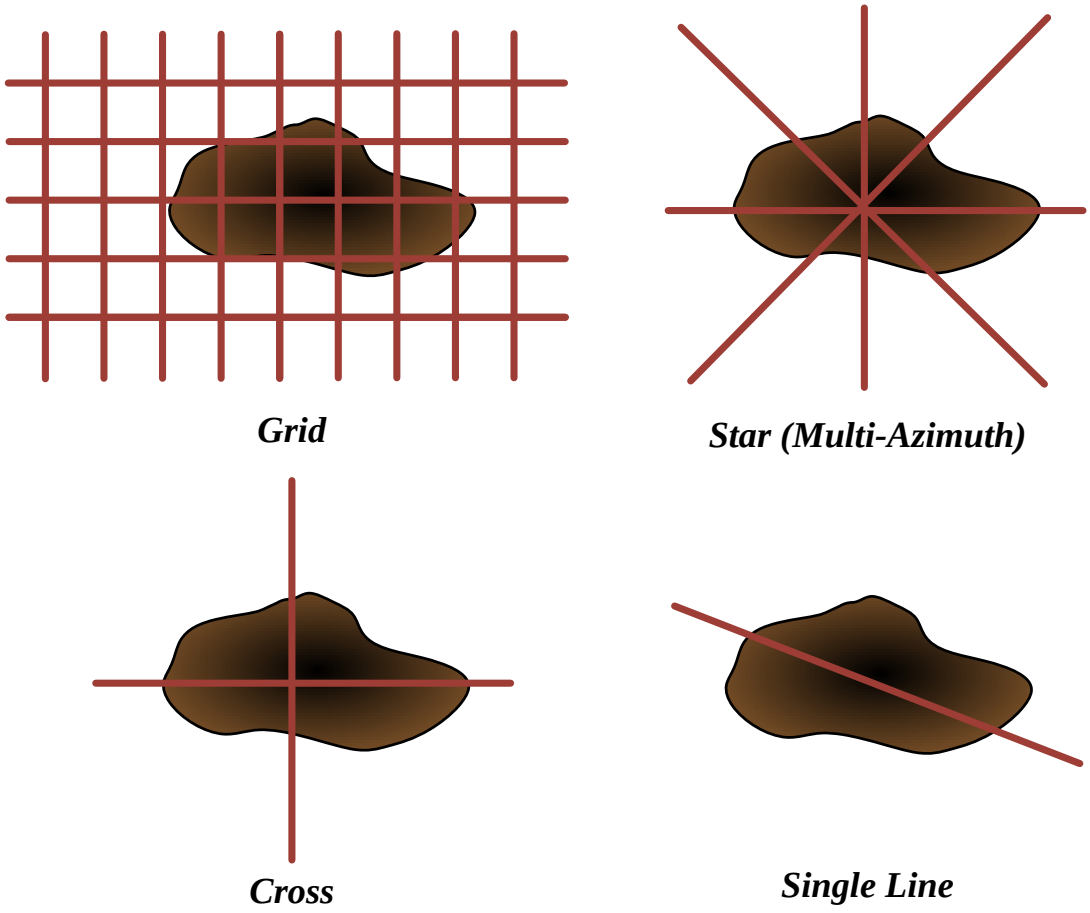

Figure 2-9: MCSEM survey layouts of transmitter and receiver lines. The purpose of the survey determines the survey layout, including the transmitter and receiver positions. Each layout has its advantages, denser transmitter-receiver grids generally have higher relative responses, however the operations are more expensive to conduct.

2.7 Visualising the Data

Analysis can be performed on a variety of modelled datasets. Visualising MCSEM data for analysis is complicated because of the infinite possibilities of transmitter-receiver arrangements, transmission frequencies and theoretical geoelectric models available for selection. The process of planning a survey becomes even more convoluted when the behaviour of the amplitude and phase of the axial (x, y, z) electric and magnetic fields needs to be visualised and understood prior the execution of the survey. The visualisation techniques that can assist in displaying the data in an intuitive format for analysis include profiles, grids, vectors, 3D shapes (polygons), scalar planes (3D Grids), isosurfaces and streamlines and streamtubes.

2.7.1 1D Profiles

Profiles are used extensively in MCSEM interpretation. They are used to describe one dimensional datasets where only one variable is being tested. For example a popular example of using profiles in MCSEM include plotting electric, magnetic field amplitude or phase against offset (for example see MacGregor et al., 2001; Phillips, 2007). Surveys are being increasingly performed in 3D, profiles do not offer the capability view 3D volumes of data, therefore other visualisation techniques need to be utilised.

2.7.2 2D Grids and contours

Grids and 2D contours can show scalar data on a 2D plane. Common uses of grids and contours in MCSEM include displaying amplitude, phase or normalised responses versus offsets. Grids with multiple contour overlays are often cluttered and convoluted makes interpretation difficult.

2.7.3 Isosurfaces

Isosurfaces represent a surface of scalar equipotential value and is the 3D contour. Much like 2D contours, multiple isosurfaces can clutter a visualisation. While 2D contours can represent 2 variables and a scalar while isosurfaces can test three variables and a scalar.

2.7.4 Vector Glyphs

Vector glyphs represent a vector in both magnitude and direction. In MCSEM they can represent the direction of the EM field both in amplitude in time. Using vector glyphs to display field paths is difficult. Vector glyphs only visualise the field direction at a point in time.

2.7.5 Polygons

Polygons are 3D sets of points to make shapes or planes. Polygons in CSEM are currently used to represent the 3D geoelectric model. The geoelectric unit or body can be represented geometrically and by a single scalar. The geometry is represented by the polygon while a scalar value (or colour) represents the resistivity. Currently anisotropy is much more difficult in a single image because anisotropy is a resistivity tensor rather than a scalar.

2.7.6 Streamlines

Used to show flux lines of electric and magnetic fields spatially and in time. Phase is contained in the streamline orientation and amplitude through either streamtube thickness or colour. Streamlines can be used to help understand the behaviour of EM fields also they can be used to orient receivers and to determine which directions to record. Cluttering is often a problem when interpreting streamlines, as only one or two fields can be shown at a given time (i.e. Magnetic and electric or scattered and total fields etc...)

3 Software design for MCSEM survey planning

A program had to be created to interface with 3D forward modelling algorithms. The software needed to import, process and export 4D forward modelled data. The developed package was consequently named CSEMoMatic because less time should be spent manipulating with data and more time spent on interpretation and survey planning. Use of the program should be easy and require minimal programming knowledge.

3.1 Overall Software Design Process

The Java programming language (Java, 2008) was chosen because of its object oriented structure. Data structures were designed for each component of a survey. For example receivers, transmitter bipoles, 1D layers and 3D bodies as individual data structures. CSEMoMatic was programmed using Java version SDK 1.6 using the eclipse programming platform. The program developed over a number of stages. Firstly the program implemented the creation survey designs over a 3D body in a 1D halfspace. Stage 2 formed data structures to handle and represent the modelled data. Lastly export formats were added so that various programs could use the output from the program. Crucial export file formats included VTK (VTK, 2008), binary volumes, CSV, ASCII and Matlab m files.

3.2 User interaction

4 steps were needed to create a survey design over a given geoelectric model.

1) Creating the geoelectric model for both 1D layering and 3D scatterers. The water column, seabed layering, and 3D scattering bodies were defined in terms of resistivity and geometry at this stage.

2) Specifying the receiver geometry. This involved entering east, north and depth positions for a receiver line, grid or theoretical volume.

3) Defining transmitter position, bipole length and transmitter orientation. East, north, inline and vertically oriented transmitters could be selected.

4) Specifying the transmitted waveform. Waveforms were characterised in terms of frequency and amplitude. The amplitude is computed automatically by normalising a 1 Amp current with the HED length.

3.3 Export Format Support

CSEMoMatic supports a number of file formats. Export functions needed to be versatile enough to sort and process large quantities of modelled data. Forward modelled surveys contain both electric and magnetic fields, each field contained a total, layered, scattered response and normalised response. These responses could then be viewed in the time domain or frequency domain for all axial directions. The number of combinations of these responses complicates how the export process was structured. Exporting files consisted of two steps:

1) Define export options. The options included selecting which electric and magnetic components to be exported, export directory and filename, also the number of time slices for a given frequency and polarisation ellipse size could be specified if needed.

2) Selecting export format. Once the export format is selected, data is sorted according to the export options.

Planning surveys requires the data to be visualised in a variety of ways. To facilitate this, a number of export formats were included. CSEMoMatic's design allows users

to export into formats most third party software packages support. The following formats were included because they allowed data to be represented in a variety of external software suites.

1) The ASCII and CSV formats were included because of their versatility.

2) Matlab m files were included to generate profiles of amplitude and phase versus offset. Profiles in this format could be visualised with both ease and speed.

3) The binary RAW file format was added as an export function because it is required for various visualisation packages. Freely available software packages such as ImageJ (ImageJ, 2008) and Drishti (Drishti, 2008) support this file format.

4) The VTK file format (VTK, 008) was chosen to be the main export format because MayaVi (MayaVi, 2008), a freely available 4D visualisation software package, contained the most current scientific visualisation techniques and processes.

To make the export window more user friendly rollover buttons were used such that each export format is explained in the bottom picture window prior to export.

Figure 3-1 : The layout of the CSEMoMatic Software package. The numbered boxes represent the sequential stages to forward modelling such that the data can be used for planning the survey.

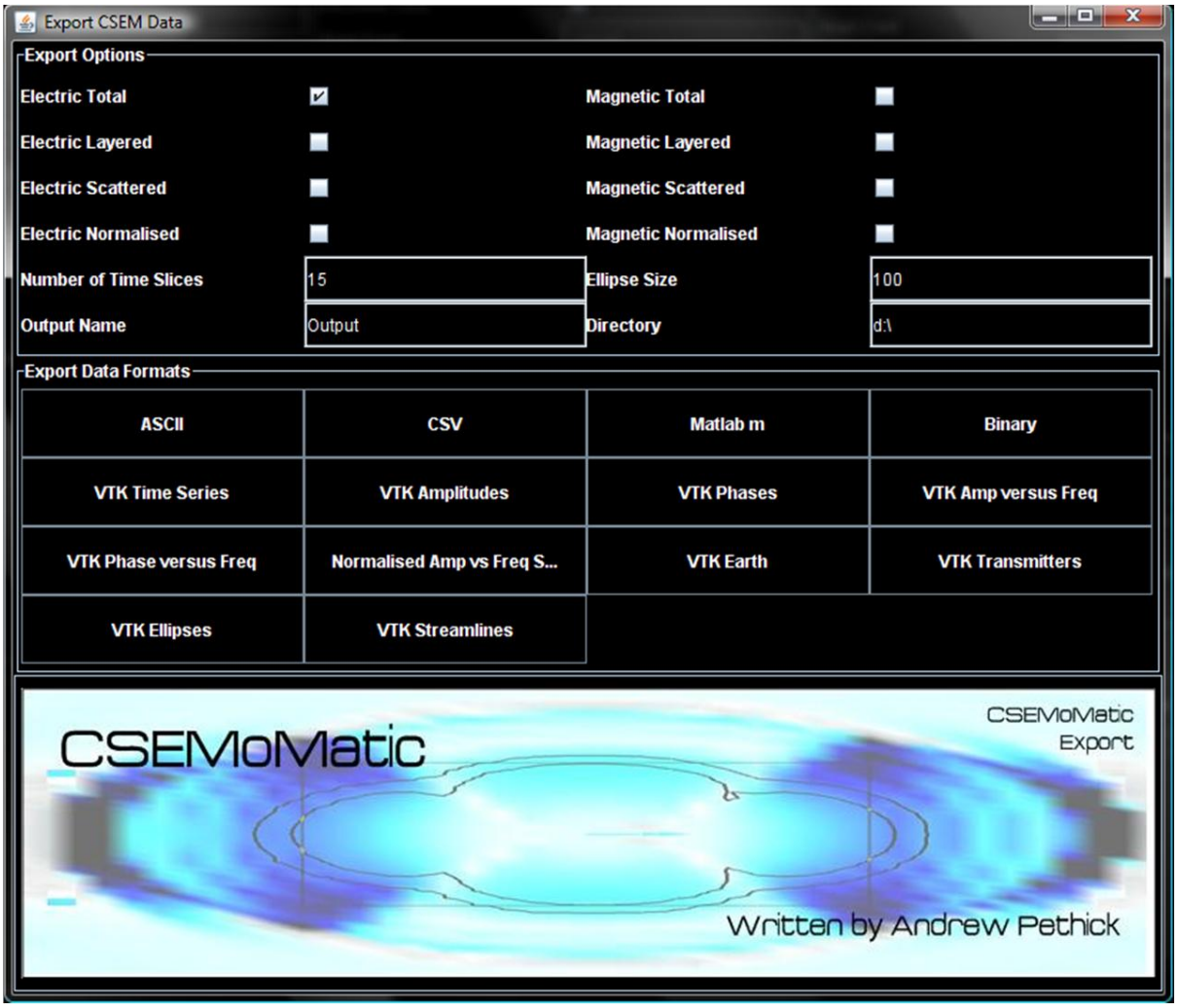

Figure 3-2: The export frame of CSEMoMatic. CSEM planning software should cater a multitude of export formats and for all different fields, electric, magnetic, total, layered, scattered or even normalised fields. In addition to export the fields, the transmitter locations and geoelectric model should be able to be exported. This example has both ASCII and binary formats, primarily the main export format is VTK form because of its versatility in visualising the EH fields.

3.4 Advantages and Pitfalls of the Software Design for CSEM Planning

A number of conclusions can be drawn from the development of CSEMoMatic. CSEMoMatic did not adequately allow users to interactively view and modify survey designs. An interactive design would graphically display the position of the bodies, receivers and transmitters. CSEMoMatic was mainly text based, this made error checking difficult and often tedious. CSEMoMatic was not meant to be a graphical and visualisation software package but an in between stage so users would not be limited to a single visualisation package. The effort into the design of the program allowed additional forward modelling algorithms to be easily integratable into the program. MCSEM survey planning and forward modelling software should be structured and intuitive for novices to use whilst offering advanced options for experts. The structured and step based interface was beneficial because the user was aware of what details were needed at each step. Lastly software created for MCSEM survey design should include a variety of export formats; even though the export process is not optimal, the variety of formats didn't limit the user to one specific software package.

4 Planning the marine controlled source electromagnetic method

Planning 3D marine CSEM surveys may seem daunting because of the large number of variables that need to be addressed. The planning process can be simplified by visualising forward modelled data in the correct manner. Several variables can be visualised simultaneously allowing interpretation to be performed quickly and with a small number of tests. The planning stage can be broken into several steps. For the purpose of outlining this process a simple geoelectric model was used.

4.1 Planning methodology

To demonstrate the following planning methodology, a simple example with a 3D rectangular hydrocarbon in a 1D halfspace was used. The model consists of three layers, an air interface, a 1500m water and a 1.5Ωm sedimentary halfspace.

The proposed planning methodology has been broken into four main steps.

1) Create the geoelectric model
2) Initialising modelling parameters
3) Optimising survey parameters
4) Evaluate chosen designs.

Each stage consists of a number of smaller steps (as seen in Figure 4-2). Firstly a reasonable projection must be selected. The projection could for example be local or in latitudes and longitudes. In the non-specific simple example a local projection was used. The water depth or bathymetry must be modelled accurately because it influences the forward modelled responses (Phillips, 2007). Seismic stratigraphy and

hydrocarbon reservoirs also have to be defined in both resistivity and thickness. If anisotropy is present, it also has to be defined at this stage.

Survey parameters need to be initialised or known prior to forward modelling. These include transmitter tow height and HED length. The tow height is limited by the depth of the water column; ideally the transmitter would be towed inside the reservoir. Practicality only allows the HED to towed 25-50m above the seafloor. Forward modelling can be time consuming so it is necessary to determine the maximum bounds and resolution required for further modelling. Once this offset has been calculated an optimal base frequency can be found by normalising the total field response with the background response. This optimal frequency can then be used to design the transmitted waveform

Once the initial parameters have been established, receiver positions and recorded directions, transmission frequencies and transmitter line locations need to optimised. The addition of a 3D body results in a computationally expensive process. Therefore the maximum transmitter receiver offset to detect the scattering response should be found for future modelling. The effectiveness of receiver and transmitter positions can then be evaluated either by using polarisation ellipses, streamlines or normalised plots to maximise the scattered response. Individual parameters can also be optimised by using geometric response indicators and sensitivity grids.

There are a number of survey configurations that can be executed. Each survey should be independently evaluated by using three steps, establishing the maximum sensitivity to the survey design, estimating the risk that the configuration may produce a false negative to detect a hydrocarbon and finally estimating the monetary cost to deploy receivers and survey the area.

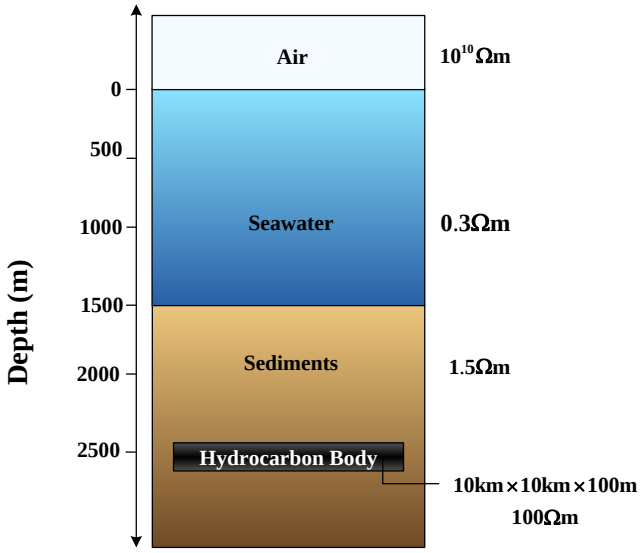

Figure 4-1: The geoelectric model used to demonstrate the planning methodology.

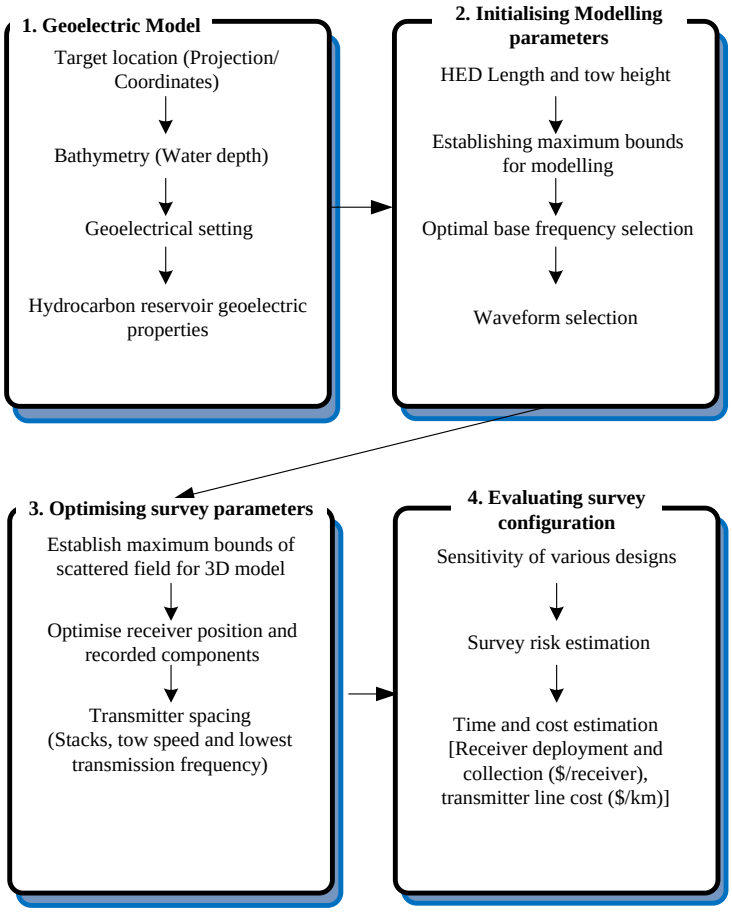

Figure 4-2 : The proposed CSEM Planning Methodology.

4.2 Designing the geoelectric model

The geoelectric model defines the area of investigation in terms of resistivity distribution (i.e. layering). A number of 3D polygons can be used to represent a geoelectric model. It is also to created its response can be modelled for various survey configurations. The geoelectric model can be based from either downhole resistivity information or approximated through seismic interpretation. Larger conductive structures can also be approximated by MT investigations.

Hydrocarbon reservoirs should be defined in lateral and vertical extents, basic morphology and resistivity. The MCSEM method cannot detect deep complex geometries. Therefore structures should be approximated to more regular geometric shapes to speed up the modelling process. Geometry should be preserved for shallow targets. 3D body should be used, even for a 2D survey.

Field responses can be visualised inside the geoelectric volume, allowing geophysicists to interactively view interactions between EM waves and geoelectric structures. A stacked seismic model can also be shown collectively with the geoelectric model. The field the maximum east-west, north-south and depth extents should be roughly estimated with the skin equation from the lowest transmission frequency and average resistivity. A survey area with the lateral extents of $40\text{km} \times 40\text{km}$ was used. The model was created with 3 layers, water ($0.3\Omega \cdot \text{m}$ at 1500m) and sediments halfspace with a resistivity of $1.5\Omega \cdot \text{m}$ and an effectively infinitely resistive air interface. A thin isotropic resistive hydrocarbon body with the dimensions of $10\text{km} \times 10\text{km} \times 100\text{m}$ at $100\Omega \cdot \text{m}$ was also added to the model. The resulting model can be seen in Figure 4-3.

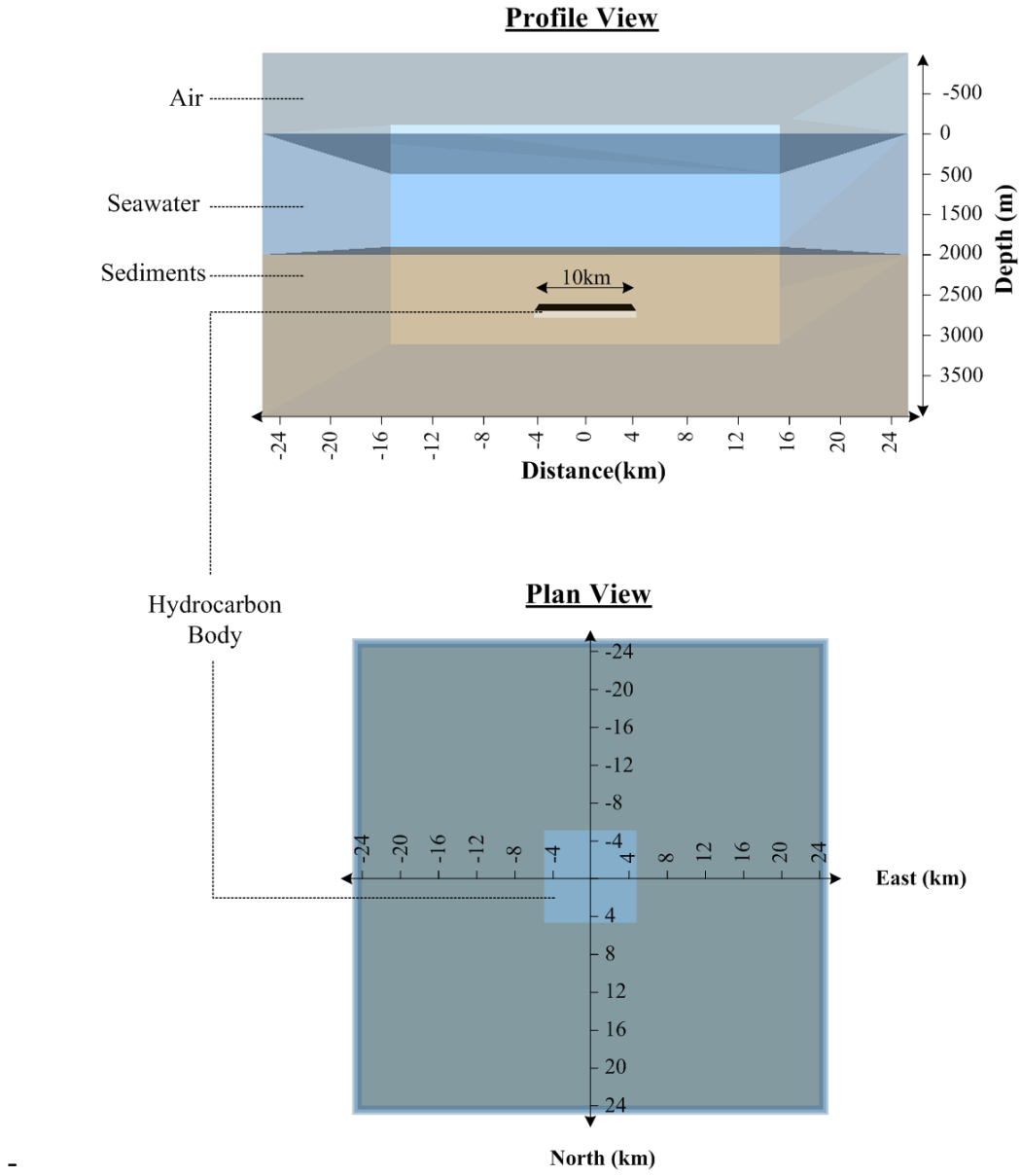

Figure 4-3: 3D Geoelectric Model Design Visualised using polydata in MayaVi.

4.3 Initialising Model Parameters

Forward modelling can be expensive in terms of modelling time and storage space. It is therefore necessary to quickly establish the maximum bounds and resolution required for further modelling. A 1D model without the hydrocarbon body was used (seen in Figure 4-1) because surveys over a 1D layered earth are quickly calculated.

The maximum offset is considered to be the maximum transmitter receiver separation that detects and EM response. The limit of for x, y and z should be calculated individually because each direction is independently measured. A threshold was considered to be 10^{-15}V/Am^2 for electric fields and 4×10^{-14}T for magnetic fields over all frequencies.

To establish the maximum bounds of the simple model, a highly resolved 25×25km grid of ocean bottom receivers was created. At near offsets (less than 2000m from the transmitter) receivers were placed 150m apart whilst at further offsets a spacing of 250m was used. A 300m east-west aligned transmitter was then placed at (0, 0).

A single transmitter position was then forward modelled over 10 frequencies ranging from 0.01 to 10Hz. The electric and magnetic field responses were then exported as a volume where x, y and z is represented by inline, crossline and log frequency respectively. Several visualisation techniques were then applied to the volume to obtain detection limit and the amplitude distribution. Amplitudes were represented by 3D grids and the noise floor was then represented by an isosurface (3D contour). Figure 4-4 demonstrates that this 3D representation is sufficient. The maximum detectable offsets of E_x decreases with increasing frequency. At 0.05Hz the inline offset is 21km whilst broadside it is at 25km. At high frequencies and at low amplitudes the algorithm becomes unstable, resulting in ringing in the data at

amplitudes smaller than 10^{-17}V/Am^2 well beyond the detectable limit. A denser grid of receivers at near offsets at high frequencies is needed to resolve the position of the noise floor.

Inline, crossline, plan and oblique slices to be easily produced by using these . Inline, broadside and plan views provide the clearest view of the noise limit of the model. Figure 4-5 shows a plan slice taken at 0.1Hz. This plan provides information about the noisefloor. It also shows the pattern of the E_x field. A low amplitude zone exists 30^o radially from the transmitter. The placement of receivers should be limited in this zone if E_x is only used. E_y receivers can detect a response in this E_x low amplitude region, but the placement of E_y should be limited in the inline and broadside regions as seen in Figure 4-7. Slices of inline and broadside grids (Figure 4-6) were obtained from the 3D model. The slices of frequency versus offset show the drop-off of the transmitter amplitude with frequency. The detection limit, represented by the white dotted line, is the position at which receivers fail to detect any signals. For example at 10Hz signals can be detected up to 3km inline and broadside from the source while, at 0.1Hz receivers can be effective with 18km broadside and 15.5km inline offsets.

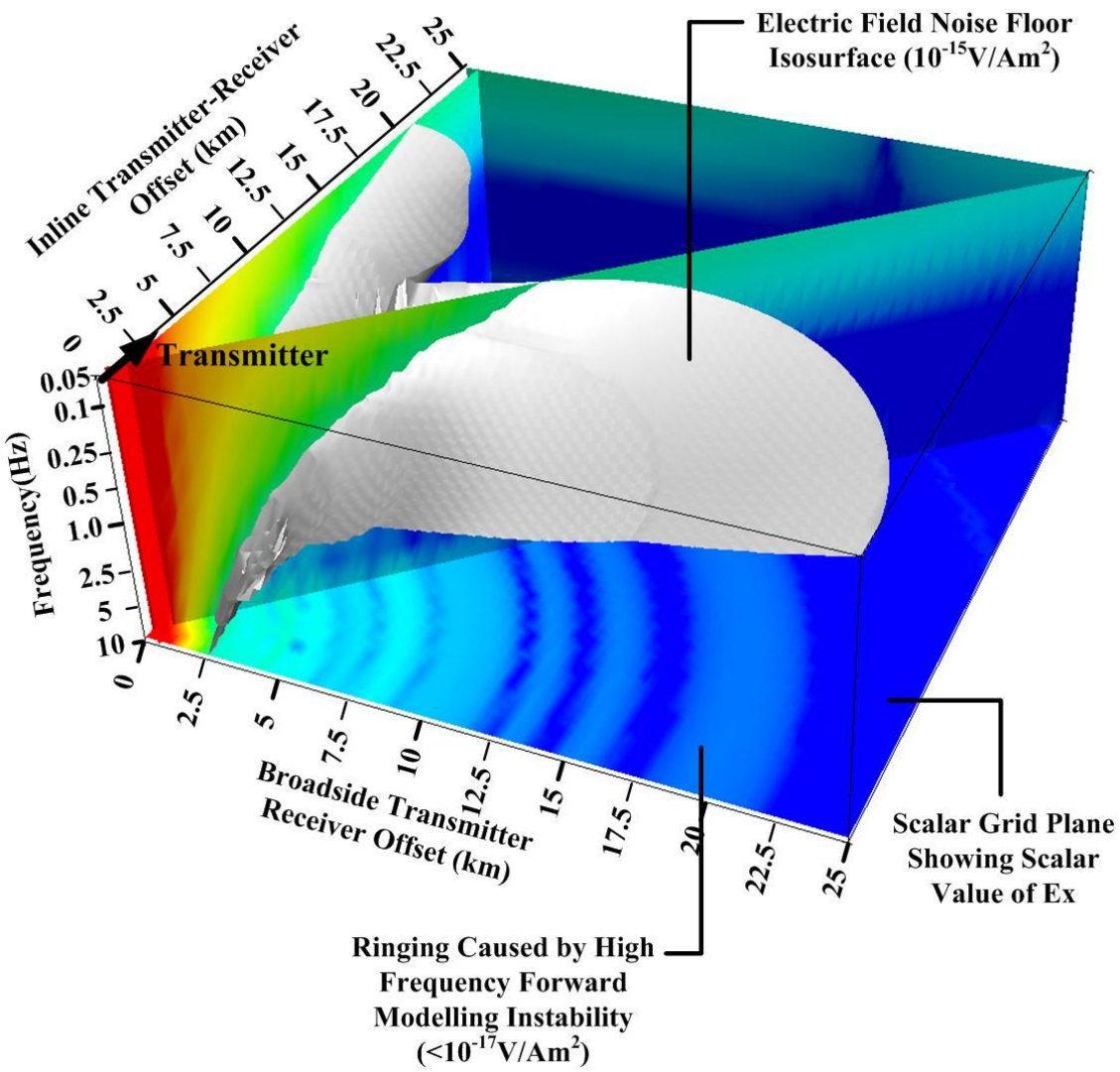

Figure 4-4: 3D representation of the detection limited and recorded signal for seafloor receivers at several transmitted frequencies. This representation shows that the noise floor broadside is 25km and the inline noise floor is 21km at 0.05Hz. This representation can also show numerical errors seen as ringing in the data at high frequencies.

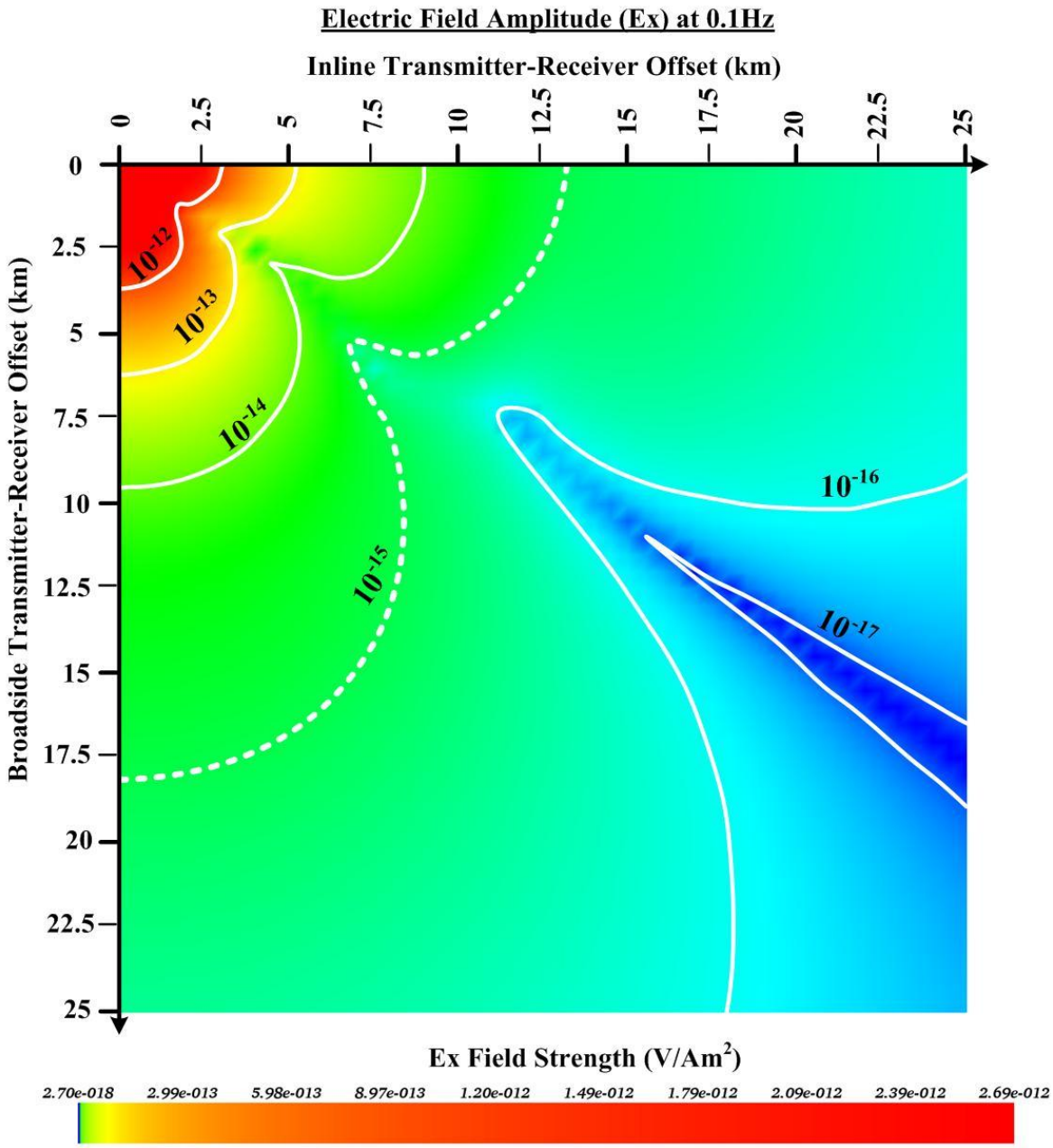

Figure 4-5: The x-component Electric Field Amplitude at a 0.1Hz transmission frequency versus offset from the transmitter located at point (0,0). The detection limit (represented by the white dotted line) is the point at which receivers fail to detect any signals. To detect the halfspace response with a fundamental transmission frequency of 0.1Hz Ex receivers can be placed up to inline 13km away from the transmitter and up to 18km broadside. It should be noted that at 30° radially from the source a low amplitude zone exists and the placement of receivers should be limited in this zone if Ex is only used.

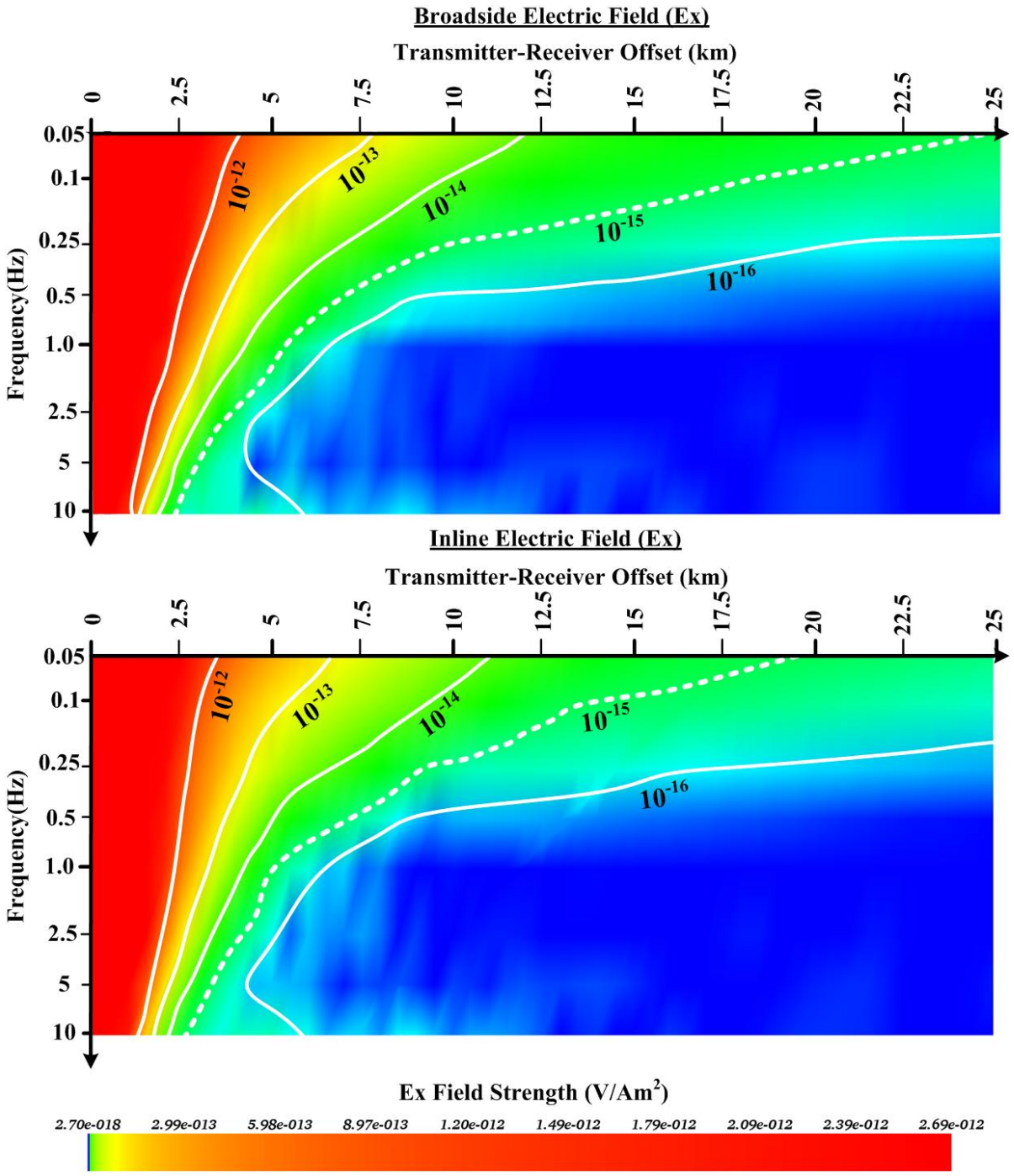

Figure 4-6: Modelled x-component electric field recorded by seafloor receivers versus frequency for both broadside(top) and inline(bottom) offsets. High frequency transmitted signals are limited by distance that they can travel. At 10Hz signals can be detected up to 3km inline and broadside from the source while at 0.1Hz receivers can be effective with 18km broadside and 15.5km inline offsets.

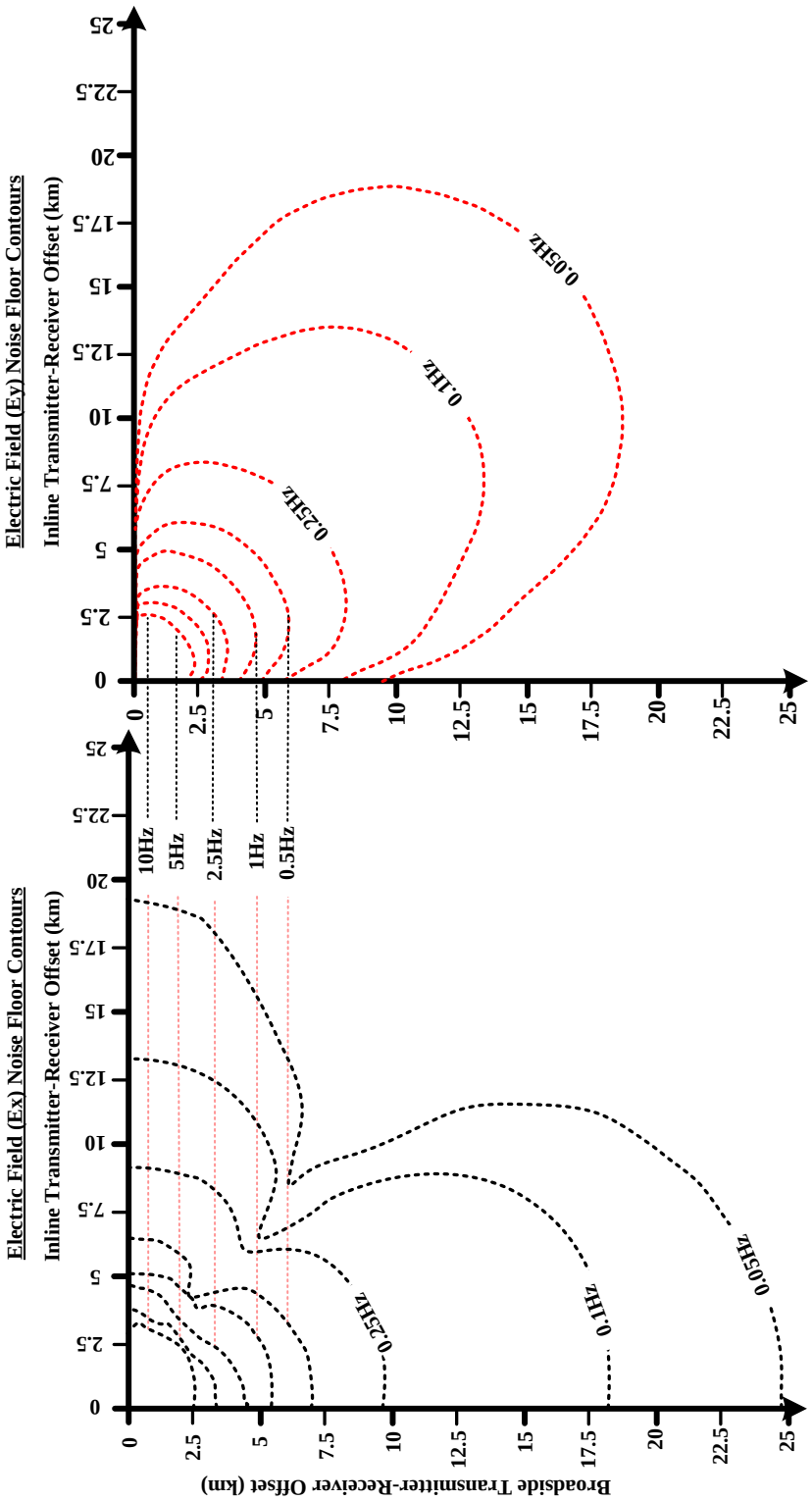

Figure 4-7: Modelled noise floor contours of both Ex and Ey fields at several operating frequencies. The halfspace response can best be detected radially by Ey and inline and broadside by Ex signals. Therefore the maximum transmitter receiver offset should be at 25km at 0.05Hz.

Representing the amplitudes in a 3D volume by several grid planes, isosurface of the noise floor and a glyph representing the transmitter position and orientation was found to be the best way to visualise the dataset for multiple frequencies. This was because the noise floor of any frequency for any direction could be determined.

The contours of the noise floors of both E_x and E_y are dissimilar. The halfspace response can best be detected radially by E_y and inline and broadside by E_x receiver components. This is useful because for a set array of receivers multiple transmission positions can be used effectively. For the given survey design receivers can be position 25 km away from the source to maximise the depth of investigation.

4.4 Optimising survey parameters

4.4.1 Optimising survey parameters using polarisation ellipses

The purpose of polarisation ellipses is to observe the range of amplitudes and phase for magnetic and electric scattered and total fields. Polarisation ellipses represent the complete cycle of the field at a specific receiver position. To create polarisation ellipses a complete time series must be computed from the amplitude and phase by using the transmitter waveform, in this case a sinusoidal function, for all Cartesian directions (E_x, E_y, E_z, H_x, H_y and H_z). The amplitude for a given time can be computed by,

$$y_t = A\sin\left(2\pi ft + \phi\right) \qquad \boxed{\begin{array}{l} A = \sqrt{\mathrm{Re}^2 + \mathrm{Im}^2} \\ \phi = \mathrm{atan2}\left(\dfrac{\mathrm{Im}}{\mathrm{Re}}\right) Rad \\ f = Frequency\left(Hz\right) \\ t = time\left(s\right) \end{array}}$$

As seen in Figure 4-8 the completed array of amplitude over the whole cycle forms the points of an ellipse. This ellipse is best represented by a polygon. Both electric

and magnetic field ellipses with its corresponding axis can be displayed simultaneously in 3D (see Figure 4-9). This representation can be used to establish the directions of maximum amplitude and can be used to infer the path of electric and magnetic fields.

Polarisation ellipses contain information regarding the phase for each of the components.

Figure 4-11 shows a simplified version of the electric field polarisation ellipses. The x-z plane is shown which assists in placing x and z receivers. The representation of the layered and scattered responses contrasts the polarisation of the fields. There appears to be a large contrast in direction at near offsets from the transmitter. At far offsets the scattered response is similar to that of the total field until 7km offset.

The information then can be used to place receivers and determine what directions to record. For example at the ocean bottom fields travel at around 45^{o} from the horizontal, therefore both x and z directions would be equally coupled. At 8-12m there appears to be a polarisation change due to the hydrocarbon body.

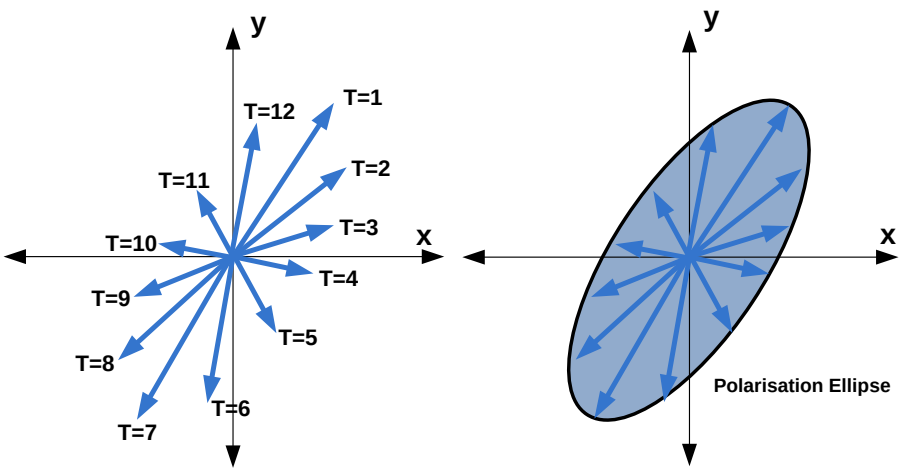

Figure 4-8: Formulation of polarisation ellipses. Electromagnetic field vectors vary in amplitude over time. The complete elliptical rotation of the field can be summarised in a polygon shape (As seen by the right shape. Therefore polarisation ellipse representation contains amplitude, and phase and polarisation directions.

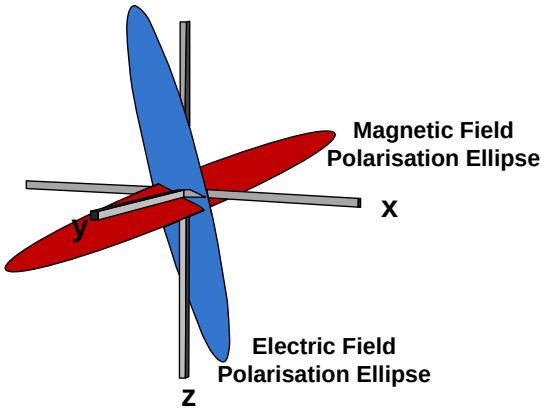

Figure 4-9 : Example of 3D magnetic and electric polarisation ellipses. Polarisation can be used to contrast electric and magnetic fields or show the differences in attributes of the scattered, total and layered responses.

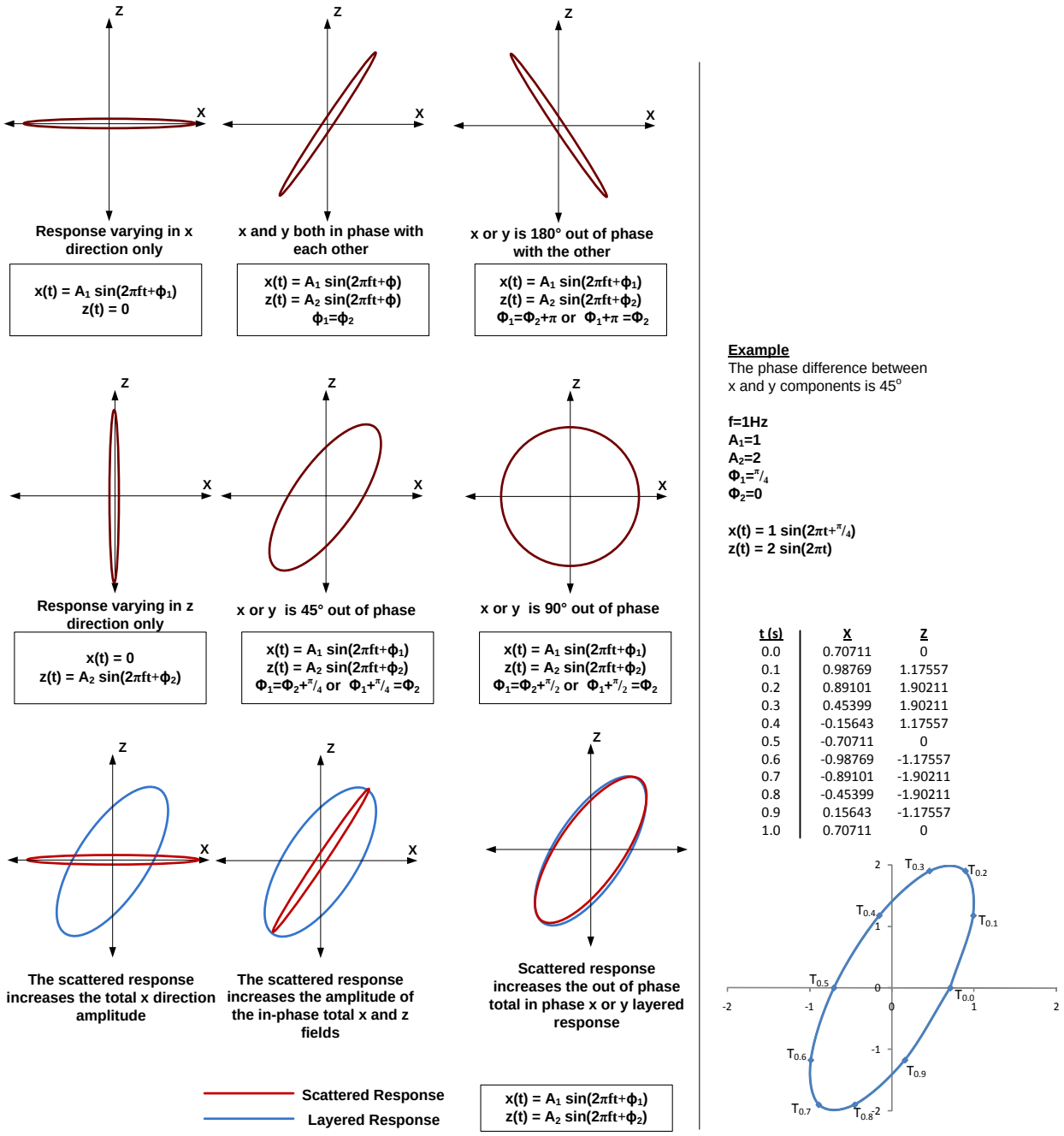

Figure 4-10: Interpretation guide of polarisation ellipses. The motion of an EM field vector can be expressed by $A\sin(\omega t+\phi)$. The amplitude (A) controls the amplitude of the polarised ellipse. The relative phase (ϕ) is the difference in phase between the receiver and transmitter. ϕ controls the angle in which it polarises.

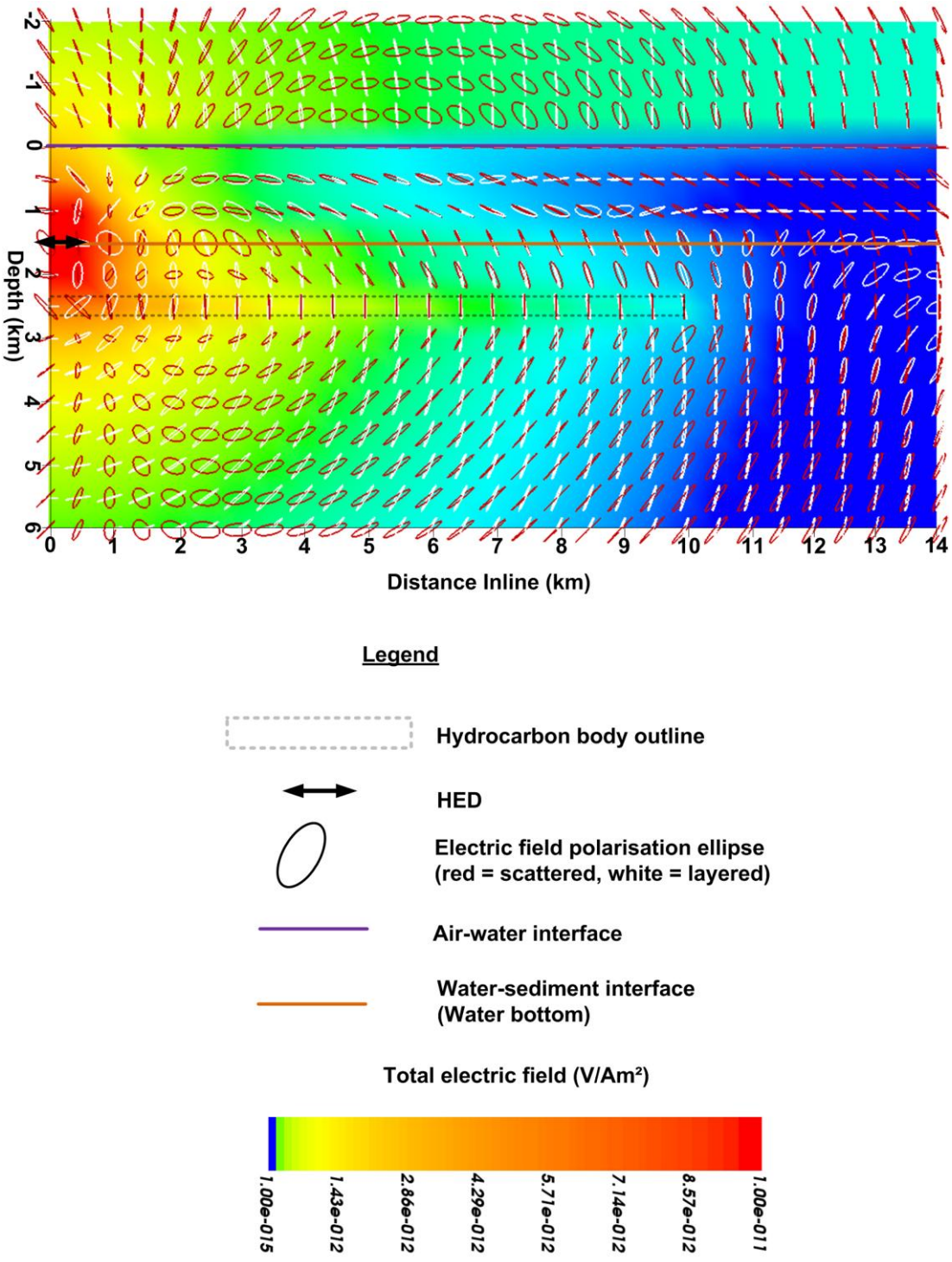

Figure 4-11: Applications of polarisation ellipses to optimise receiver positions. The above Figure shows an inline cross-section displaying total and scattered polarisation ellipses. Deviation between the scattered and total responses signifies a variation in polarity of the signal. The best position to place a receiver to detect a change in direction of the signal is between 8-12km

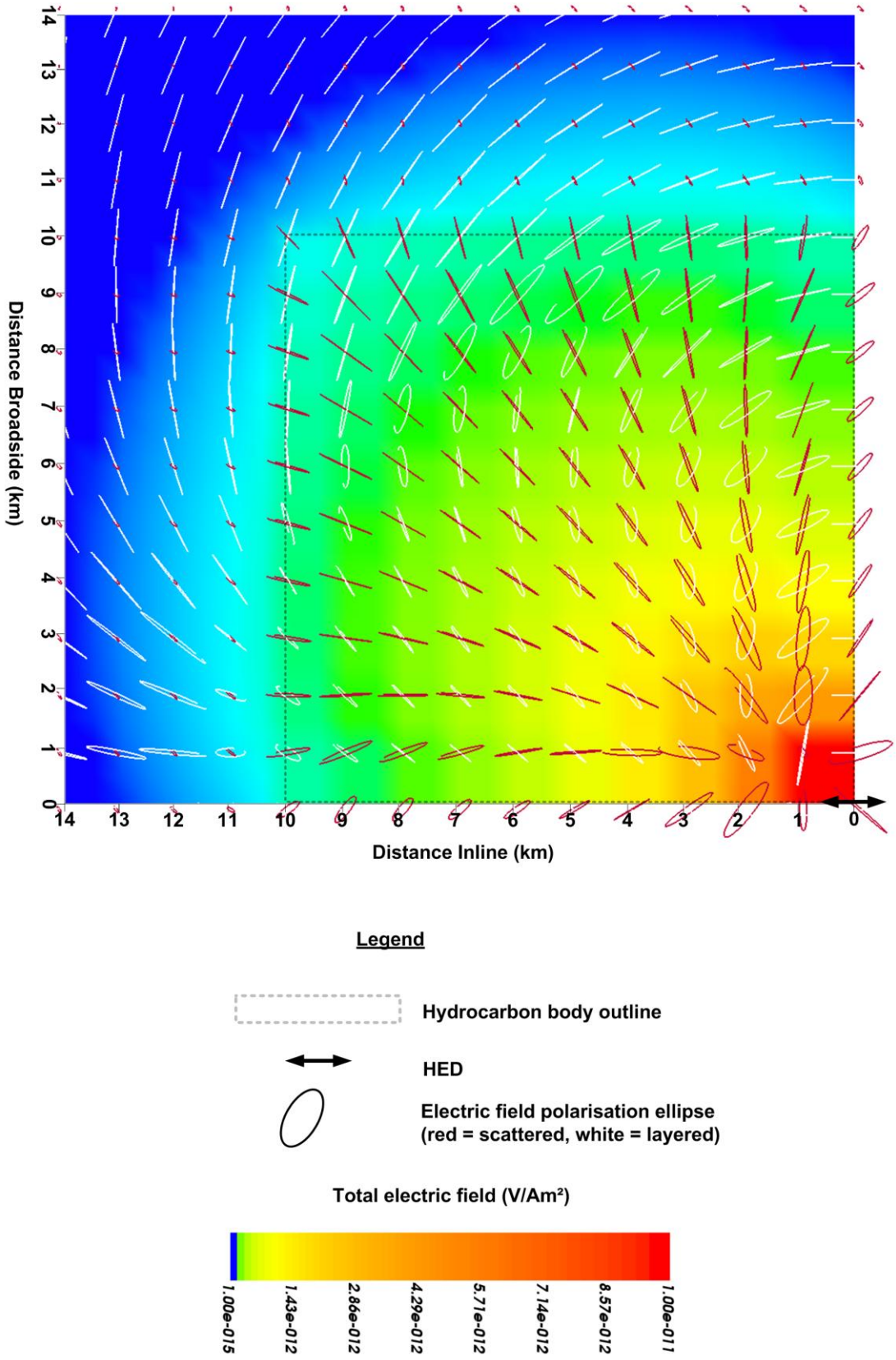

Figure 4-12: Plan view of ocean bottom scattered and layered polarisation ellipses.

4.4.2 Optimising survey parameters using streamtubes

Streamlines or streamtubes assist in understanding the behaviour of the electromagnetic fields and optimising receiver positions and recorded components. In the following examples streamtubes are used to represent the flux lines; the direction the field takes when travelling from the positive end of the transmitter bipole to the negative pole. This representation shows direction and amplitude of the field shown in a single 4D visualisation. The scattered and layered responses can be compared so that receiver position and recorded field orientations can be optimised.

Flux lines show the forward modelled path the transmitted wave travels through the earth. It shows the fields interaction with the earth in terms of amplitude and direction. Streamtube/streamline visualisations assist in understanding the behaviour of EM field propagation through a conductive earth. Figure 4-13. Firstly, the most noticeable about the diagram is that the electric field appears to be the same shape as a bar magnet. Flux lines leave from the positive end of the bipole and return at the negative pole. In this way we can understand the behaviour of electric fields by using streamlines. Secondly, at the air water interface the streamlines become parallel. The virtually 'infinite' resistivity contrast between the conductive water column and resistive air causes the electric fields to channel along the interface of the more resistive layer. When the field travels along the air-water interface it attenuates less than if travelling through water. The high amplitude wave travelling on this path is considered to be the 'air-wave'. Secondly the CSEM method is entirely diffusive due to the low transmission frequency, there appears to be no reflection at layer boundaries contrary to popular literature (Kong et al., 2002) only channelling of the electric field. The bottom right image of Figure 4-13 contains the area in which various fields can be recorded. E_x and E_z fields can be recorded inline with the HED,

whilst E_x is the only field that can be recorded broadside with the transmitter and finally E_y and E_z can be recorded radially from the source.

Electric and magnetic field lines vary in time due to the time harmonic waveform, therefore the variation in both direction and amplitude should be observed. Figure 4-14 shows the electric and magnetic scattered field lines at time 0.0s and 0.8s for a transmission frequency of 0.25Hz. It is revealed that both the electric and magnetic flux lines at these two times show similar shapes with no major directional changes (except for polarity). Streamlines constantly change position making it difficult to compare each time slice. Interpreting all time slices independently is also exhaustive. Due to the small variations in direction only one time slice needs to be analysed to observe the general behaviour of the electromagnetic field. Streamlines may not help detect subtle changes in the direction of the EM field, rather streamlines assist understanding the behaviour of the EM wave so receivers can be positioned for maximum coupling.

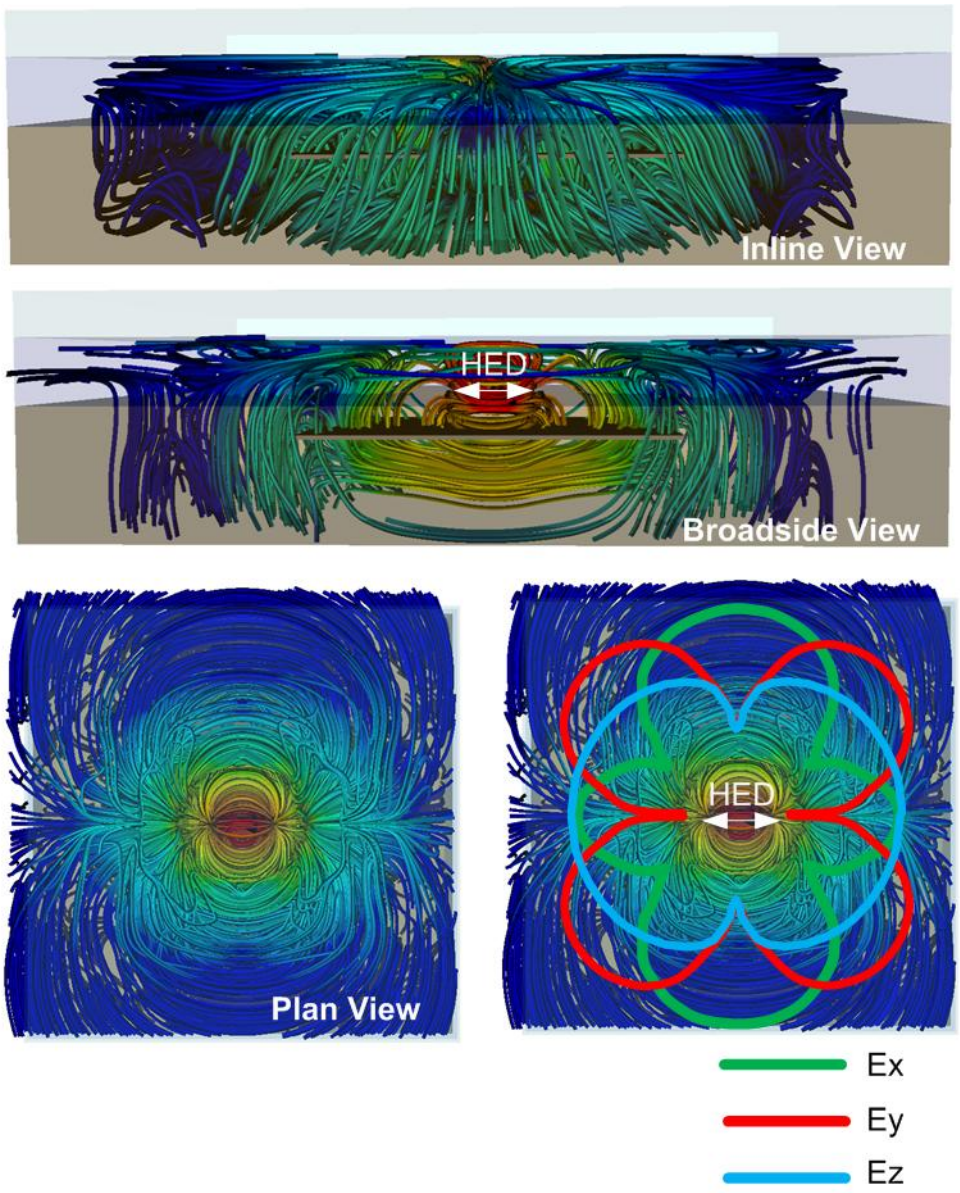

Figure 4-13 : Layered electric field streamtubes (flux lines) at time 0.0s from 3 viewpoints. Streamlines represent the lines of flux of the electric fields, the total electric field amplitude is shown by the colour (red=high and blue=low). These views illustrate the behaviour of EM field and assist in the positioning of receivers. The inline view displays the variation in the y-z plane while the broadside shows x and z directional variations and the plan view shows x and y changes. The bottom right image overviews where receivers can be positioned.

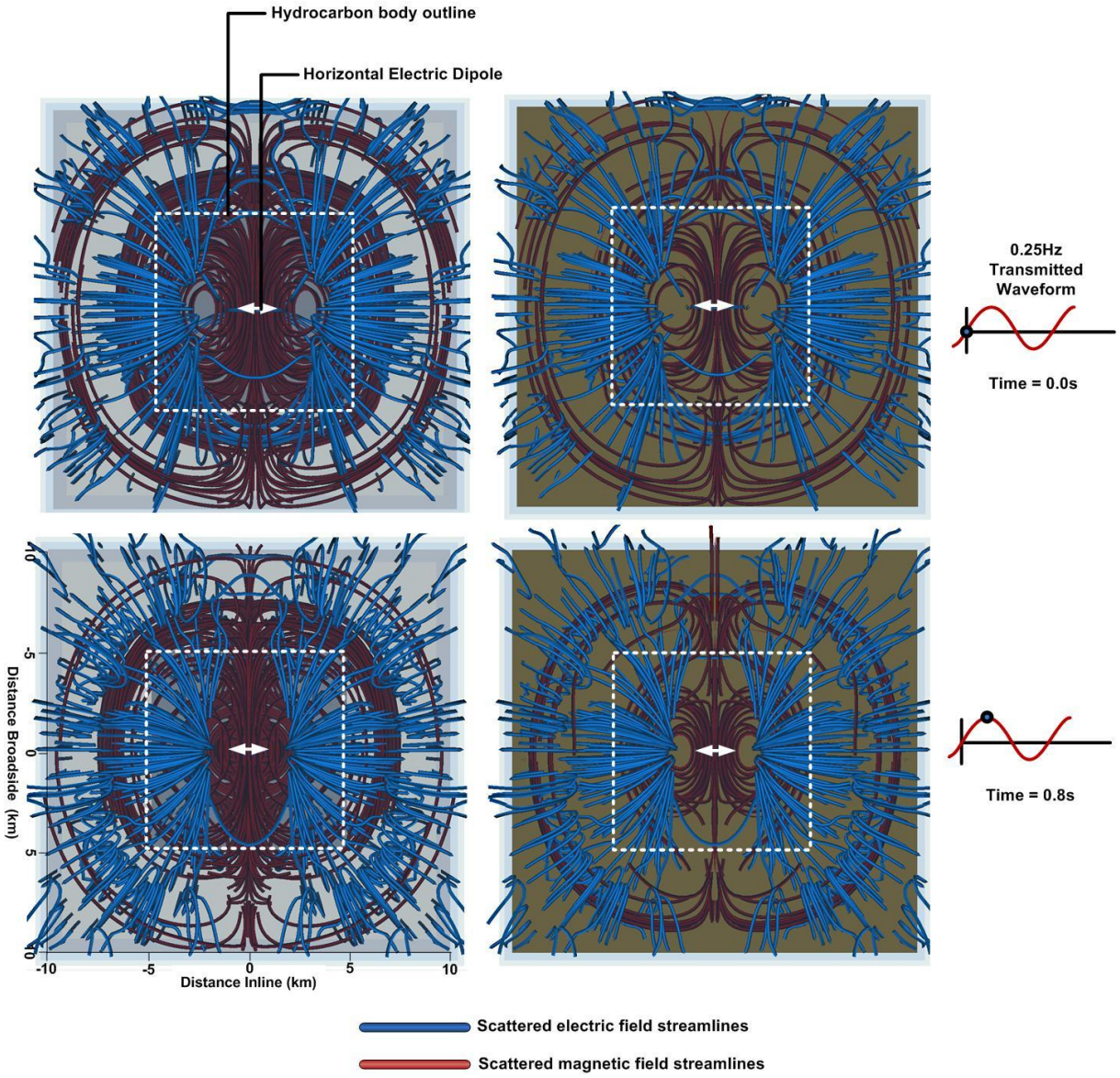

Figure 4-14 : Contrast of the variation in scattered field flux lines at 0.0s and at 0.8s with a transparent seafloor (left) and with flux lines blanked below sea floor (right). There are no major changes in the direction of the flux lines for these two times for either electric or magnetic fields.

Total field lines are not the only flux lines that should be visualised. In fact the scattered signal is the best response to visualise to optimise receiver position and recording directions. Figure 4-15 is a visualisation of the scattered field lines from inline and broadside directions and contrasted with both transparent and opaque ocean bottoms. The ocean bottom was made opaque because seafloor receivers are used. From this representation a number of observations can be made. Firstly it appears that the scattered field (both electric and magnetic fields) intersects with the body at perpendicular angles. This is the nature of EM fields at a resistive interface. Secondly the inline view shows that E_y fields do not contribute to the received signal unless recorded broadside of the body which is unlike the layered response. Since E_y fields contribute broadside of the HED, this component should be recorded. Thirdly E_x can be recorded broadside and inline from the transmitter. The vertical scattered electric field is the most influential out of the three components because at the scattered flux lines are near vertical at the ocean floor. If possible the E_z field component should be recorded. Since the magnetic field vectors are perpendicular to the electric field vectors, H_z is insensitive at the ocean floor because the fields are almost horizontal. H_x can be recorded radially from the source while H_y receivers can be placed both inline and broadside from the HED.

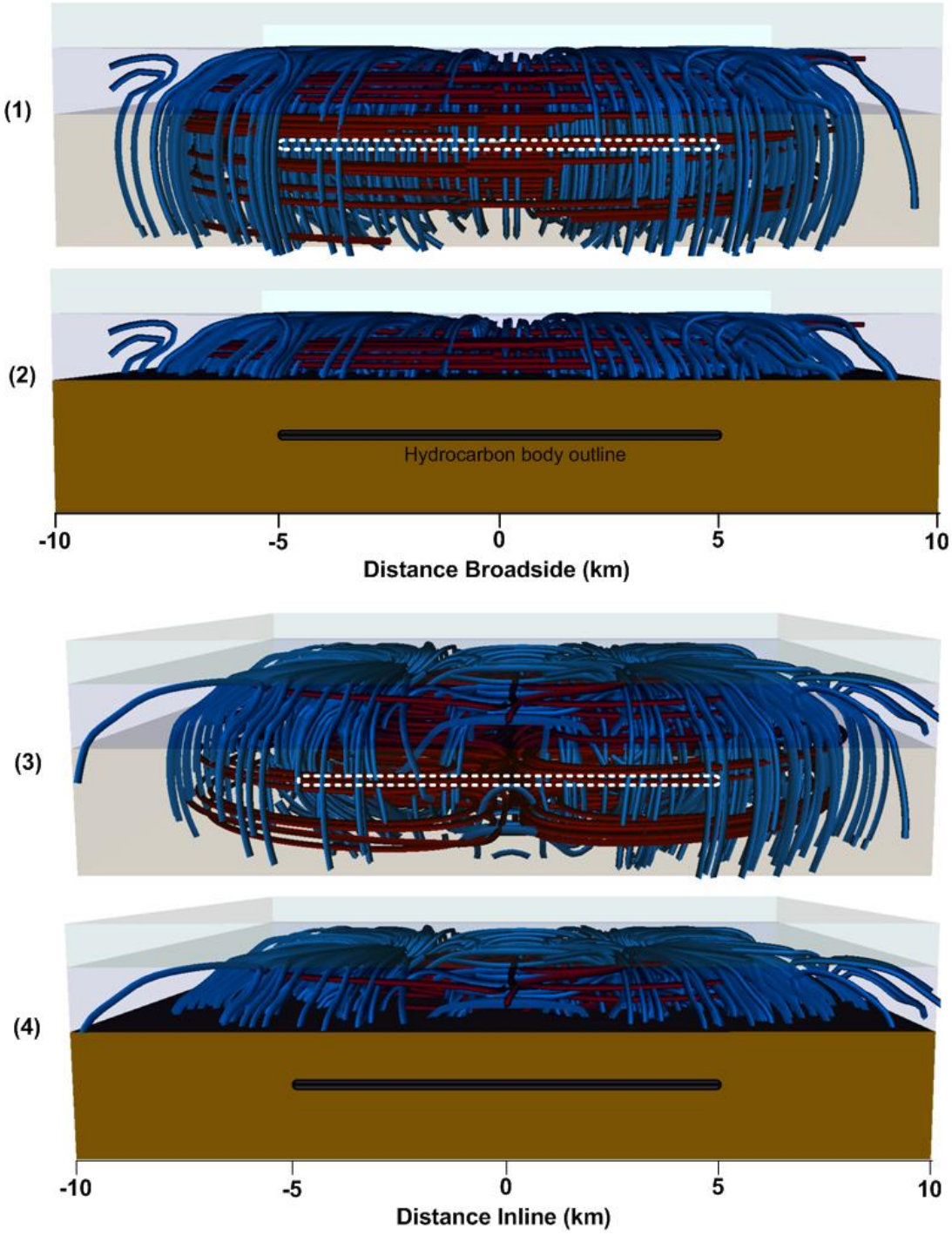

Figure 4-15: Streamlines at time = 0s of inline electric (blue) and magnetic field (red) for (1) inline view (top), (2) inline view with opaque seafloor, (3) broadside view and (4) broadside view with opaque seafloor (bottom). The view which blocks flux lines below the sea floor is helpful for optimising receiver positions. It appears that the influential component of the scattered field is the vertical electric field, which can be recorded any position. While the scattered vertical magnetic field

should not be recorded because it does not contribute to the recorded signal (the scattered magnetic response is horizontal to the ocean floor).

4.4.3 Optimising survey parameters using sensitivity and geometric response indicator grids

Survey geometry influences the success of a survey. One measure of sensitivity is the normalised field. The normalised field is a ratio of the total field response and the background (layered) response. The presence of hydrocarbon generally results in increased normalised responses. Receivers and transmitter lines should be positioned to maximise the normalised response.

Firstly the layered and scattered responses are forward modelled for the proposed survey configuration. The normalised field is then determined by using,

$$Normalised\ Field = \frac{Layered + Scattered\ Response}{Layered\ Response}$$

The overlapping area between the total and scattered noise floor is considered to be the detectable area (See Figure 4-16). Only in this region should the normalised response be calculated. A transmitter line over stationary ocean bottom receivers produces a number of normalised plots (See Figure 4-17).

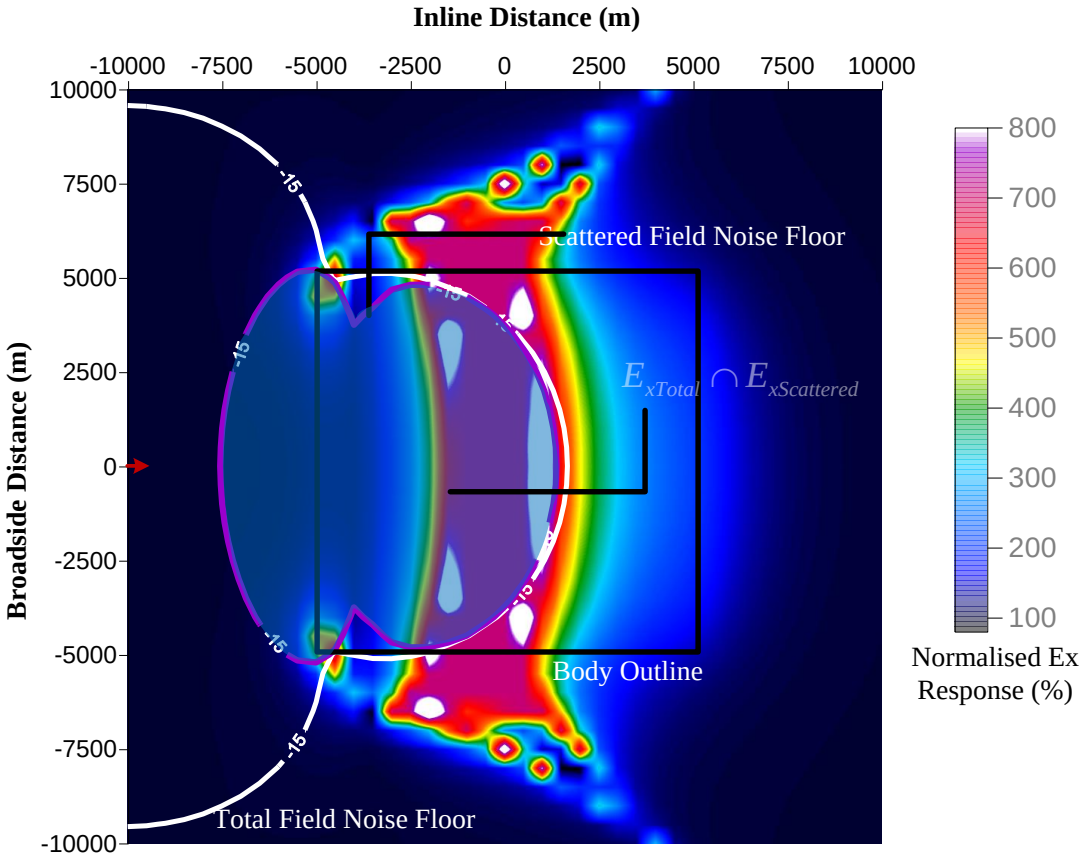

Figure 4-16 : The normalised E_x field response for one transmitter position at 0.25Hz. The normalised response = $^{\text{Total amplitude}}/_{\text{Layered amplitude}}$ and it represents the sensitivity of the receiver position to the hydrocarbon plate. The white contour represents the total field noise floor whilst the purple line signifies the detectable scattered field response. The overlapping area of the total and scattered field response shows the detectable area of the hydrocarbon body. At inline offsets of 7.5km there is a jump in the normalised response and at this position receivers should be placed to get the maximum response from the transmitter.

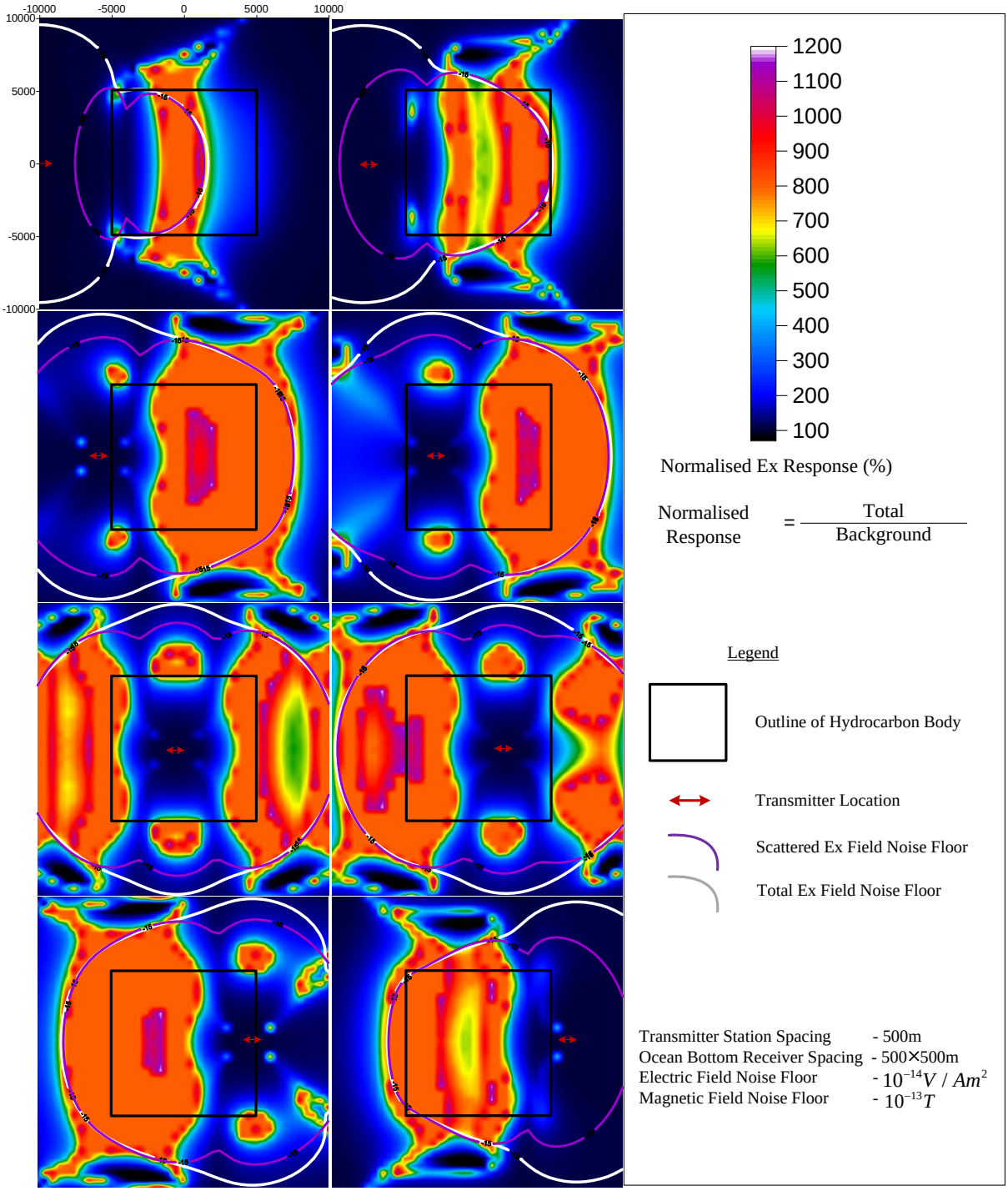

Figure 4-17 : The normalised Ex field response for a transmitter line over the centre of a resistive plate. When the transmitter is located over the plate the offsets required to obtain a large normalised response decreases. At most transmitter positions there is a dramatic increase in the normalised field around 5to 7km inline from the transmitter.

A number of conclusions can be drawn from viewing the normalised plots. The maximum normalised response is inline with the transmitter. In Figure 4-16 there is a marked jump in the normalised response at offsets greater than 7km. At offsets nearest to the noise floor the normalised response is the greatest. It also appears from Figure 4-17 that there is an increased normalised response when the transmitter is over the hydrocarbon body. This evidence reinforces the theory that the transmitted signal is only affected by the hydrocarbon at incident angles close to 90°. The normalised field changes for each transmitter location. Figure 4-17 shows the normalised inline electric field at several transmitter locations for a survey line over the centre of the hydrocarbon body. The position of the transmitter affects the normalised response. When the HED is directly over or near the edge of the hydrocarbon reservoir there is a dramatic increase in the normalised response. Therefore the transmitter or receiver needs to be placed near or above the body to receive a response. A whole transmitter line or series of readings which contains a normalised response is necessary to characterise the detectability of a hydrocarbon body.

Viewing all normalised plots for each transmitter position is impracticable. Several Normalised grids for several transmitter positions can be encapsulated into one image. A sensitivity plot can be created by finding the maximum response for all receivers over all transmitter positions. For example if a receiver has a normalised response of 1.1, 1.5 and 1.2 for transmitter positions T_{x1}, T_{x2} and T_{x3} respectively the maximum normalised response for that transmitter line would be 1.5.

$$E_{(x,y)} = \begin{cases} Max\left(E_{Normalised(x,y,t_n)}\right), & E_{scattered} > \mathrm{E}_{Noise\ Floor} \text{ and } E_{total} > \mathrm{E}_{Noise\ Floor} \\ 1 & otherwise \end{cases}$$

$$H_{(x,y)} = \begin{cases} Max\left(H_{Normalised(x,y,t_n)}\right), & H_{scattered} > \mathrm{H}_{Noise\ Floor} \text{ and } H_{total} > \mathrm{H}_{Noise\ Floor} \\ 1 & otherwise \end{cases}$$

$E_{(x,y)}$ = Maximum detectable electric field normalised response for transmitter series for receiver $(\mathrm{x,y})$

$H_{(x,y)}$ = Maximum detectable magnetic field normalised response for transmitter series for receiver $(\mathrm{x,y})$

$E_{Normalised(x,y,t_n)}$ = Set of the electric field normalised response for each transmitter position for receiver $(\mathrm{x,y})$

$H_{Normalised(x,y,t_n)}$ = Set of the magnetic field normalised response for each transmitter position for receiver $(\mathrm{x,y})$

Another approach to evaluate a range of survey parameters in a single grid is by using geometric response indicators (GRI). The GRI represents the sensitivity of the survey configuration with the geometry of the body. Each possible survey design generates hundreds of response curves. GRI's can be use encapsulate a whole survey to create maps of suitable 'attributes'. These maps compare of merits of various survey designs. (Ridyard, 2006). The first step to generating GRI grids is to firstly create a suite of common offset magnitude maps by interpolating the modelled data at the midpoint locations. The second step is to sort the bin into magnitudes and lastly is to compute the GRI by using a weighted sum of the amplitudes of the most responsive offsets (See Figure 4-19) (Ridyard, 2006).

$$GRI = Max[\frac{\sum_{n=1}^{N} Magnitude(n)}{\sqrt{n}}]$$

For the following examples, it is not the value of magnitude that is important, rather it is to examine which components and areas are sensitive to the hydrocarbon and which aren't. Figure 4-18 shows sensitivity grids for a single transmitter line with 500m transmitter location increments, 500m receiver spacing at the optimal base frequency of 0.25Hz. Each component has a pattern of sensitivity to the hydrocarbon body. We can look at the patterns of sensitivity to place the receivers. In this example

if only E_x, E_y and H_x and H_y were recorded receivers placed on the corners of the body will not detect a normalised response. Since the Hz normalised field is negligible its use should be limited. Most receivers record the E_x, E_y, H_x and H_y fields. Therefore the receivers should be placed both directly over the plate and off the edge by a maximum of 5km.

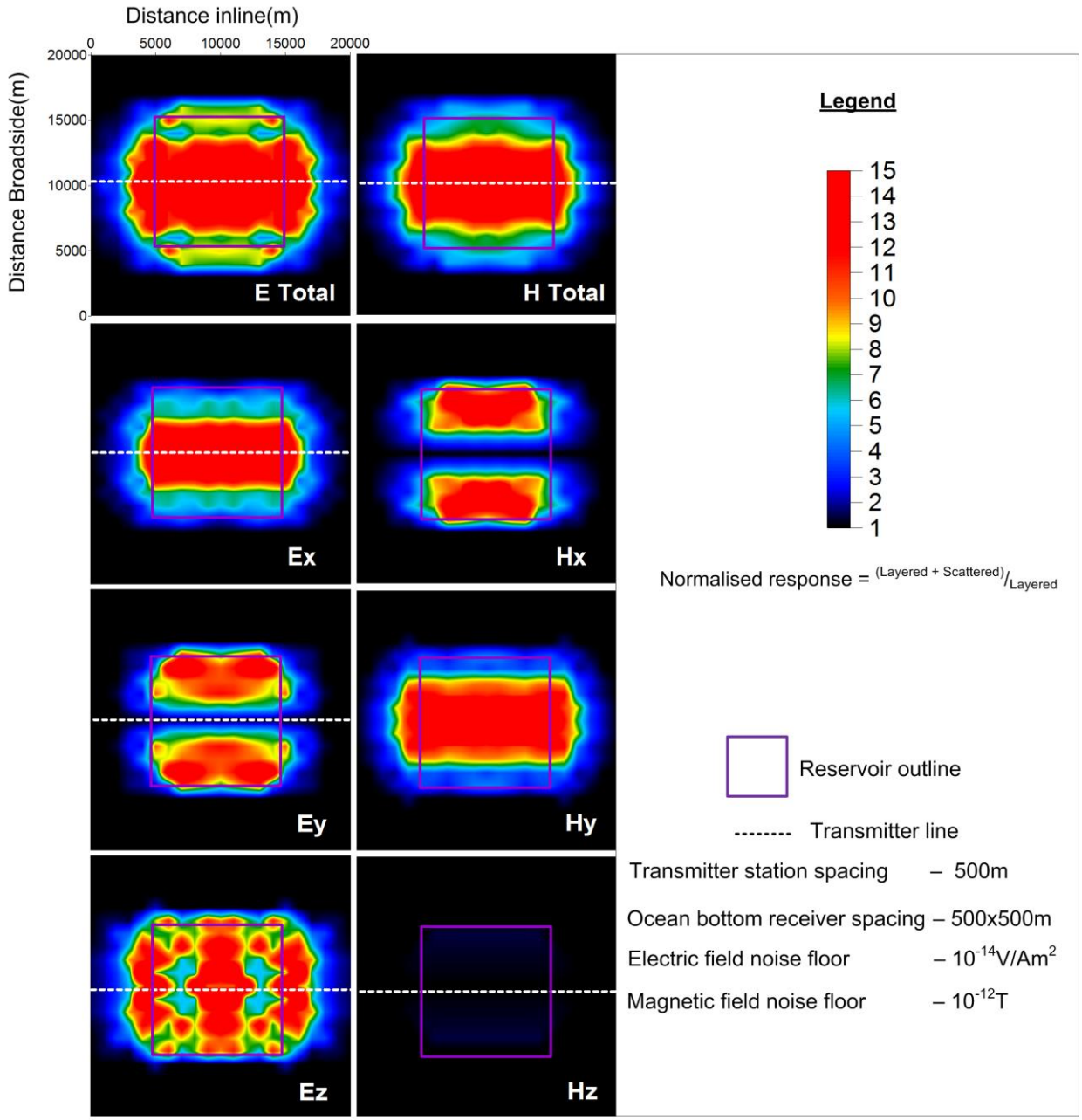

Figure 4-18: Maximum sensitivity grids for all recorded components for a single transmitter line at 0.25Hz. Ex, Ez and Hy is sensitive to inline recordings while Ey and Hy are sensitive to broadside recordings and Hz is insensitive to the hydrocarbon all together.

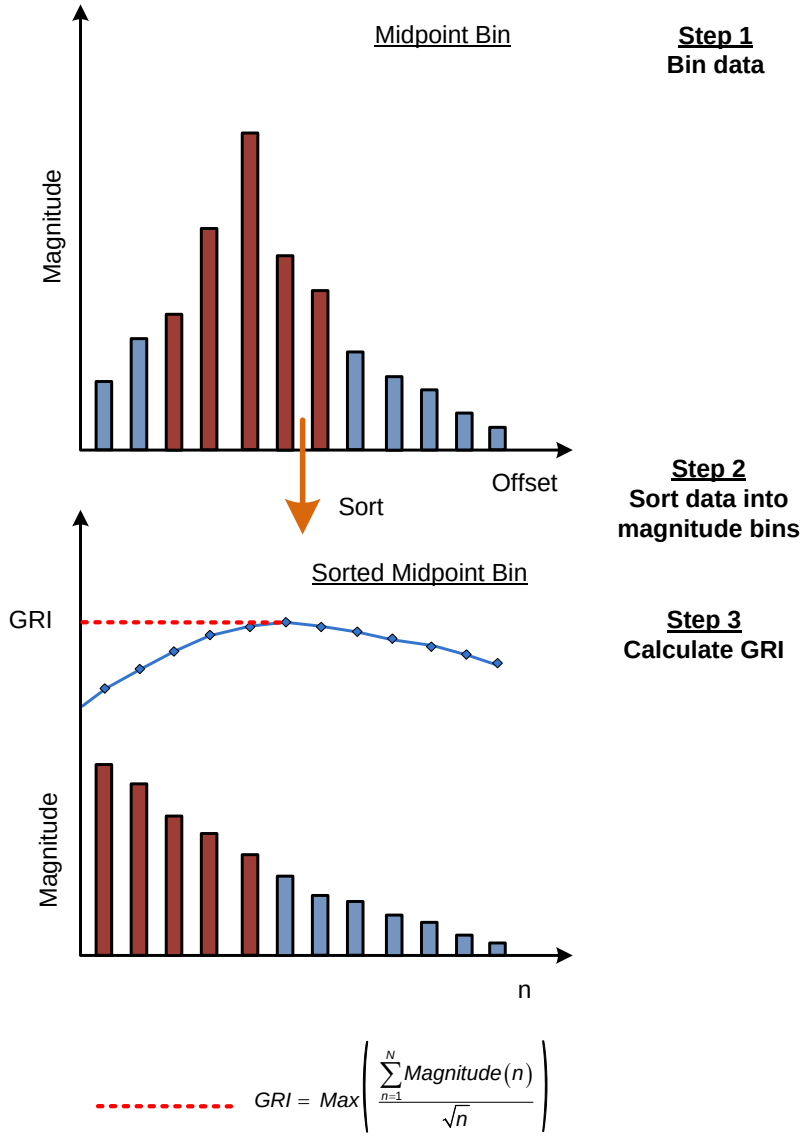

Figure 4-19: Calculating the Geometric response indicator (GRI). The GRI is a modelled attribute that describes the amount of scattered EM energy expected to reach the sea floor receivers. In effect it shows how well the modelled survey configuration maps out the geoemetry of the anomalous feature. At each location the GRI is the weighted sum of the modelled amplitudes of most responsive offsets. (reproduced from Ridyard et al., 2006)

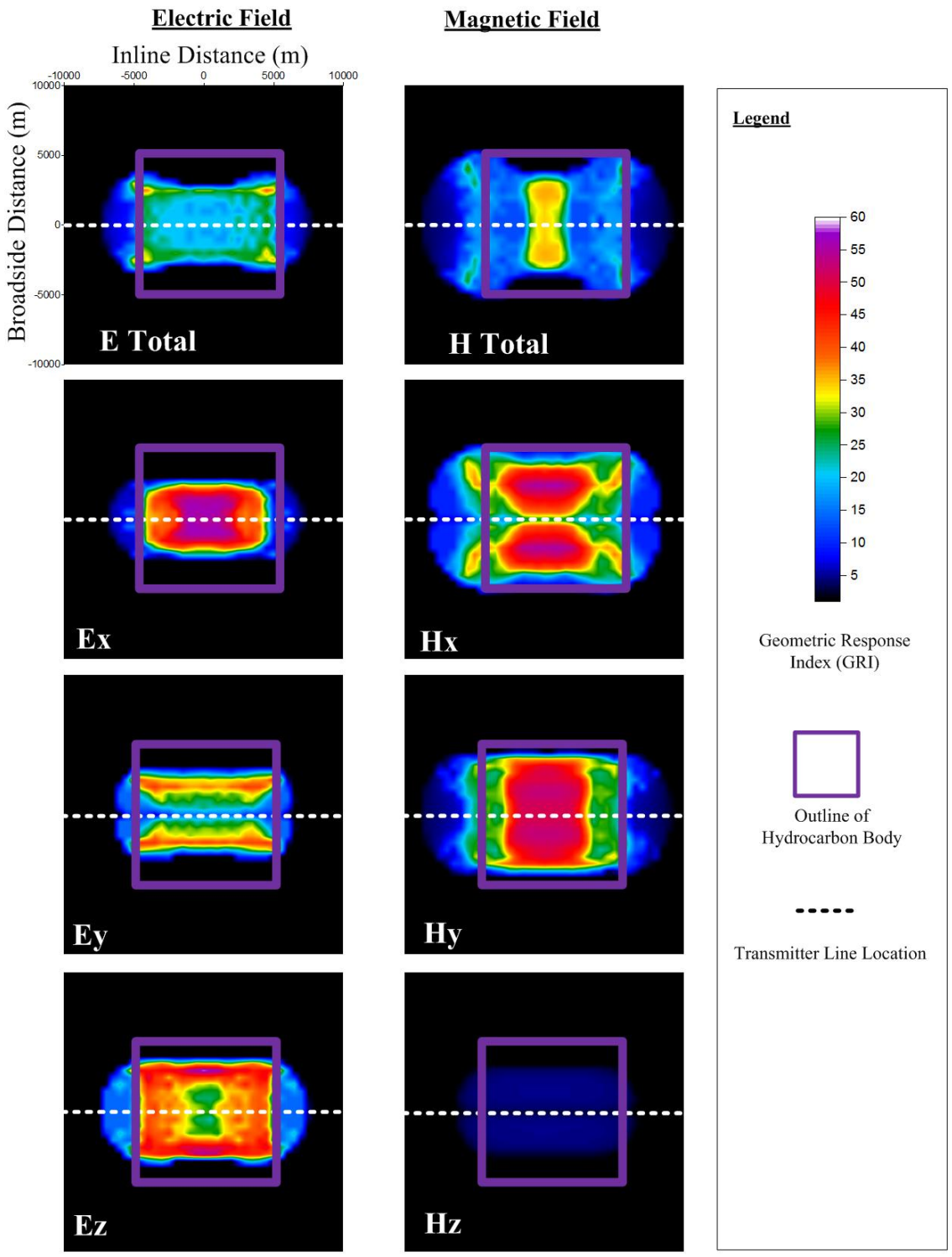

Figure 4-20 : Geometric response indicator for a single transmitter line at 0.25Hz. This shows how well each of the detectable signal components map out the geometry of the body. These show similar results to the maximum sensitivity grid in Figure 4-18. It appears that E_z and E_x is sensitive to inline geometry of the body while H_y is sensitive to the broadside geometry. H_z is insensitive to the geometry of the body.

4.4.4 Optimising receiver spacing

Changes in the receiver and transmitter line spacing impacts both the time required to record the survey and the resolution of the data (Ridyard et al., 2006). Therefore there is always a trade off between resolution and cost of survey. Spatial sampling and receiver positions are designed to meet the objectives of the specified survey types. Wide spaced grids help perform a recognisance survey over a large area where as closely spaced receivers can be used to perform a 3D survey to characterise a field for appraisal and development.

Figure 4-21 contrasts the maximum normalised response between a grid of ocean bottom receivers with a spacing of 2x2km and 500x500m. The 2x2km spacing represents a 2D survey performed over a field with unknown extents and the 500x500m sampling represents a high resolution 3D survey performed over a known field. At 2kmx2km the extents inline with the transmitted line can be resolved within 2km. This resolution is acceptable such that a more highly resolved survey can be performed over this area. At 500x500m the extents can be resolved within 500m.

4.4.5 Optimising transmitter spacing

The transmitter spacing is calculated from the minimum transmission frequency and the number of stacks required (See Table 4-1). Therefore there is a trade off between resolution and data precision. When transmitter spacing is minimised, the resolution increases but the precision decreases. The point of modelling variations in transmitter spacing is to determine the maximum transmitter spacing that can sufficiently resolve the hydrocarbon reservoir. For example if survey conditions were undesirable because of high atmospheric, natural or system noise, a minimum required number of stacks and transmission base frequency is known such that a survey will not

needlessly be performed if the conditions are not met. This precision is not the only issue, the airwave is also a problem. Stacking also reduces the maximum transmitter-receiver offset. While stacking the transmitter is not stationary. Far offset data may be swamped by the airwave if many stacks are performed. The furthest offset that can be resolved without influenced by the airwave is reduced distance the ship travels to perform all stacks. The offsets that the airwave starts to dominate the responses is seen in Table 2-2.

Sensitivity grids can be used to contrast the differences in transmitter spacing positions. Under normal surveying conditions a tow speed of 1-5 knots is achievable. For a transmitting a 0.01Hz base frequency and a tow speed of 1 to 5knots, transmitter spacing is between 51 and 257m.

Figure 4-22 contrasts the fields with 2km and 500m transmitter spacing. At 2km transmitter positions and the data is ‘under sampled’ resulting in bands in the maximum normalised field for the entire survey. This spacing would be the equivalent of a 0.01Hz signal stacked 8 times. For a transmitter spacing of 500m, the plate is more resolvable and a distinguishable pattern of sensitivity is visible.

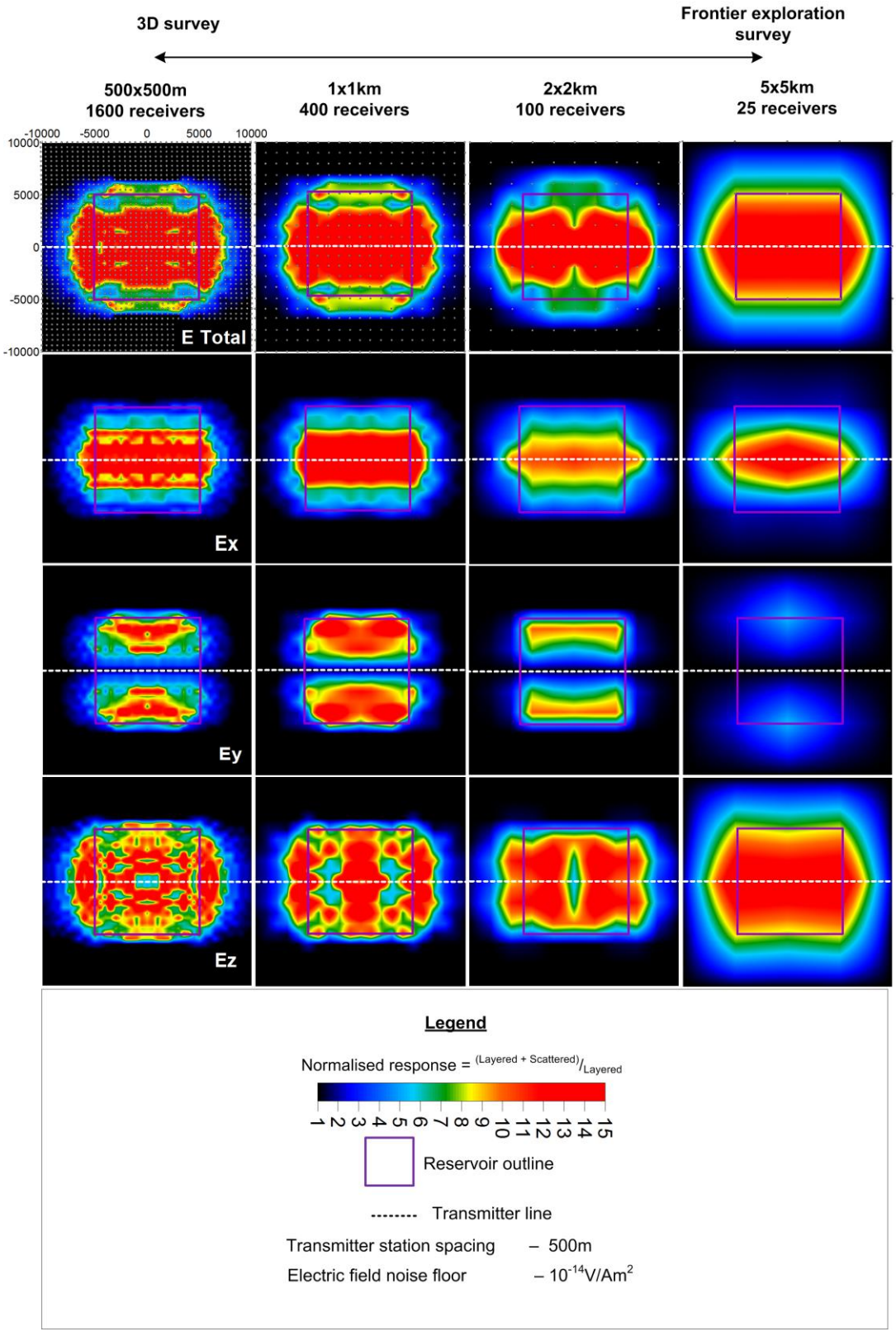

Figure 4-21 : Maximum sensitivity grids of the total electric field for several receiver spacing's. For exploration surveys a spacing of 5km would be adequate for a reservoir of 10x10km. To characterise a field a higher resolution is needed, a spacing of 1x1km appears to be sufficient for this purpose.

Number of stacks	Transmission frequency (Hz)				
	0.01	0.05	0.25	1	2.5
1	51.44	10.29	2.06	0.51	0.21
2	102.89	20.58	4.12	1.03	0.41
3	257.22	51.44	10.29	2.57	1.03
4	205.78	41.16	8.23	2.06	0.82
5	257.22	51.44	10.29	2.57	1.03

Tow speed 1 knot = 1.852km/h = 0.51m/s

Number of stacks	Transmission frequency (Hz)				
	0.01	0.05	0.25	1	2.5
1	257.22	51.44	10.29	2.57	1.03
2	514.44	102.89	20.58	5.14	2.06
3	771.67	154.33	30.87	7.72	3.09
4	1028.89	205.78	41.16	10.29	4.12
5	1286.11	257.22	51.44	12.86	5.14

Tow speed 5 knot = 9.26km/h = 2.57m/s

Table 4-1 : The transmitter spacing in metres for various base transmission frequencies and number of stack at 1 knot and 5 knots. This is used in conjunction with the airwave table (Table 2-2), GRI and maximum sensitivity plot, to determine the maximum allowable transmitter spacing.

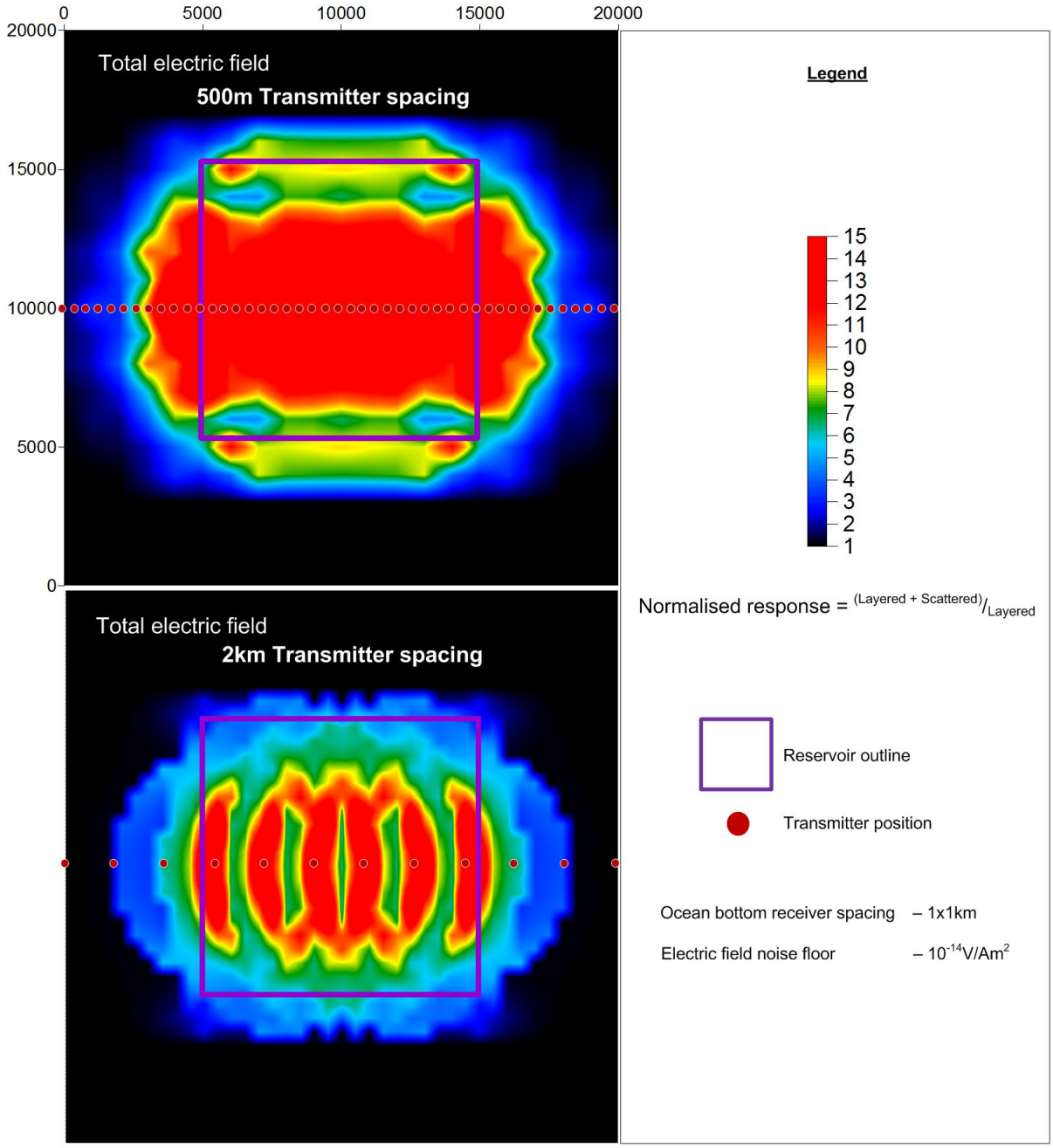

Figure 4-22 : Sensitivity grids of the total electric field showing the effect of transmitter spacing between 2km and 500m. At 2km transmitter spacing the resolution is insufficient to model the plate, as seen by the banding patterns from the lack of sampling. At 500m it is the equivalent of transmitting a 0.01Hz signal, with 2 stacks travelling at 5knots. This transmitter spacing is sufficient to model the hydrocarbon.

4.4.6 Effect of transmission frequency

Transmission frequency content affects the resolution, depth of penetration, amplitude of normalised response and onset of airwave. The resolution and depth of penetration should be optimised. Low frequencies, as seen by the skin depth, have high penetration into the earth due to the low attenuate. If the transmission frequency is too low, it may be insensitive to thin resistive targets and can result in low resolution of the target. By viewing the effect of the transmission frequencies on sensitivity of the survey we can confirm the optimal transmission frequency and test whether the resolution is adequate. Figure 4-23 shows the variation in the sensitivity of the electric field components at various frequencies. Several observations can be made from this Figure, firstly at low frequencies the maximum normalised response is diffuse whereby the variations in maximum amplitude of sensitivity are more gradual over the plate. The total-E field's pattern of sensitivity is circular, while at 0.25Hz the pattern is sharper and contains information about the geometry of the body. This is probably due to the circular diffusion of the field. Secondly it appears that the most influential component on the total field response is the vertical electric field. At 0.05Hz and 0.25Hz the vertical electric field dominates the normalised response. Since the survey configuration is the most sensitive to the E_z component, the component should be recorded. It is sufficient to record only E_x and E_y fields at 0.05-1Hz to resolve the extends of the field It also appears that at 0.05Hz it is still sensitive to the 100m thick hydrocarbon despite its longer wavelength. Also higher frequencies resolve the edge more effectively than lower frequencies and the amplitudes also decrease either side of the optimal transmission frequency, as seen in Figure 4-23.

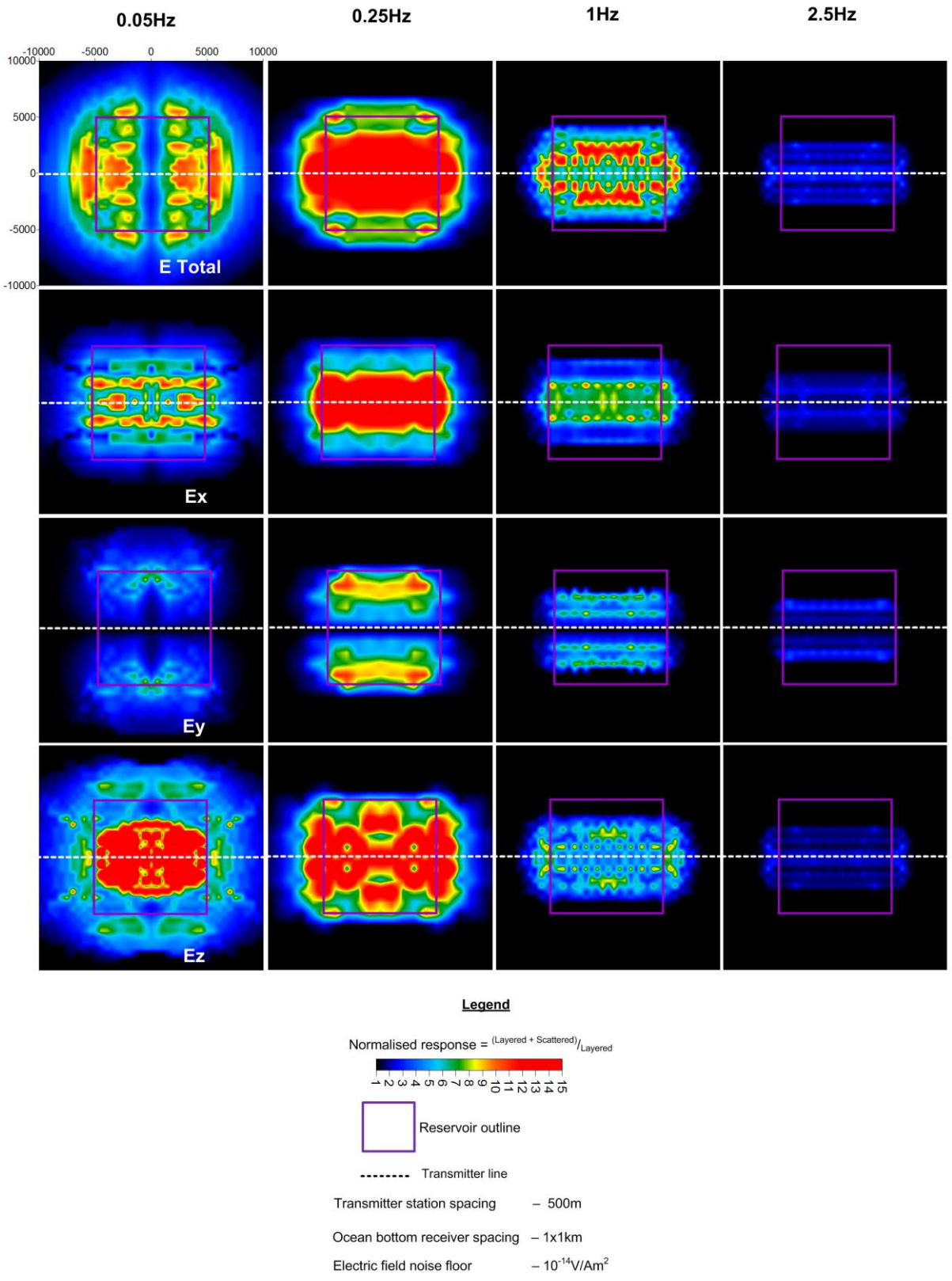

Figure 4-23 : Maximum sensitivity grids comparing all electric field components and a range of transmission frequencies.

4.4.7 Effect of Transmitter Line Orientation

The position of the transmission line determines how the body is energized. The hydrocarbon body must be located between the transmitter-receiver pair to record a change in the electric field. The purpose of testing transmitter line locations is to maximise the coverage of the target whilst also reducing the number of lines required to characterise the target. This is done by viewing the GRI and maximum sensitivity responses of various transmitter line positions. Several transmitter line locations should be trialled to both optimise normalised response, or to obtain a background response free of interference from the hydrocarbon.

Figures, Figure 4-24 and Figure 4-25 show the maximum normalised response and geometric response indicator for several transmitter line positions. The maximum normalised response occurs near the edges and over the body regardless of the transmitter line location. A transmitter line location over the body generates the maximum normalised response and can be detected using fewer receivers. Therefore with carefully planned transmitter lines, fewer receivers are necessary. Since this is a simple model it is the maximum normalised response is generated from a transmitter line directly over the centre of the body. From these figures only three lines are necessary to characterise the plate, two over the north and south edges and one over the centre. To obtain a background response a transmitter line has to be performed over 2.5km from the edge of the body.

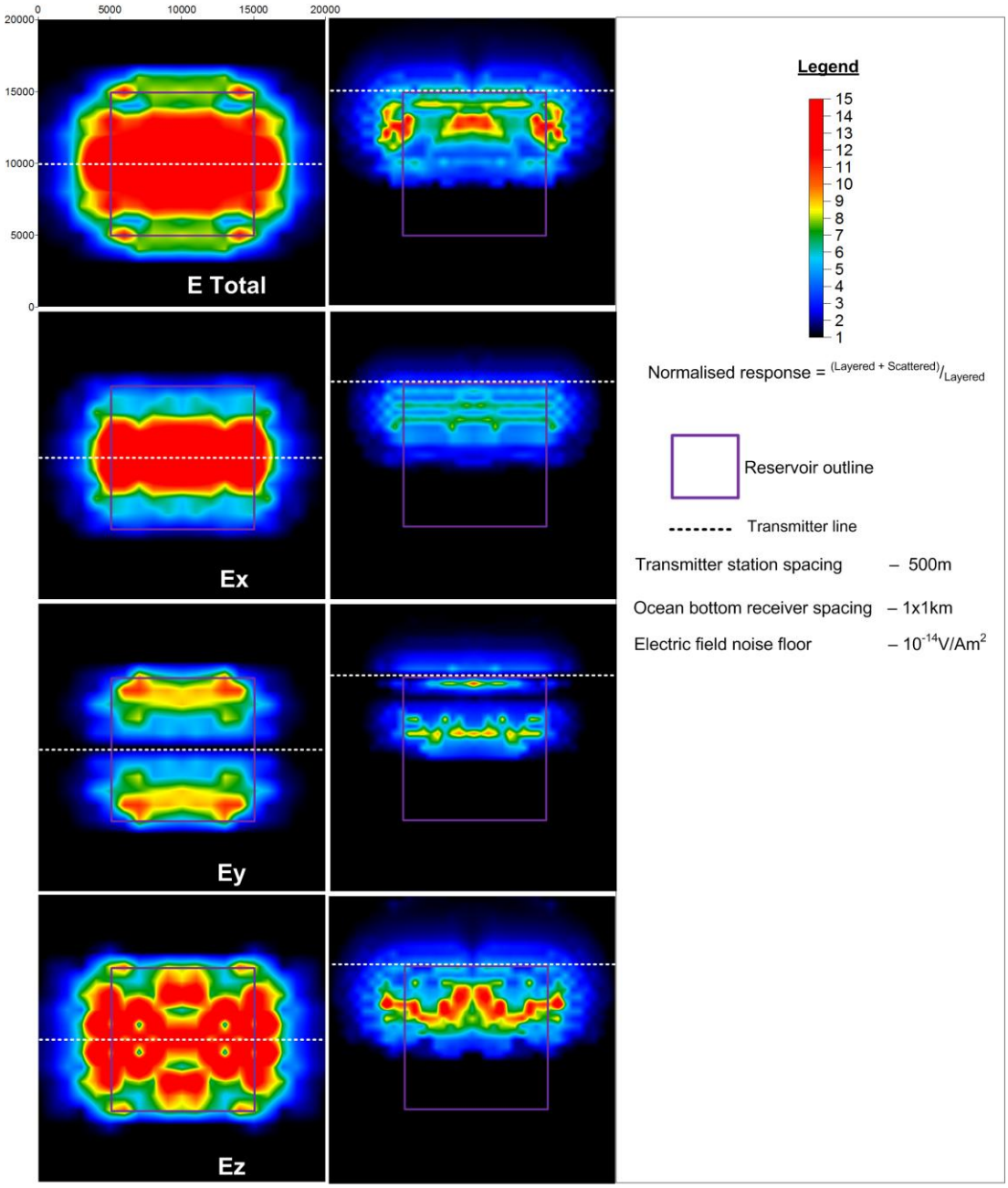

Figure 4-24 : Maximum sensitivity grid of x, y and z electric field components for two transmitter line locations.

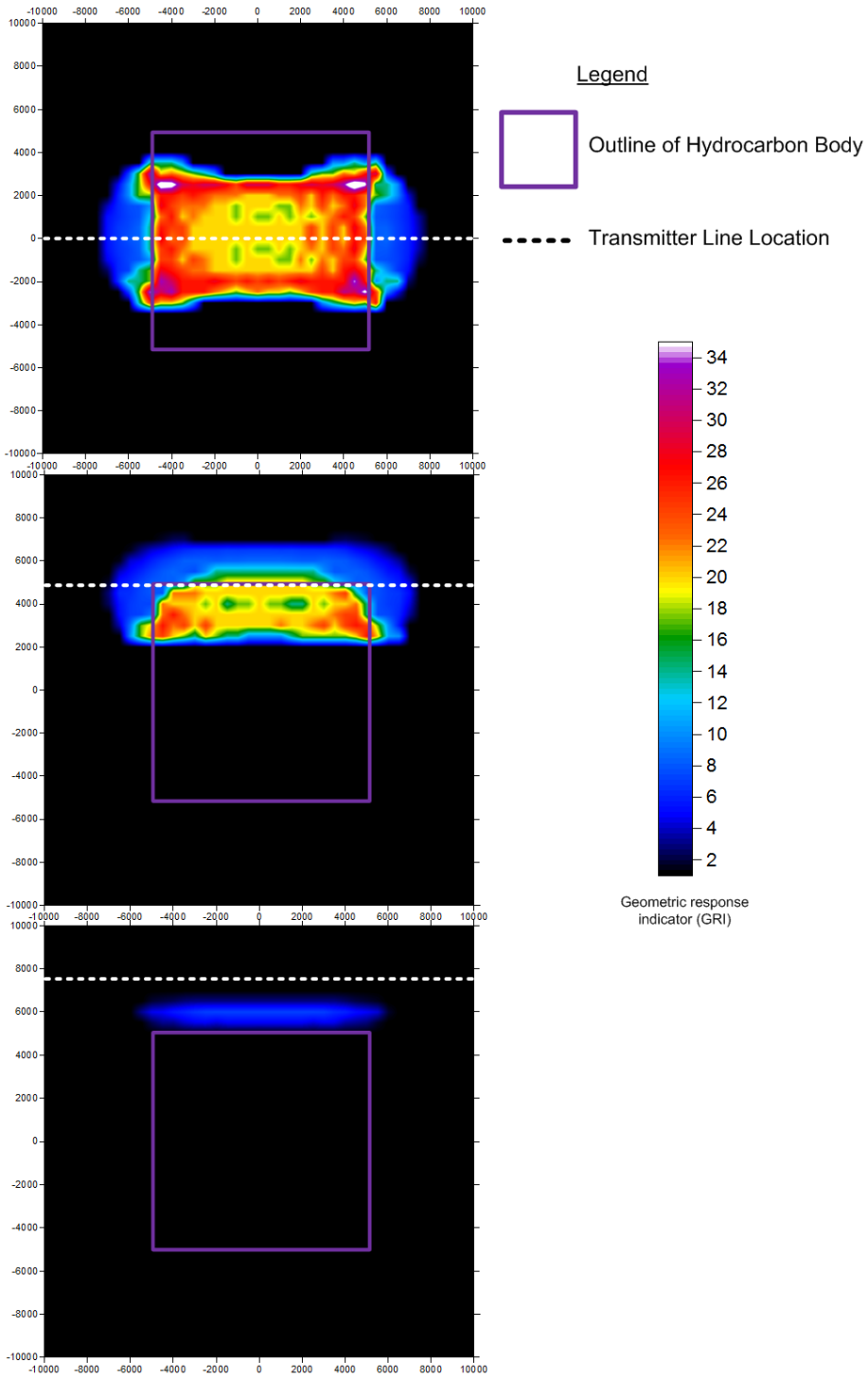

Figure 4-25 : Geometric response indicator for transmitter lines over centre, top edge and 2.5km off edge. The transmitter line over the centre of the body generates the maximum GRI. To obtain a background response a transmitter line has to be performed more than 2.5km from the edge of the body.

4.5 Evaluating survey design

4.5.1 Evaluating the hydrocarbon response for survey configurations

The output survey design consists of the equipment used, receiver locations, transmitter line locations, transmitted waveform, number of stacks and transmitter tow height. Due to the large number of survey parameters, it is best to evaluate all possible optimised survey configurations simultaneously by using the maximum normalised response and by creating GRI. At this stage of survey planning the final receiver positions and transmitter line locations can be selected.

A number of survey styles have been performed over the simple model (See Figure 4-26 and Figure 4-27). The main survey styles include single line, cross, multi-azimuthal (star) and grid survey. The single line and cross survey's were included for recognisance designs, to identify resistive bodies and body edges. Both could identify the resistive body, only the cross could identify the true extents of the body to within 2km. The star and grid 3D surveys were able to characterise the field to within 200m of the edge of the body. It is also apparent that there is a larger normalised response and GRI for both of these survey designs compared to the 2D surveys.

Finally it also is apparent that the recorded electric field characterises the edges of the hydrocarbon better than the magnetic field. The magnetic field identifies the centre of the body more effectively.

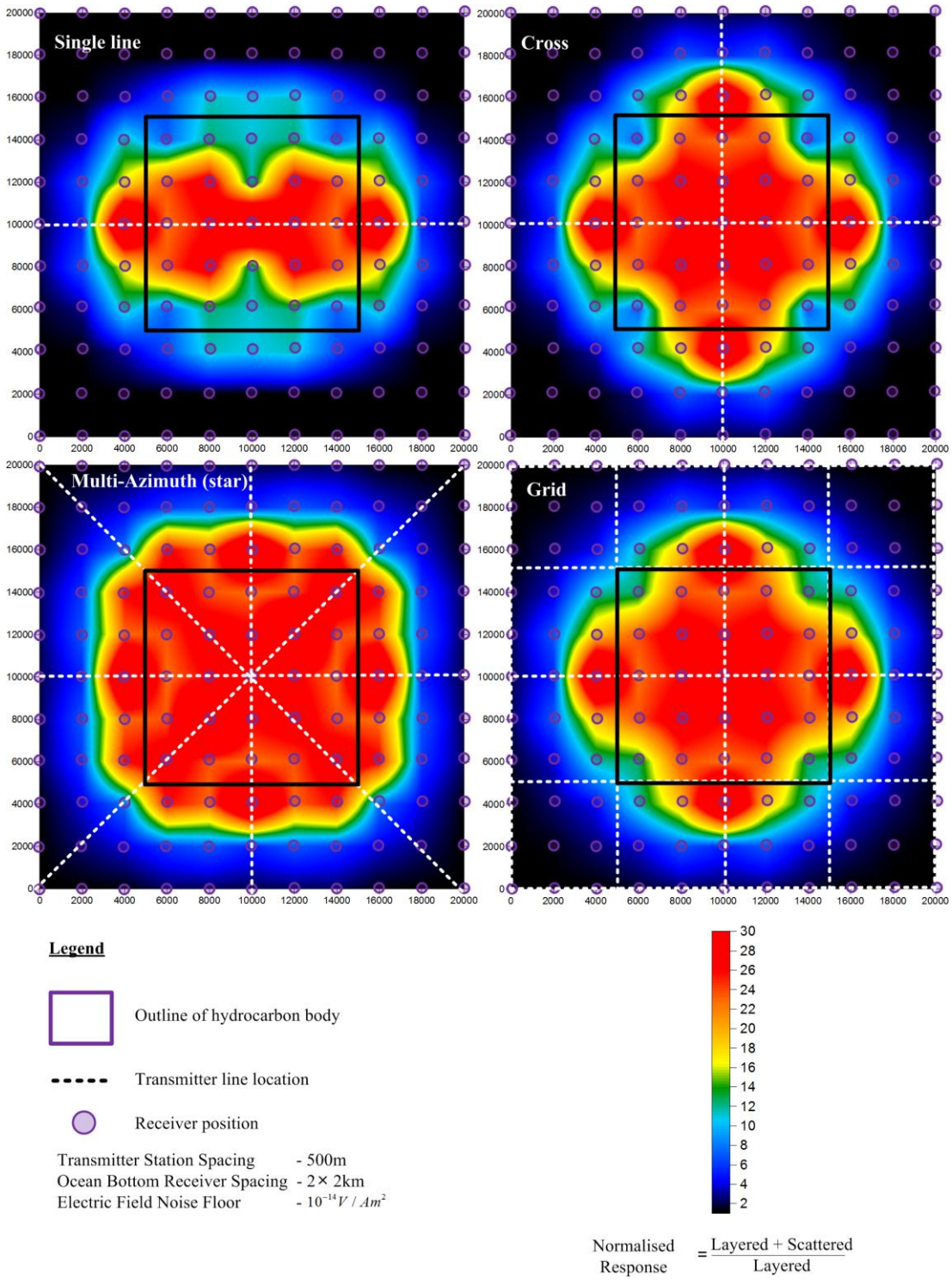

Figure 4-26 : Maximum normalised total electric field response for several 3D survey styles.

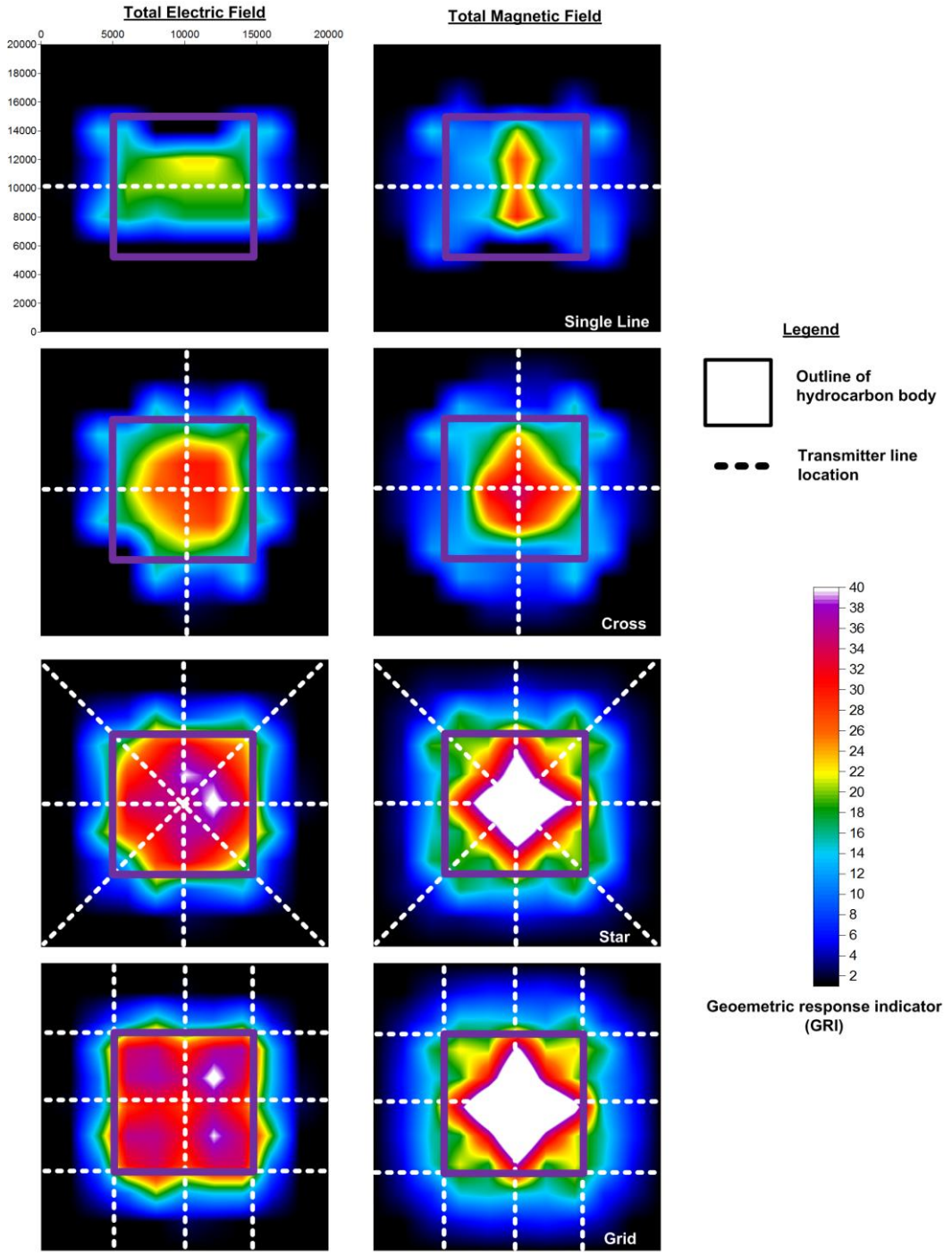

Figure 4-27 : GRI of several survey styles (2x2km receiver spacing). The star and grid surveys perform the best job at defining and characterising the geometry of the hydrocarbon. The star survey is superior to the grid style because it minimises the number of transmitter lines required. The asymmetries are caused by the asymmetrical binning and transmitter positions.

4.6 Output survey plan

The output survey design should include the plans to deploy and collect ocean bottom receivers and the parameters used to survey the prospect area. The crucial areas of a survey plan were considered to be crucial boat type, receiver selection, transmitter selection, waveform, projection, receiver deployment positions and transmitter line orientations. The before mentioned planning procedures were used to create the survey plan on Figure 4-28.

Proposed Date : 23-Oct-2002	Example Selection
Boat	
Name	Polar Bjorn
Receiver storage capacity	400 receivers
Receiver	
Name	Scripps Mach III
Electric field noise floor	10^{-15}V/Am^2 at 1Hz
Magnetic field noise floor	10^{-12}T at 1Hz
Electric field directions	X,Y and Z
Magnetic field directions	X and Y
Transmitter	
Name	DASI III
Total transmitted current	1000A
Dipole length	300m
Source dipole moment	300000Am
Tow height	20m
Maximum tow speed	2 Knots
Waveform	
Base frequency	0.01Hz
Waveform type	Cox
Minimum required stacks	3
Location	
Projection	IGS 50
Location area coordinates	20000E-34000E and 100N-16000N

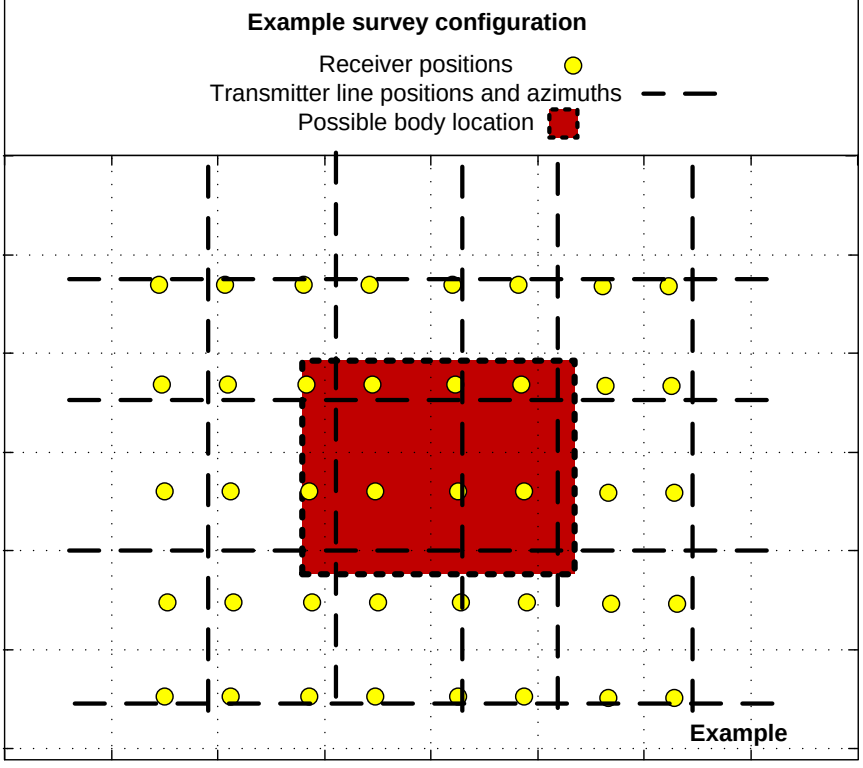

Figure 4-28 : Example survey plan

5 Conclusions

The three main areas investigated:

1) CSEM software development

2) Visualisation techniques

3) Planning procedures

Development of a CSEM Software Package

i. The CSEM package (CSEMoMatic) was written in the Java programming language. Object oriented design principles governed the program design. This allowed simple importation and organisation of survey geometry and its associated forward modelled data. Processing procedures included normalisation of the EM field and binning routines for the creation of geometric response indicator grids.

ii. A number of export file formats were necessary. ASCII and CSV were included for generic purposes, Matlab m files for profiles and binary and VTK for advanced 3D and 4D visualisation packages.

iii. A four step process was applied to modelling a CSEM survey. This involved defining the (1) geoelectric model (2) receiver positions (3) transmitter locations and (4) transmitted waveform.

iv. Each button in CSEMoMatic was linked to an information screen for usability. This displayed the purpose and details of the operation.

Examine a range of visualisation techniques

i. X, y, z or total field amplitudes for the electric or magnetic field were represented by 3D scalar planes.

ii. Various attributes were represented using isosurfaces. The noise floor in three dimensions was visualised using this. Several 3D time slices over entire transmitted waveforms were used to clarify the 4D nature of EM fields.

iii. Flux lines of either the magnetic or electric fields were best represented by streamlines. The 3D path of the electric and magnetic fields could be represented by this. The responses from a hydrocarbon body and layered fields could be compared using visualisation method.

iv. A 4D animation of a EM vector can be encapsulated by a 3D polygon by using polarisation ellipses. Phase, amplitude and directional information can be extracted using the visualisation method. Layered and scattered polarisation ellipses were compared to optimise the positions of receivers.

Develop a planning procedure/method for marine CSEM

A 4 Step planning methodology was constructed:

1) Creating the geoelectric model
2) Initialising survey parameters
3) Optimising survey parameters
4) Evaluating the survey design

Receiver and transmitter line positions and orientation are optimised to obtain the largest normalised response by using the 4 step approach. The number of receivers and transmitter lines are minimised whilst maximising the received response. The approach designed to be generic and could be applied to 2D and 3D surveys.

Several representations were used to facilitate the planning methodology.

i. Normalisation plots and geometric response indicator grids were used together to independently test survey parameters and to evaluate the complete survey design.

ii. Streamlines and polarisation ellipses were used to optimise receiver positions. Both were used to observe the likely areas where the scattered response would be influential compared to the layered response.

6 Recommendations

To understanding the EM field behaviour streamlines of a single time snapshot should be analysed.

GRI's and maximum normalised sensitivity grids should be used in favour of streamlines because they are insensitive to small variations in the field's polarity.

Maximum normalised sensitivity grids and geometric response indicator (GRI) grids should be used together to evaluate survey designs. The normalised response shows the amplitude while the GRI evaluates the survey's effectiveness to characterise the target's geometry.

Secondly by using CSEM simultaneously with seismic survey, the number of false positive reservoirs will be reduced. Therefore it is highly recommended that research be put into a planning methodology which results in a coupled CSEM, MT and seismic survey design.

A commercially available package should be created that incorporates both planning and visualisation packages. CSEMoMatic incorporated a text based interface, making visualising the survey design difficult. A modern CSEM planning software system should integrate a 2D imaging window to show receiver and transmitter line positions and allow several grid overlays. Typical GIS functions should be included. Future EM software packages should integrate a 3D visualisation window into the interface. The software should be easily updated with modern visualisation algorithms. OpenGL (OpenGL, 2008) or Direct3D (Direct3D, 2008) could be used for this purpose.

It is difficult to obtaining the geoelectric model for forward modelling and inversion. 1D borehole information is not representative of either the structure on a regional or reservoir level. The use of a downhole marine CSEM survey or vertical MCSEM method should be investigated. VMCSEM transmitter dipole can be lowered into the borehole while seafloor receivers and detect the signal. Since the transmitter is stationary, much lower frequencies than 0.01Hz can be practically used. This method could provide high signal to noise ration because low amplitude, high frequency signals can be stacked hundreds of times.

References

Chave, A.D., Constable, S.C., and Edwards, R.N., 1991, Electromagnetic methods in applied geophysics: Volume 2, Applications, edited by Misac N. Nabighian Society of Exploration Geophysicists Tulsa, Oklahoma

Constable, S.C., Orange, A.S., Hoversten, G.M., and Morrison, H.F., 1998, Marine magnetotellurics for petroleum exploration part I: A sea-floor equipment system: *GEOPHYSICS*, **63**, 816-825.

Cox, C.S., 1981, On the electrical conductivity of the oceanic lithosphere: *Physical Earth Planetary International*, **25**, 196-201.

Direct3D, Retrieved November 1st, 2008, from http://www.gamesforwindows.com/en-US/AboutGFW/Pages/DirectX10.aspx.

Drishti, Retrieved November 2nd, 2008, from www.anusf.anu.edu.au/Vizlab/drishti.

Eidesmo, T., Ellingsrud, S., MacGregor, L.M., Constable, S., Sinha, M.C., Johansen, S., Kong, F.N., and Westerdahl, H., 2002a, Sea Bed Logging (SBL), a new method for remote and direct identification of hydrocarbon filled layers in deepwater areas: *first break*, **23**, 144-152.

Eidesmo, T. and Ellingsrud, S., 2002, How electromagnetic sounding technique could be coming to hydrocarbon E&P: *first break*, 20, 142-143.

Ellingsrud, S., Eidesmo, T., Johansen, S., Sinha, M.C., MacGregor, L.M., and Constable, S., 2002, Remote sensing of hydrocarbon layers by seabed logging (SBL): results from a cruise offshore Angola: *The Leading Edge*, **21**, 972-982

Flosadóttir, Á.H., and Constable, S., 1996, Marine controlled-source electromagnetic sounding: *Journal of Geophysical Research*, **101**, 5507-5517.

Gribenko, A. And Boulaneko, M., 2005, Rigorous 3-D inversion of marine CSEM data based on the integral equation method, University of Utah.

Hohmann, G.W., 1975, Three-dimensional induced polarization and electromagnetic modeling: *GEOPHYSICS*, **40**, 309-324.

Hohmann, G.W., 1988, Electromagnetic methods in applied geophysics: Volume 1, Theory, edited by Misac N. Nabighian: Society of Exploration Geophysicists, Tulsa, Oklahoma.

Hoversten, M.G., Newman, G.A., Geier, N., and Flanagan, G., 2006, 3D modeling of a deepwater EM exploration survey: *GEOPHYSICS*, **71**, 239-248.

ImageJ. Retrieved November 1st, 2008, from www.rsbweb.nih.gov/ij/

Java. Retrieved November 1st, 2008, from http://java.sun.com/.

Johansen, S.E., Amundsen, H.E.F., Røsten, T., Ellingsrud, S., Eidesmo, T., and Bhuyian, A.H., 2005, Subsurface hydrocarbons detected by electromagnetic sounding: *first break*, **23**, 31-36.

Keys, K.W., 2003, Application of broadband marine magnetotelluric exploration to a 3D salt structure and a fast-spreading ridge: Ph.D. Thesis, University of California.

Kong, E.N., Westerdahl, H., Ellingsrud, S., Eidesmo T., and Johansen S., 2002, 'Seabed logging': A possible direct hydrocarbon indicator for deepsea prospects using EM energy: *Oil & Gas Journal*, **100**, 30-36.

Li, Y., and Constable, S., 2007, 2D marine controlled-source electromagnetic modeling: Part 2 - The effect of bathymetry: *GEOPHYSICS*, **72**, 63-71.

MacGregor, L.M., 2006, *OHM short course; Section-1*, *Section-2*: Marine electromagnetic sounding for hydrocarbon applications, Perth 27 - 29 March.

MacGregor, L.M., Andreis, D., Tomlinson, J., and Barker, N., 2006, Controlled-source electromagnetic imaging on the Nuggets-1 reservoir: *The Leading Edge*, **25**, 984-992.

MacGregor, L.M., Sinha, M.C., and Constable, S., 2001, Electrical resistivity structure of the Valu Fa Ridge, Lau Basin, from marine controlled-source electromagnetic sounding: *GEOPHYSICS*, **146**, 217-236.

MacGregor, L.M., Constable, S. and Sinha, M.C., 1998, The RAMESSES experiment – III. Controlled-source electromagnetic sounding of the Reykjanes Ridge at 57°45'N: *Geophysics Journal International*, **135**, 773-789.

MayaVi, Retrieved November 2nd, 2008, From www.mayavi.sourceforge.net/.

Mehta, K., Nabighian, M., Li, Y., and Oldenburg, D., 2005, Controlled source electromagnetic (CSEM) technique for detection and delineation of hydrocarbon reservoirs: an evaluation.

Mittet, R., Løseth, L. and Ellingsrud, S., 2004, Inversion of SBL data acquired in shallow waters: Presented at the 66th EAGE Conference & Exhibition.

OHM Surveys. Retrieved July 1st, 2008, from www.ohmsurveys.com

OpenGL, Retrieved, November 31st, 2008, from www.opengl.org.

Peace, D.G., 2005, How to Plan for a Successful C.S.E.M. Survey: Presented at the 2005 Offshore Technology Conference.

Peace, D.G., Meaux, D., Johnson M. and Taylor, A., 2004, Controlled souce electro-magnetics for hydrocarbon exploration: Houston Geological Society, **47**, 3.

Phillips, S., 2007, Feasibility of the marine controlled source electromagnetic method for hydrocarbon exploration; Western Australia: BSc Honours thesis, Department of Exploration Geophysics, Curtin University of Technology.

Pound, G. 2007, Multi-Transient EM Technology at PGS: Tech Link, 7, 4.

Ridyard, D., Wicklund, T., Lindhom B., 2006, Electromagnetic prospect scanning moves seabed logging from risk reduction to opportunity creation : *first break*, **24**, 61-64.

Sheriff, R.E., 1991, Encyclopedic dictionary of applied geophysics: Society of Exploration Geophysics, Tulsa, Oklahoma.

Spiess, F.N., Macdonald, K.C., Atwater, T., Ballard, R., Carranza, A., Cordoba, D., Cox, C., Garcia, V.M.D., Francheteau, J., Guerrero, J., Hawkings, J., Haymon, R., Hessler, R., T. Juteau, Kastner, M., Larson, R., Luyendyk, B., Macdougall, J.D., S. Miller, Normark, W., Orcutt, J., and Rangin, C., 1980, East Pacific Rise: Hot springs and geophysical experiments: *Science*, **207**, 1421-1433.

Tompkins M., Weaver R. and MacGregor, L.M., 2004, Sensitivity to Hydrocarbon Targets Using Marine Active Source EM Sounding: Diffusive EM Imaging Methods, OHM.

VTK, Retrieved November 1st, 2008, from www.vtk.org/pdf/file-formats.pdf.

WesternGeco. Retrieved July 1st, 2008, from http://www.westerngeco.com/content/services/electromagnetic/wgem.asp?.

Appendix A – The CSEM Method

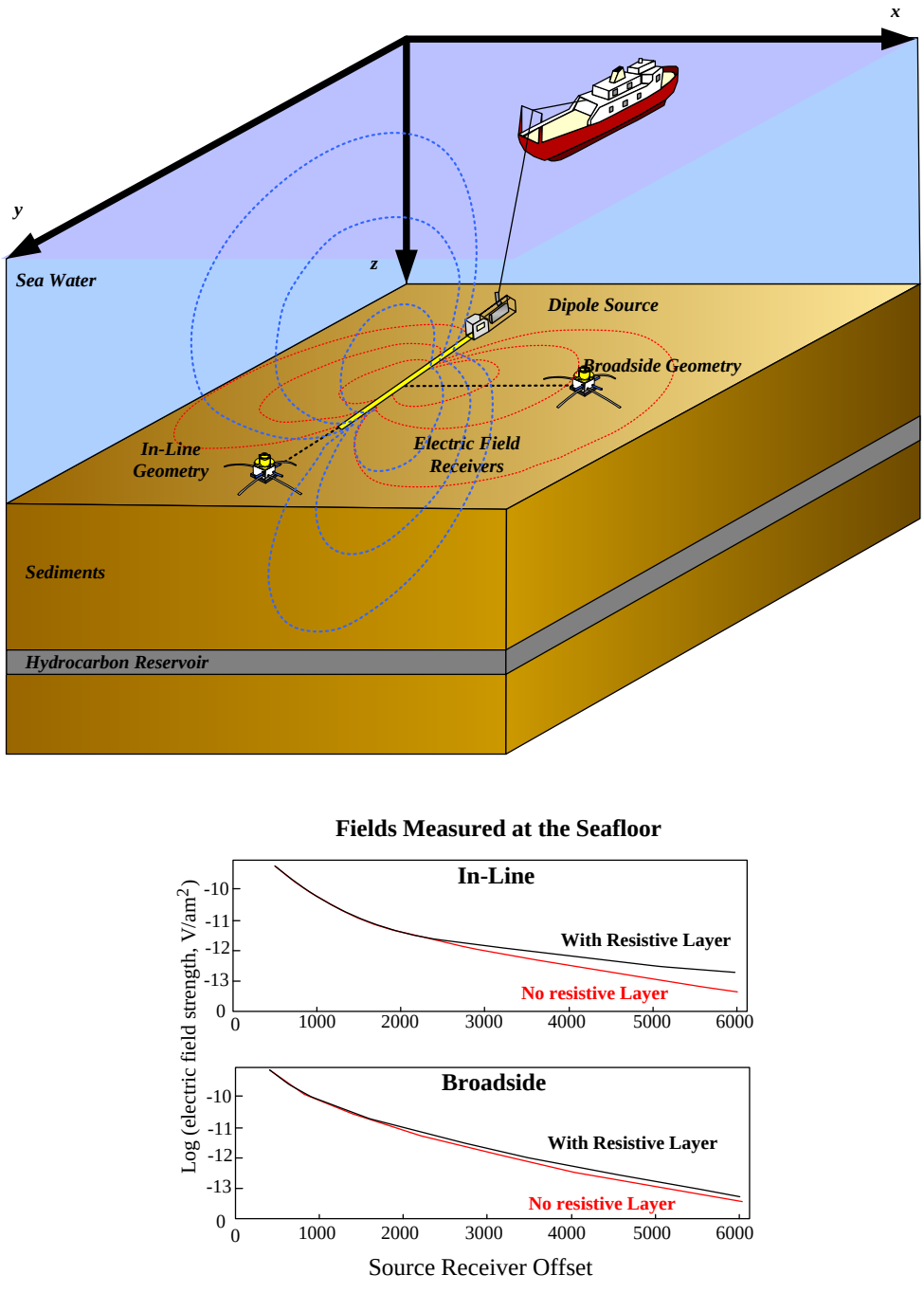

Figure A1 : (Top) Survey geometry and basic EM radiation pattern. (Bottom) The expected response from inline and broadside receivers (MacGregor, 2001)

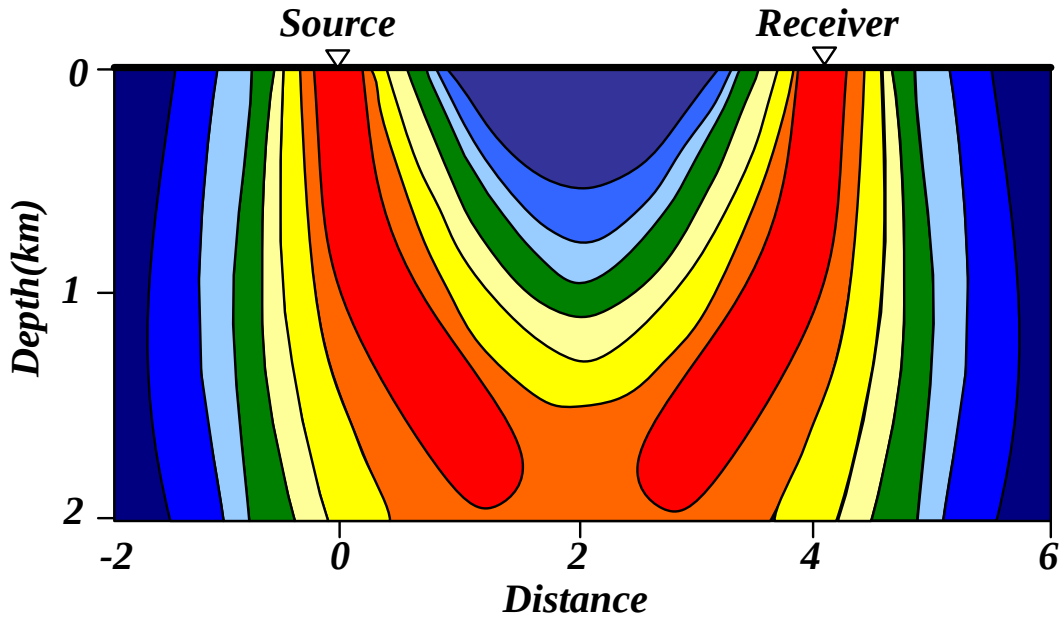

Figure A2 : Influence from receiver. For the isotropic case, the greatest sensitivity is located between the source and receiver. (MacGregor, 2001)

Appendix B – Visualisation techniques

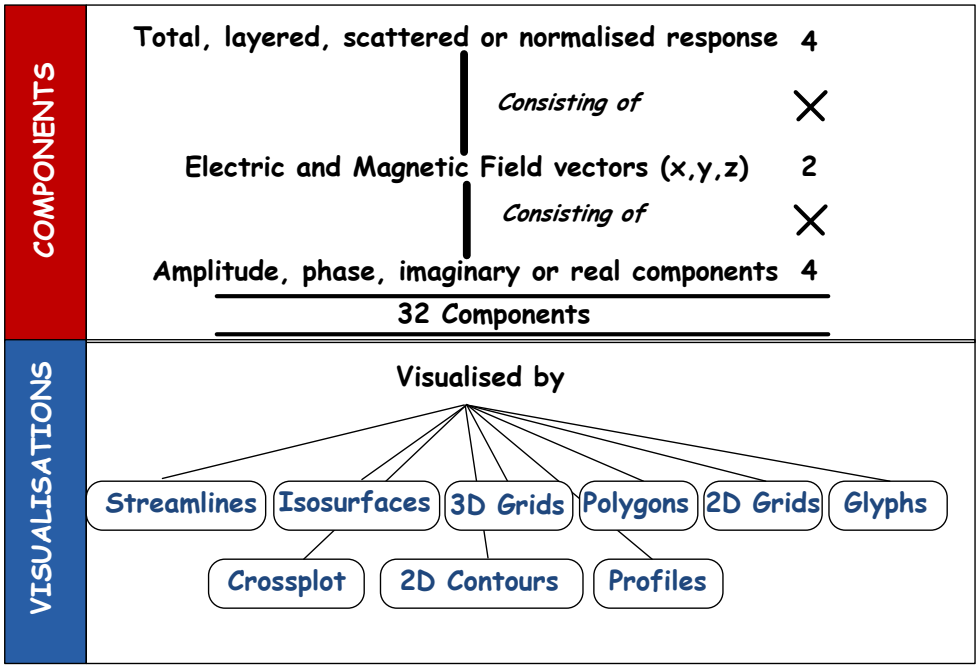

Figure B1: CSEM multispectral components and the various visualisation techniques. The method is problematic for visualisation due to the large number of components which can be represented. Therefore it is best to choose visualisation techniques which can intuitively represent multiple components at once to simplify the problem.

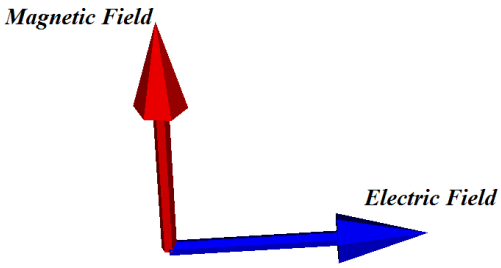

Figure B2: Magnetic and electric field glyphs. Glyphs represent both the direction and magnitude of EM vector.

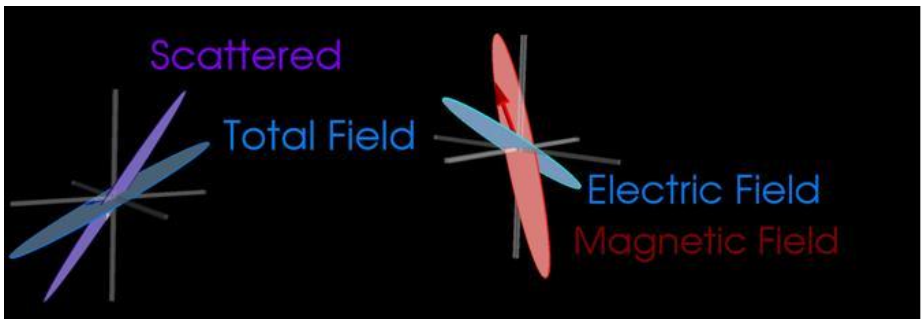

Figure B3: Example uses of polarisation ellipses. Polarisation ellipses simplify the 4D movement of the EM vector. Polarisation ellipses can be used for detecting changes between scattered, total and layered field responses, or electric and magnetic responses.

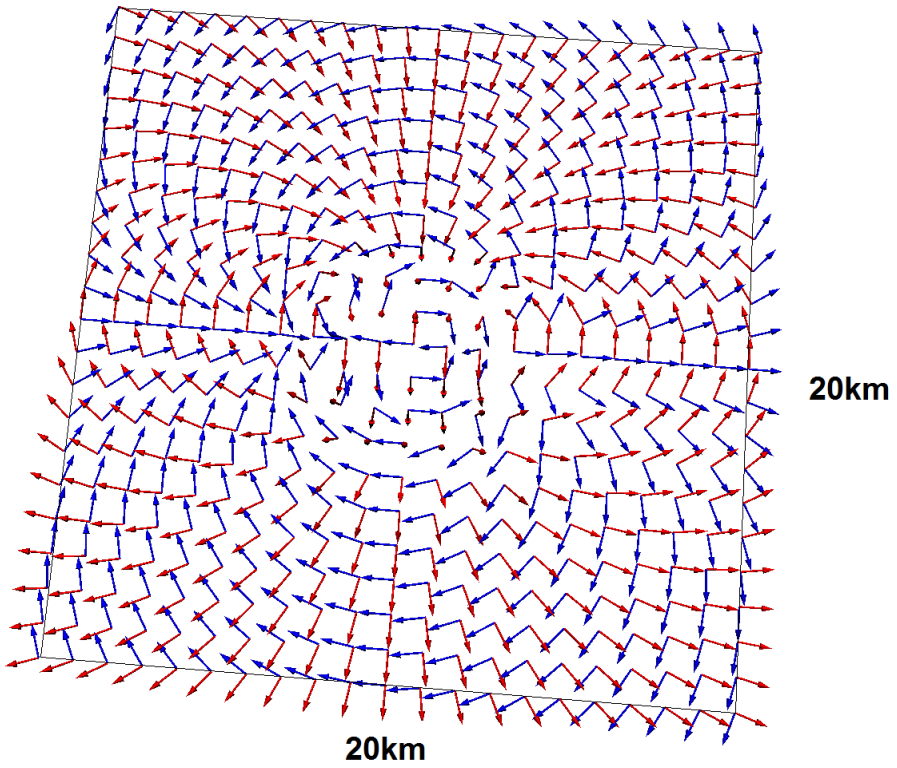

Figure B4: A single time interval of the Electric (blue) and Magnetic field (red) glyphs. Glyphs show direction of the electric and magnetic field for a single time step. Glyphs can be animated to show the changes in direction and amplitude in real time stereo (i.e. a 3D movie).

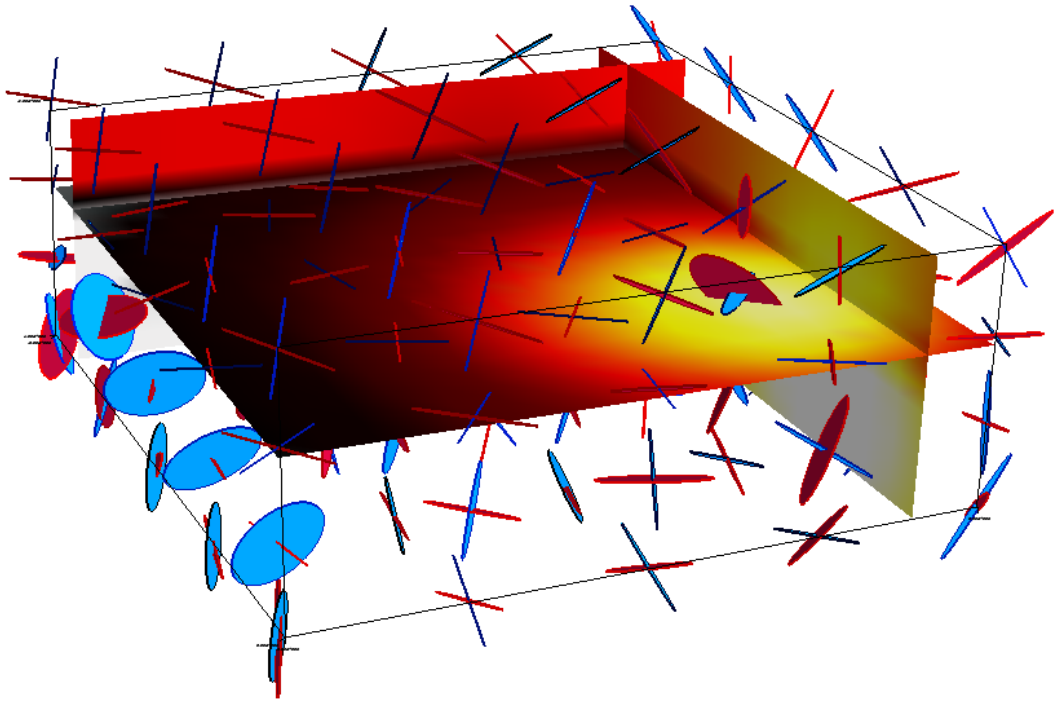

Figure B5: Example of a 3D volume of polarisation ellipses and scalar planes of the same volume seen in B3. Generated in MayaVi.

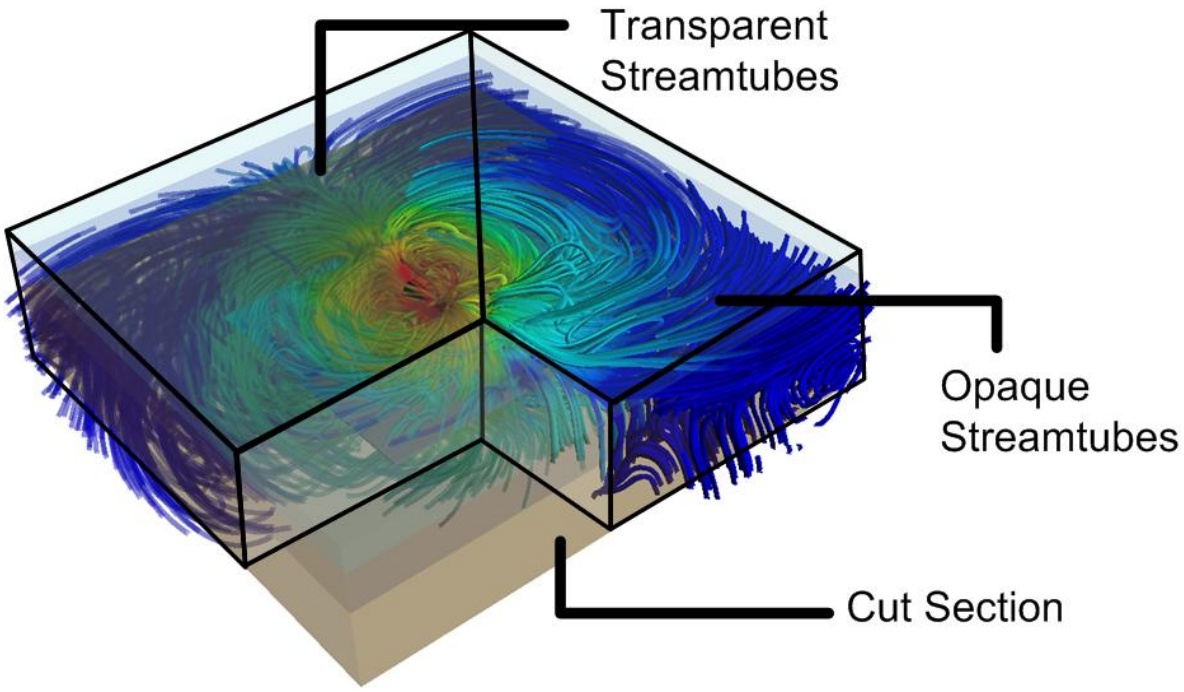

Figure B6: Example of 3D streamlines. There is a number of ways to manipulate streamlines, including making them transparent to better understand the overall nature of the field or it can also be done by creating a cross section or slice to better see what the field is doing in a single area.

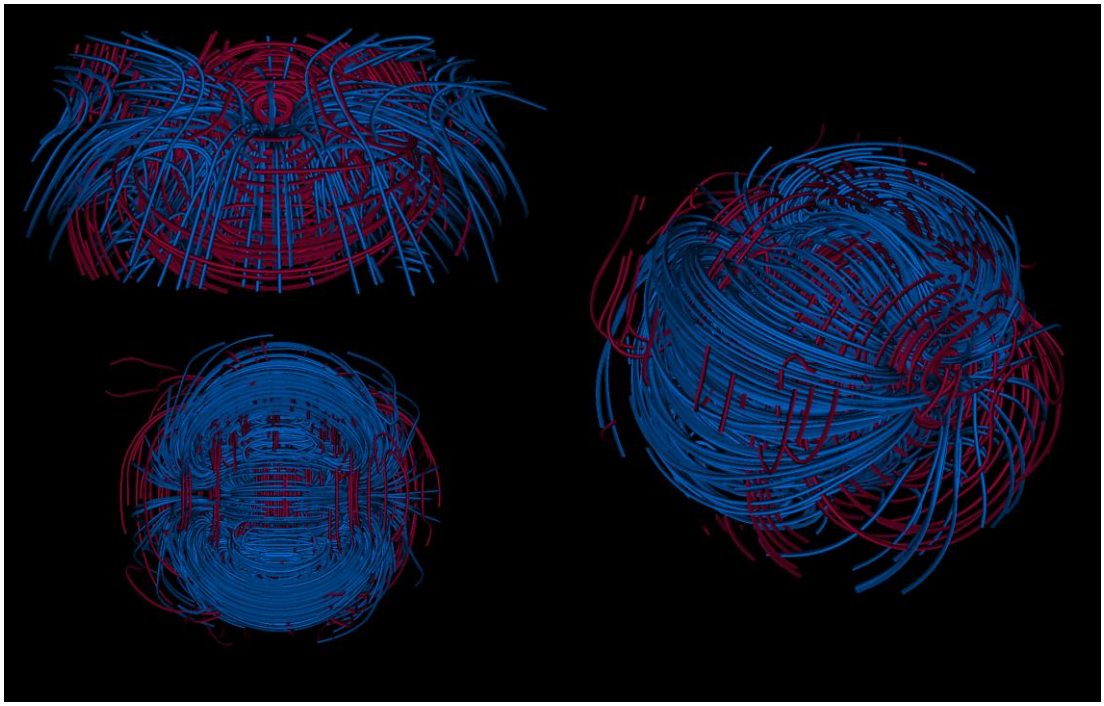

Figure B7: Streamlines of the electric field (blue) and magnetic field (Red)

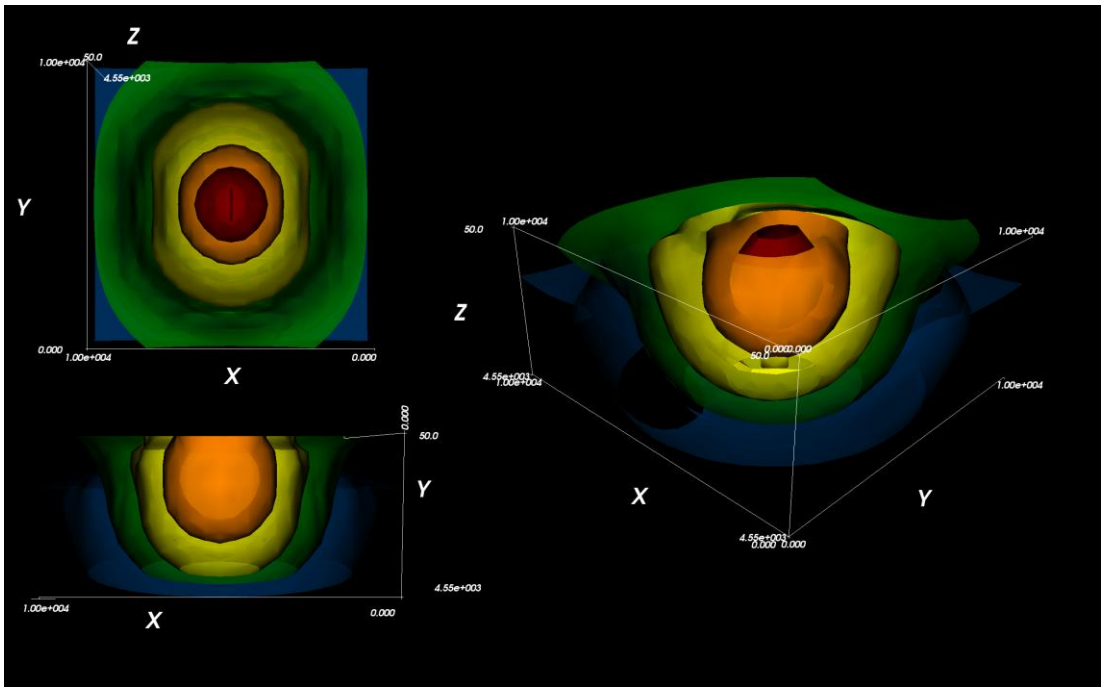

Figure B8: Example of isosurfaces at 10^{-15}(Blue), 10^{-14}(Green), 10^{-13}(Yelow), 10^{-12}(Orange), 10^{-11}V/Am^2(Red),being used to represent the total electric field behaviour for a single time slice. Generated in MayaVi.

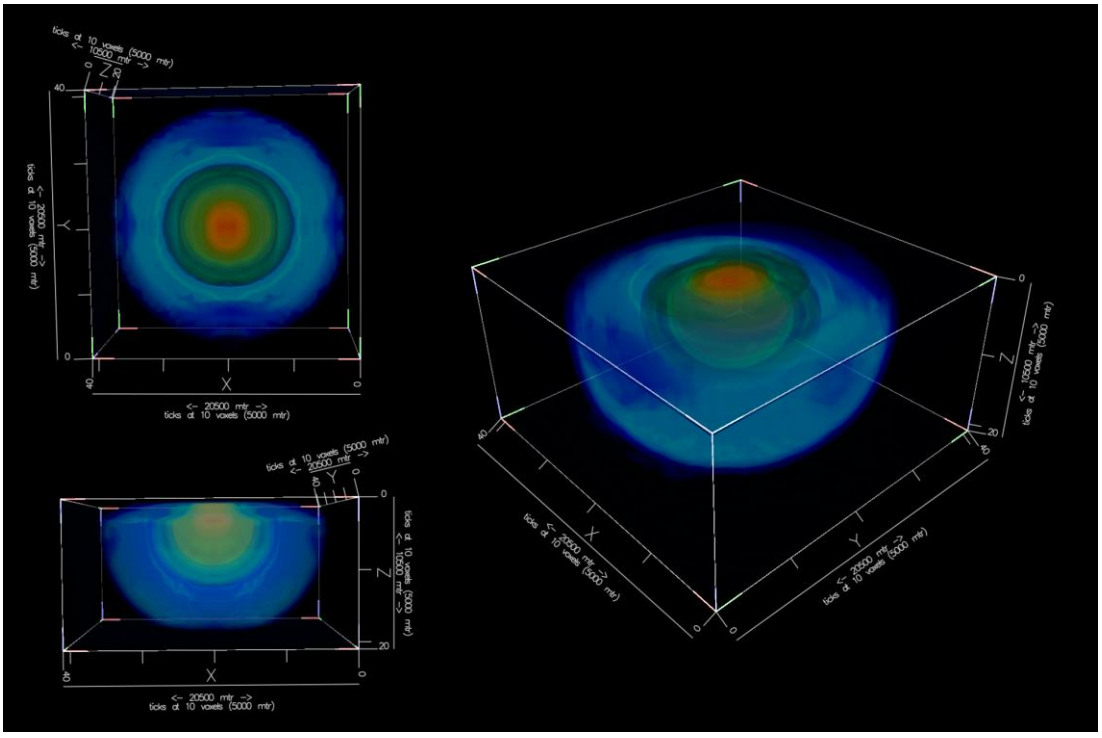

Figure B9: Example of isosurfaces being used to represent the total electric field behaviour for a single time slice. Generated in Drishti.

Appendix C - Modelling

Modified Integral Equation Code

1D layered earth forward modelling algorithms mainly consist of Fourier or Bessel integrals which can be easily evaluated numerically. A frequency domain modified integral equation code is used here to numerically simulate real marine CSEM survey data. This code provides efficient evaluation of 1D layered earth models excited by current bipole(s). The coupled vector field can be calculated at any point in space. Primary and secondary fields are calculated individually. Real and imaginary components of the electric field (E) and magnetic field (H) are calculated for all Cartesian vectors (Ex, Ey, Ez, Hx, Hy and Hz) of the coupled vector field from which amplitude and phase can be derived.

The approach of Hohmann (1988) is followed with application to a simple model that consists of; the air/water interface, water column, host sediments, and a target layer (hydrocarbon reservoir) over a halfspace. Due to attenuation in the earth only low frequencies are of interest, so displacement currents can be ignored. Frequency domain equations used by this integral equation code are obtained by performing a Fourier transformation of the time domain equations described below.

If the displacement currents are neglected, the coupled space and time dependence of electric and magnetic fields can be described by Maxwell's equations as functions of position, r and time, t:

$$\nabla \times E(r,t) = -\mu_0 \frac{\partial H(r,t)}{\partial t} - \mu_0 \frac{\partial m_p}{\partial t}(r,t) \quad (1)$$

and

$$\nabla \times H(r,t) = \sigma E(r,t) + J_p(r,t) \quad (2)$$

Here m_p is the primary magnetic current and J_p is the primary electric current. Taking the curl of equation (1) and substituting into equation (2) yields a vector diffusion equation for the electric field:

$$\nabla \times \nabla \times E + \mu_0 \sigma \frac{\partial E}{\partial t} = -\mu_0 \frac{\partial J_p}{\partial t} - \mu_0 \nabla \times \frac{\partial m_p}{\partial t} \quad (3)$$

Taking the curl of equation (2) and substituting equation (1) yields a diffusion equation for the magnetic field:

$$\nabla \times \left(\frac{\nabla \times H}{\sigma} \right) + \mu_0 \frac{\partial H}{\partial t} = \nabla \times \left(\frac{j_p}{\sigma} \right) - \mu_0 \frac{\partial m_p}{\partial t} \quad (4)$$

Equations (3) and (4) demonstrate the fact that due to attenuation in the earth, CSEM frequencies must be so low such that we deal with a diffusion of EM energy rather than the propagation of a wave. Hence the low resolution of the resistivity distribution within the earth than can be obtained from the marine CSEM method. We can now apply the vector identity

$$\nabla \times \nabla \times A = -\nabla^2 A + \nabla(\nabla \cdot A)$$

Equation (3) becomes

$$-\nabla^2 E + \nabla(\nabla \cdot E) + \mu_0 \frac{\partial E}{\partial t} = -\mu_0 \frac{\partial J_p}{\partial t} - \mu_0 \nabla \times \frac{\partial m_p}{\partial t} \quad (5)$$

Taking the divergence of equation (2) gives

$$\nabla \cdot (\sigma E) = \sigma \nabla \cdot E + \nabla \sigma \cdot E = -\nabla \cdot J_p$$

Substituting for $\nabla \cdot E$ into equation (5) gives

$$\nabla^2 E + \nabla\left(E \cdot \frac{\nabla \sigma}{\sigma} \right) - \mu_0 \sigma \frac{\partial E}{\partial t} = \mu_0 \frac{\partial J_p}{\partial t} - \rho \nabla \left(\nabla \cdot J_P \right) + \mu_0 \nabla \times \frac{\partial m_p}{\partial t} \quad (6)$$

Assuming that the source is in a region of homogenous conductivity the following identity can be used:

$$\nabla \times \phi A = \phi \nabla \times A - A \times \nabla \phi$$

Equation (4) can be written as

$$-\nabla^2 H + \nabla\left(\nabla \cdot H \right) - \sigma \left(\nabla \times H \right) \times \nabla \rho + \mu_0 \sigma \frac{\partial H}{\partial t} = \nabla \times J_p - \mu_0 \sigma \frac{\partial m_p}{\partial t}$$

The divergence of the magnetic field is non-zero only at a magnetic source; taking the

divergence of equation (1) shows that:

$$\nabla \cdot H = -\nabla \cdot m_p$$

Giving

$$\nabla^2 H + \ \sigma \left(\nabla \times H \right) \times \nabla \rho - \mu_0 \sigma \frac{\partial H}{\partial y} = \mu_0 \sigma \frac{\partial m_p}{\partial t} - \nabla \left(\nabla \cdot m_p \right) - \nabla \times J_p \quad (7)$$

Equations (6) and (7) are the general equations for the total electric and magnetic fields valid at any point in space. Either equation can be solved numerically by time stepping, and then the other field can be calculated from equations (1) and (2). The primary fields which apply at any point in a layered earth if there is no body present satisfy the following two equations:

$$\nabla \times E_p = -\mu_0 \frac{\partial H_p}{\partial t} - \mu_0 \frac{\partial m_p}{\partial t} \qquad (8)$$

$$\nabla \times H_p = \sigma_{layering} E_p + J_p \qquad (9)$$

Where $\sigma_{layering}$ is the normal layered earth conductivity with no body present. These primary fields are in the form of integrals that can be evaluated numerically. To obtain equations in the frequency domain, a Fourier transformation is performed on time domain equations (6) and (7) using the following integrals, assuming $e^{i\omega t}$ time dependence:

$$F(r,\omega) = \int_{-\infty}^{\infty} f(r,t) e^{-i\omega t} dt$$

$$F(r,\omega) = \frac{1}{2\pi} \int_{-\infty}^{\infty} f(r,\omega) e^{i\omega t} d\omega$$

Equation (6) then becomes

$$\nabla^2 E + \nabla\left(E \cdot \frac{\nabla\sigma}{\sigma} \right) + k^2 E = i\omega\mu_0 J_P - \rho\nabla\left(\nabla \cdot J_P\right) + i\omega\mu_0 \nabla \times M_P \qquad (10)$$

Equation (7) then becomes

$$\nabla^2 H + \sigma\left(\nabla \times H\right) \times \nabla\rho + k^2 H = i\omega\mu_0 M_P - \nabla\left(\nabla \cdot M_P\right) - \nabla \times J_P \qquad (11)$$

Equations (10) and (11) are the general frequency domain equations for the total electric and magnetic fields valid for every point for a layered earth, i.e. in the absence of any bodies embedded in the layered earth. For the total field, away from the source, either equation can be solved numerically, where the other component

can be found using the frequency domain versions of equations (1) and (2). (Phillips, 2007)

Modelling 3D bodies in a layered earth using integral equations

For a 3D body embedded in a layered earth we must consider the total field as the summation of the primary field as the response of the layered earth, plus the secondary field as the scattering response of a body embedded within the layered earth. Subtracting (8) from equation (1) and equation (9) from equation (2) gives the time domain equations for the secondary field due to the body:

$$\nabla \times E_s = \mu_0 \frac{\partial H_s}{\partial t} \quad (12)$$

and

$$\nabla \times H_s = \sigma E_S + \sigma_{body} E_P$$

or

$$\nabla \times H_s = \sigma_{layering} E_S + J_s \quad (13)$$

where

$$J_s = \sigma_{body} E$$

Note $\sigma_{body} = \sigma - \sigma_{layering}$ is the point conductivity of the 3D body. The quantity J_s is the scattering current of the body and is the source of the secondary field. The equation for E_s is the same as that for E in equation (6), without the magnetic source terms and with J_s replaced by $\sigma_{body} E_P$

$$\nabla^2 E_S + \nabla\left(E_S \cdot \frac{\nabla\sigma}{\sigma}\right) - \mu_0\sigma\frac{\partial E_S}{\partial t} = \mu_0\sigma_{body}\frac{\partial E_p}{\partial t} - \nabla\left(E_p \cdot \frac{\nabla\sigma_{body}}{\sigma}\right) \quad (14)$$

Since E_S is zero in the body, which is the only place where E is not zero, the secondary magnetic field can be derived by modifying equation (7) in a similar way to which we modified equation (6)

$$\nabla^2 H_S + \nabla\times H_S \times\nabla\rho - \mu_0\sigma\frac{\partial H_S}{\partial t} = \mu_0\sigma_{body}\frac{\partial H_p}{\partial t} - \sigma\nabla\left(\frac{\nabla\sigma_{body}}{\sigma}\right)\times E_p \quad (15)$$

The reasons for solving equations (14) and (15) rather than the equations for the total field are that the secondary fields require fine discretisation which involves dividing the 3D body into a number of cells and treating each cell as a source. The code used here uses the principle of symmetry for the body and reciprocity to reduce computation time. To obtain equations in the frequency domain, a Fourier transformation is performed on time domain equations (14) and (15) assuming $e^{i\omega t}$ time dependence:

Equation (14) then becomes

$$\nabla^2 E_S + \nabla\left(E_S \cdot \frac{\nabla\sigma}{\sigma}\right) + k^2 E_S = -k_a^2 E_S - \nabla\left(E_p \cdot \frac{\nabla\sigma_{body}}{\sigma}\right) \quad (16)$$

Equation (15) then becomes

$$\nabla^2 H_s + \sigma\left(\nabla\times H_S\right)\times\nabla\rho + k^2 H_s = -k_a^2 H_s - \sigma\nabla\left(\frac{\sigma_{body}}{\sigma}\right) \quad (17)$$

For the secondary field solutions the other component can be calculated using the frequency domain versions of equations (12) and (13):

$$\nabla \times E_s = i\omega\mu_0 H_s \quad (18)$$

$$\nabla \times H_s = \sigma_{layering} E_s + J_s \quad (19)$$

In order to formulate an integral equation we need to treat J_s as a source current. In a wholespace the secondary electric field is given by

$$E_s = -i\omega\mu_0 A_s - \nabla V_s \quad (20)$$

where A_s and V_s are the secondary vector and scalar potentials for the Lorentz gauge given by

$$A_s(r) = \int_v J_s(r')G(r,r')dv'$$

and

$$V_s(r) = -\rho_{layering} \int_v J_s(r')G(r,r')\,dv'$$

where G is the scalar EM Green's function:

$$G(r,r') = \frac{e^{-uk_{layering}|r-r'|}}{4\pi|r-r'|}$$

For a body in a halfspace, an additional term given by Hohmann (1975) for a homogenous earth and in Wannamaker, et al. (1984) for a layered earth, must be added to expression (20) to account for the layering response.

Adding the primary field to the secondary field of expression (20) we get a singular Fredholm integral equation for the total electric field which is written as

$$E(r) = E_p(r) + \int_v \tilde{G}(R,r') \cdot \sigma_{body}(r') E(r')\,dv' \quad (21)$$

where $\tilde{G}$ is a tensor Green's function. Effectively the 3D body has been replaced by a volume of scattering current. Equation (21) is limited to a 3D body within a layered earth (1D) and as such forms the basis of the modified integral equation code used here to forward model real hydrocarbon deposits as 3D bodies within a layered earth model that consists of the air/water interface, water column, host sediments, and a 3D target body (hydrocarbon reservoir) (Hohmann, 1988; Phillips, 2007).

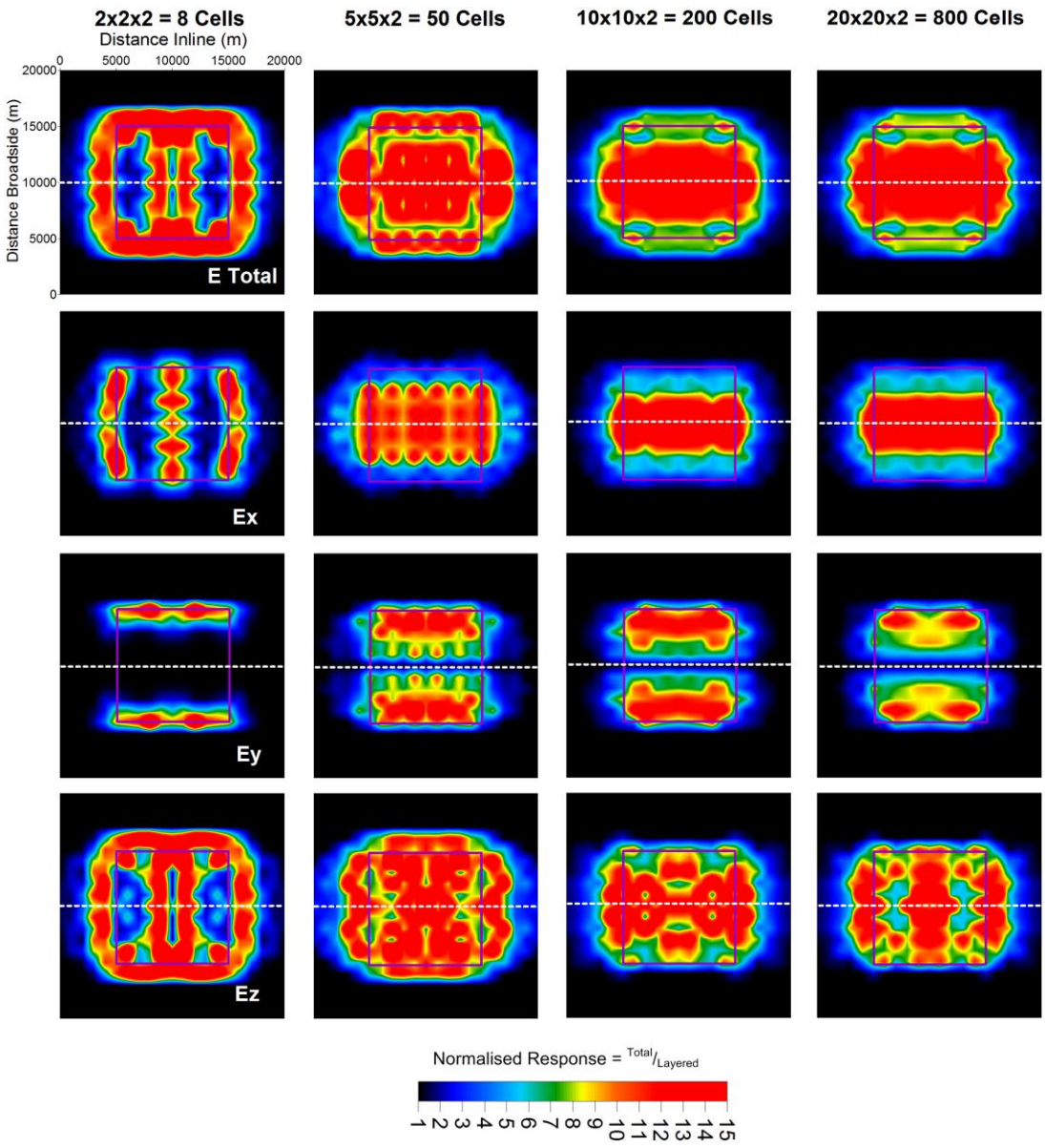

Figure C1 : Figure showing the effect of hydrocarbon discretisation on the maximum normalised sensitivity for a single transmitter at 0.25Hz transmission frequency.

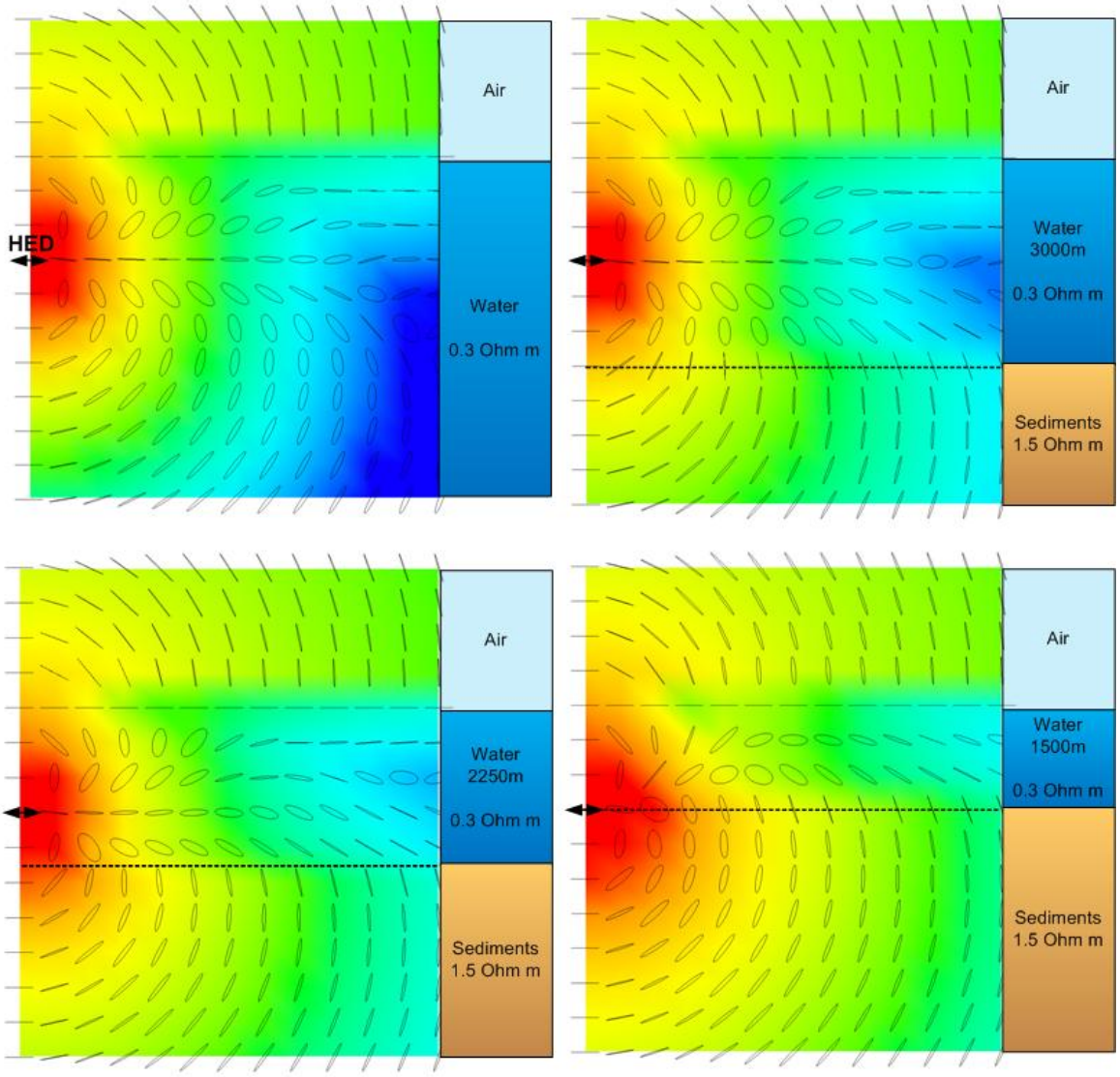

Figure C2: The effect of water depth on total electric field polarisation ellipses for a single transmitter at 0.25Hz transmission frequency. The colours represent electric field amplitude.

Appendix D - CSEMoMatic

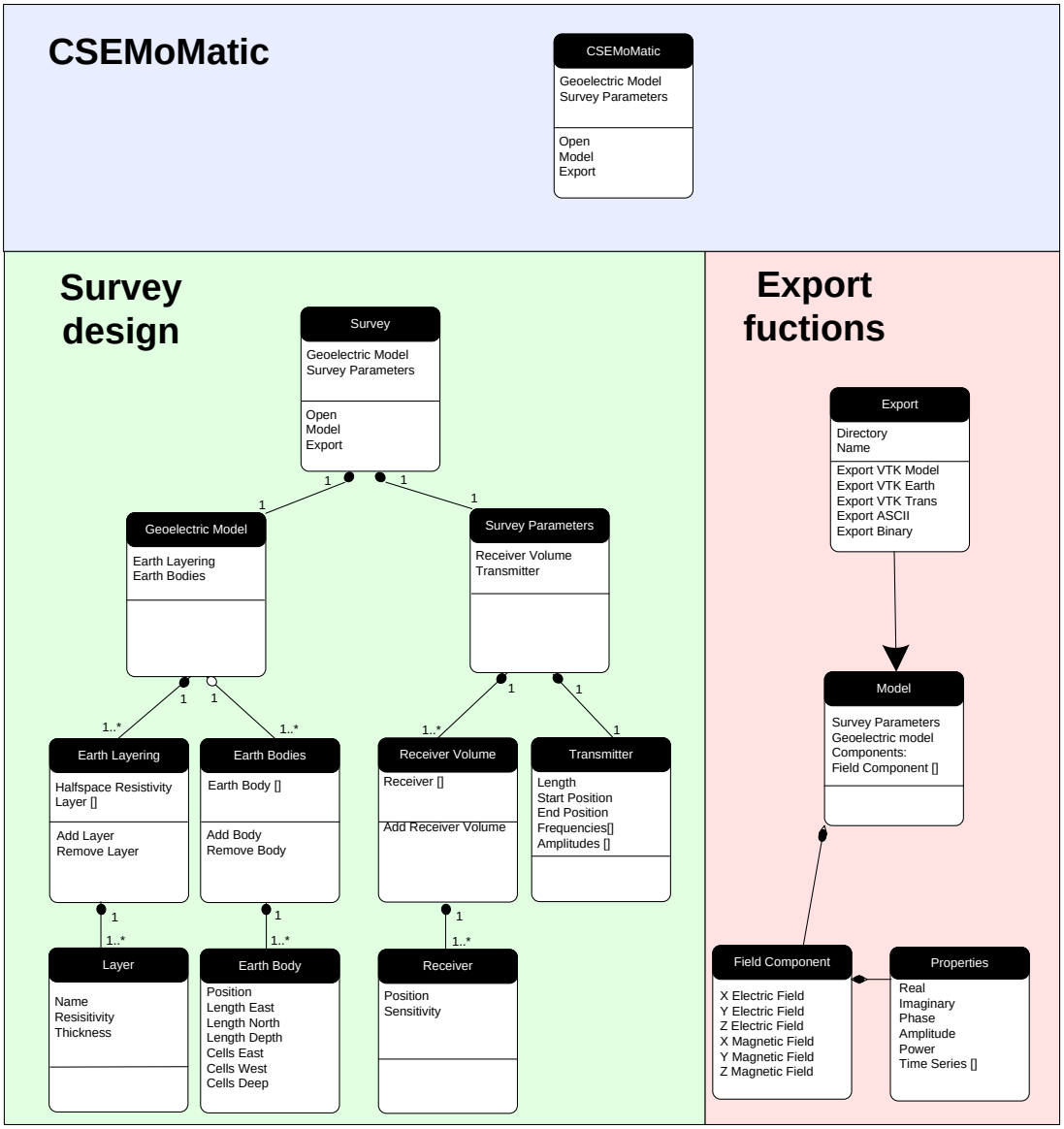

Figure D1 : An example UML class diagram structure of CSEMoMatic. This examples the use of object oriented programming.

CSEMoMatic – Supported file formats

ASCII	A tab delimited ASCII file with EM component sorted by receiver and transmitter position. An EM component consists of receiver position, transmitter position, layered, scattered, total and normalised response for the electric and magnetic field vectors.
CSV	A comma separated variable file with the same structure as the ASCII file.
Matlab	A Matlab m file containing datasets and profile plotting options.
Binary	A binary formatted file using the Intel-endian float-datatype. This binary export can be used for the freely available visualisation package Drishti.
VTK Time Series	A 4D series of visual tool kit files of a sinusoidal time series of the modelled volume.
VTK Amplitude	A 3D volume of the amplitude vector of the EM field
VTK Phase	A 3D volume of the phase vector of the EM field
VTK Amp versus frequency	A 3D volume of ocean bottom receivers versus frequency for the modelled amplitude vectors
VTK Phase versus frequency	A 3D volume of ocean bottom receivers versus frequency for the modelled phase vectors
VTK Earth	A VTK file format of the polygons making up the earth model
VTK transmitter	A VTK file format of a polygon representing the transmitter
VTK Ellipse	Polygons representing both the polarisation ellipses and axis
VTK Streamlines	A normalised 4D sinusoidal time series of the EM vector with amplitude 100
Surfer Grid	An ASCII formatted surfer grid file of the amplitude, normalised amplitude and GRI of the modelled survey.

Table D1 : CSEMoMatic supported file formats.